UNIVERSITY *of the*
WESTERN CAPE

RESERVOIR CHARACTERIZATION OF WELL A-F1, BLOCK 1, ORANGE BASIN, SOUTH AFRICA

A master's thesis in Petroleum Geoscience

by

Adrian Williams

Submitted in partial fulfilment of the requirements for the degree of Magister Scientiae (MSc) in the Faculty of Science, Earth Sciences Department University of the Western Cape, Bellville, South Africa.

April 2018

Supervisor: Dr. M. Opuwari

Abstract

The Orange basin is relatively underexplored with 1 well per every 4000km^2 with only the Ububhesi gas field discovery. Block 1 is largely underexplored with only 3 wells drilled in the entire block and only well A-F1 inside the 1500km^2 3-D seismic data cube, acquired in 2009.

This study is a reservoir characterization of well A-F1, utilising the acquired 3-D seismic data and re-analysing and up scaling the well logs to create a static model to display petrophysical properties essential for reservoir characterization.

For horizon 14Ht1, four reservoir zones were identified, petro-physically characterized and modelled using the up scaled logs. The overall reservoir displayed average volume of shale at 24%, good porosity values between 9.8% to 15.3% and permeability between 2.3mD to 9.5mD. However, high water saturation overall which exceeds 50% as per the water saturation model, results in water saturated sandstones with minor hydrocarbon shows and an uneconomical reservoir.

Keywords

Orange Basin

Hydrocarbon

Reservoir characterization

Seismic interpretation

Petrophysical analysis

Up scaling

Static modelling

Property modelling

Declaration

I declare that **Reservoir Characterization of Well A-F1, Block 1, Orange Basin, South Africa** is my own work that it has not been submitted before for any degree or examination in any other university, and that all the sources I have used or quoted have been indicated and acknowledged by means of complete references.

Adrian Williams

April 2018

Signed: _____

Dedication

This work is dedicated to;

My mother,

who devoted herself to ensuring I had an education.

My beautiful baby girl,

Amelia Hannah Trudy Williams

born on 29-09-17.

My Lord and Saviour who strengthens me.

‘Commit your works to the Lord

And your plans shall succeed.’

Proverbs 16:3

Acknowledgements

Thank you to my supervisor, Dr Opuwari for supervising this work and the patience and time invested at critical moments.

Thank you to the Petroleum Agency of South Africa (PASA) for providing the data that was used in this thesis and their assistance.

Thank you to Schlumberger for their continuous support of the UWC Earth Science department; many good scientists are being produced through your generosity.

The postgraduate and administrative staff in the background keeping things together.

To my fellow postgraduate students, especially those who gave input to my work and gave encouragement, it is appreciated. A special thank you to Nehemiah Dominick, Moses Magoba and Ayodele Lasisi, for the assistance with this project. I am glad to call you fellow scientists and friends.

Yafah, thank you for your support in this time when it seemed this work would never come to fruition. It took longer than planned, thank you for your patience and understanding. It is greatly appreciated.

To my mom who first gave me the opportunity for a better education, thank you for giving me the tools to learn. To my brother who always told me to just get it done, thank you. To my sister who now inspires me through her own academic achievements, thank you. To my family and friends, thank you for your continuous support and check-ups on me, even late at night.

To the special person who believed in me the most, who encouraged me to complete this degree, your belief in me has driven me to complete this work.

There is light at the end of the tunnel, eventually.

Table of Contents

List of Figures

List of Tables

List of Appendices

1. Introduction

Reservoirs are formed by geological processes which are complex in nature and require a multi-disciplinary approach to mitigate the uncertainties in decision analysis and reservoir management. Two key disciplines involved in improving the understanding of reservoirs and decreasing the risk exposure is the use of geophysics and petrophysics in reservoir characterization. Due to subsurface complexities and the high cost of data acquisition, limited data sets need to be analysed and used in a coherent manner to define the three-dimensional properties of a reservoir (Ma, 2011).

Petrophysical properties such as porosity, permeability, volume of shale and water saturation are necessary for successful evaluation and determining the quality of the reservoir and whether it is economically viable. Static reservoir modelling is one method, where seismic data interpretation provides the models structural framework and petrophysical log data provides the reservoir properties. Static models allow deterministic and probabilistic reserves to be calculated, furthermore, uncertainties can also be calculated with risk assessments to provide reliable estimations (Stegers, 2012).

South Africa's petroleum offshore resources have been largely under explored with imports required to meet more than half of the energy requirements. Between 1970 and 1994, only the state owned oil company, Soekor, operated due to other companies withdrawing business from the country due to political sanctions. In 1994 the offshore areas were opened to international investors for operating and exploration licenses. In the offshore area, over 300 exploration wells have been drilled (PASA, 2012).

The well data is older pre-sanction Soekor data as in the case of this study of well A-F1 although 3-D seismic was acquired over the area in 2009 by Cairn India and Petro SA, who own 80% and 20% rights to block 1 respectively (PASA, 2015).

This project aims to perform a reservoir characterization on well A-F1, by analysing the well logs and interpreting the 3-D seismic data, integrating the well logs along with the 3-D seismic data to create a static model for reservoir characterization.

1.1 Location of study area

The Orange basin lies on the western offshore of South Africa and covers an estimated area of 160 000km^2. The basin is seen as underexplored with 1 well per every 4000km^2 with only the Ububhesi gas field discovered on the South African side of the border with the Kudu gas field discovered on the Namibian side. Block 1 highlighted in figure 1.1, is largely underexplored with only 3 wells drilled in the entire block and only well A-F1 (most northerly positioned well) drilled inside the 1500km^2 3-D seismic cube which was acquired in 2009 (PASA, 2015).

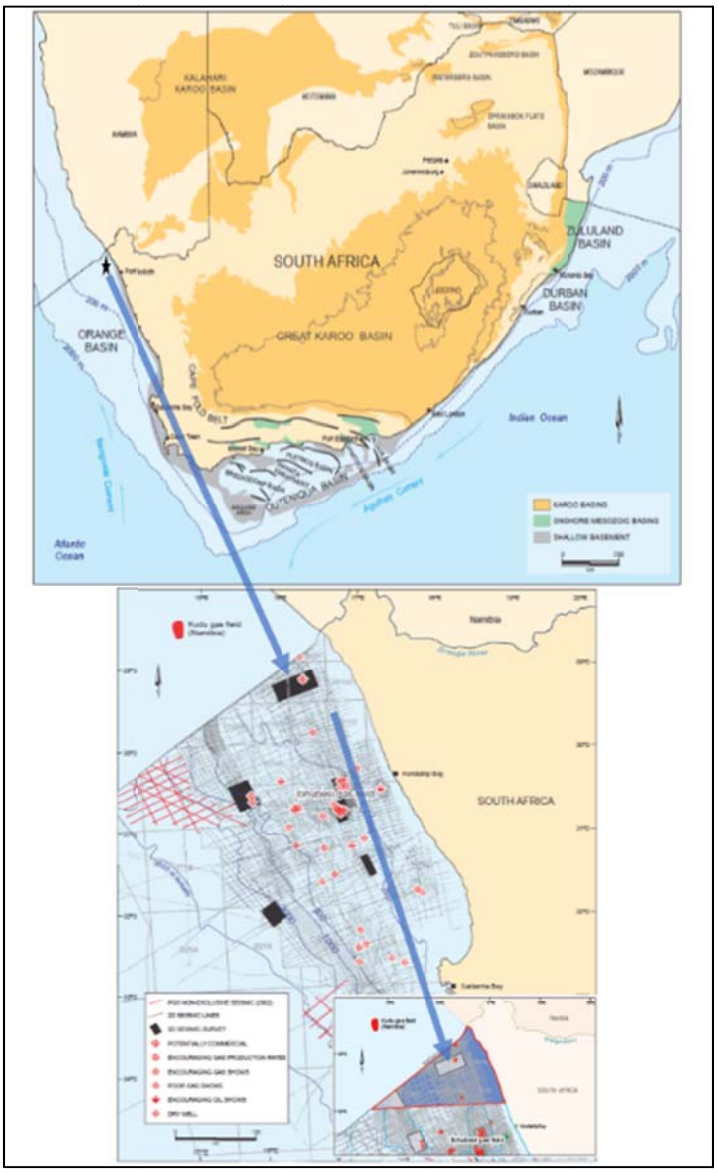

Figure 1.1 Location of well A-F1, Block 1, Orange Basin, West Coast of South Africa (PASA, 2015).

1.2 Problem statement

The Hautevarian play is the only play in which oil has been found in the Orange Basin, which was discovered in the AJ graben at well A-J1. The basin is however seen mainly as gas prone. Well A-F1 study area is in close proximity to the Kudu gas field with suggestions the aeolian play extends southwards into the South African portion over the Orange River border (PASA, 2015).

1.3 Aims of this study

The aim of this study is to characterize reservoirs by performing a static modelling of block 1, well A-F1, horizon 14Ht1, in order to increase the knowledge base of the non-marine Hautevarian play of the syn-rift succession in the marginal graben province.

1.3.1 Objective of the study:

Seismic analysis

- Perform a detailed seismic interpretation of the 3-D seismic dataset.

Petrophysical evaluation of log data

-Condition logs.

-Lithological log (from gamma ray log).

-Log calculations (Volume of shale, Porosity, Permeability, Water Saturation).

-Cut-off determinations.

Develop a static reservoir model

-Velocity modelling.

-Domain conversion.

-Produce 3-D grid model.

-Up scaling of petrophysical logs.

-Produce faces model.

-Produce petrophysical models (porosity, permeability, volume of shale, permeability)

2. Geological Background of the Orange Basin

2.1 Regional Geology

The Orange Basin extends approximately 500km on the west coast along the South African shoreline and is delineated by the border between South Africa and Namibia by the mouth of the Orange River (figure 1.2). Exploration of the basin started in 1974 with the discovery of the Kudu Gas field in southern Orange Basin in Namibia (Brown et al., 1995).

The Orange Basin is the largest of the South African basins; bound by the northwest Kudu arch of southern Namibia and the Agulhas-Columbine Arch on the south east edge as seen in figure 2.0 (Muntingh and Brown, 1991).

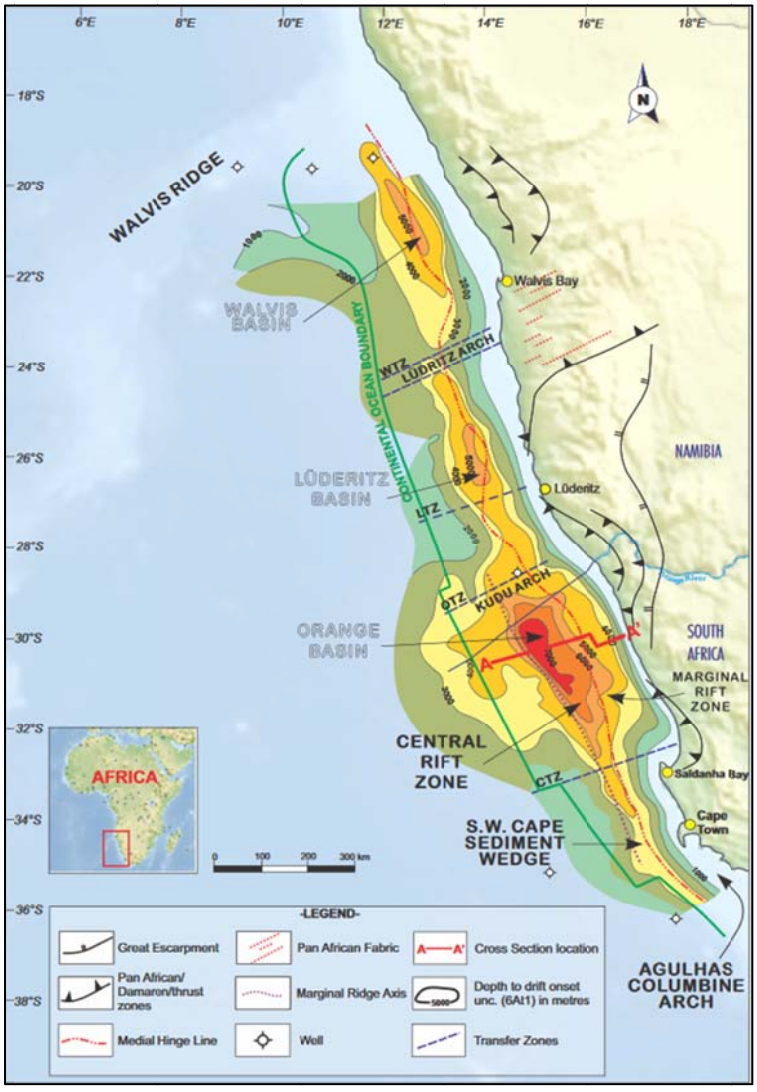

Figure 1.2 Structural Framework of Southwest Africa (PASA, 2015).

2.2 Depositional History and Basin Evolution

The depositional history of the Orange basin is characterized by four tectono-stratigraphic sequences by (Barton, 1993) and described by (Salomo, 2012) in terms of the northern deep water areas. Each tectonic stage described further below is shown in figure 2.1, with multiple unconformities present due to periods of erosion.

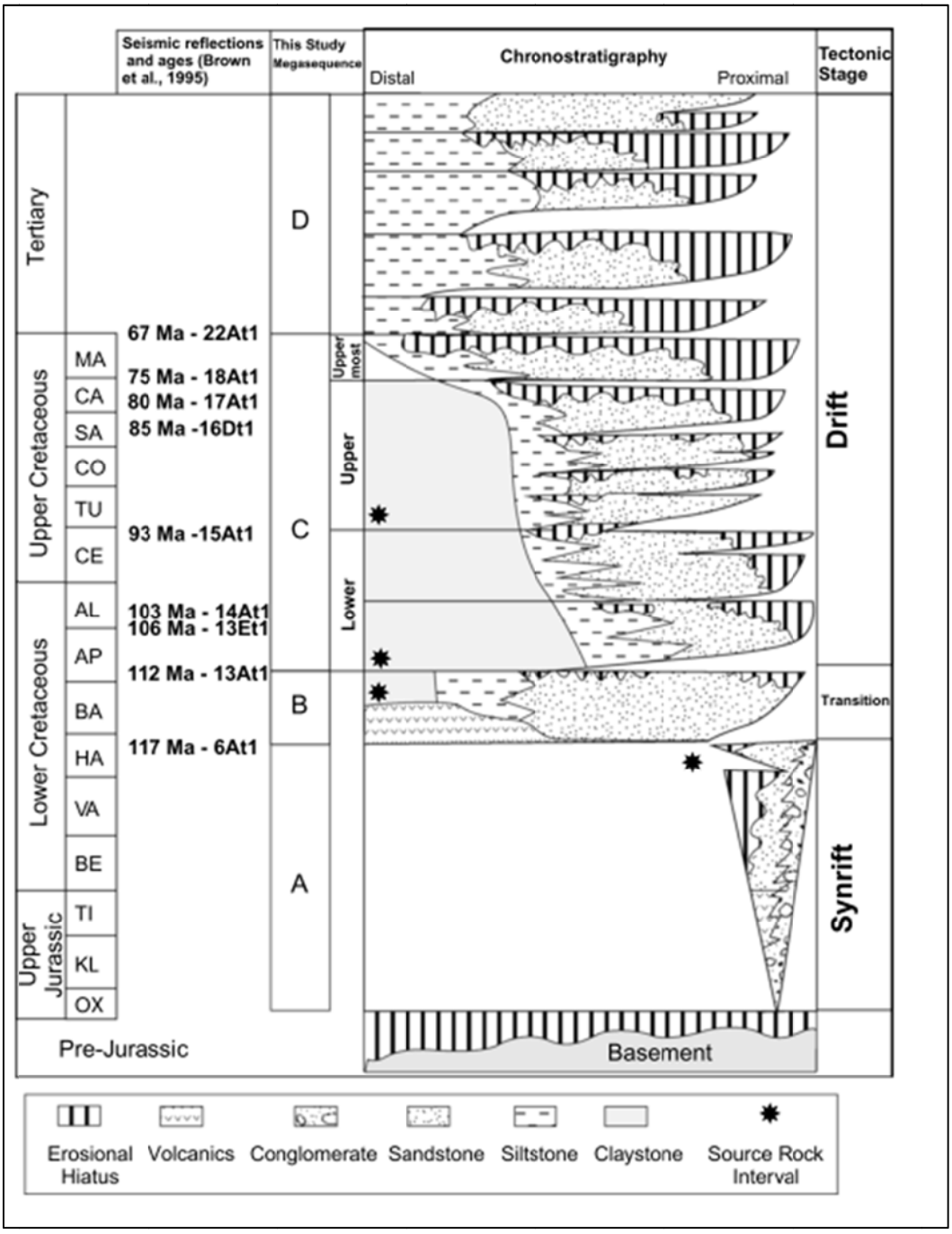

Figure 2.1 Chronostratigraphy and Tectonic stages (PASA, 2015).

2.2.1 Synrift Phase

Extensional stresses associated with the breakup of Gondwana land resulted in the formation of N-S trending graben systems in figure 2.2, which filled with Lower Cretaceous siliciclastics, volcanics and fluvial sediments. The medial hinge is a flexural high which separates the graben systems in a lateral fashion (Salomo, 2012). The synrift sequences from the basement to 6At1 have been identified in the marginal rift sequences and consist of course clastics with fluvial/lacustrine sediments and abundant volcanics, whereas within the central rift it consists mainly of lavas which are pronounced towards the west. The Rifting phase and onset of the drift phase is dated at 117Ma (Barton, 1993).

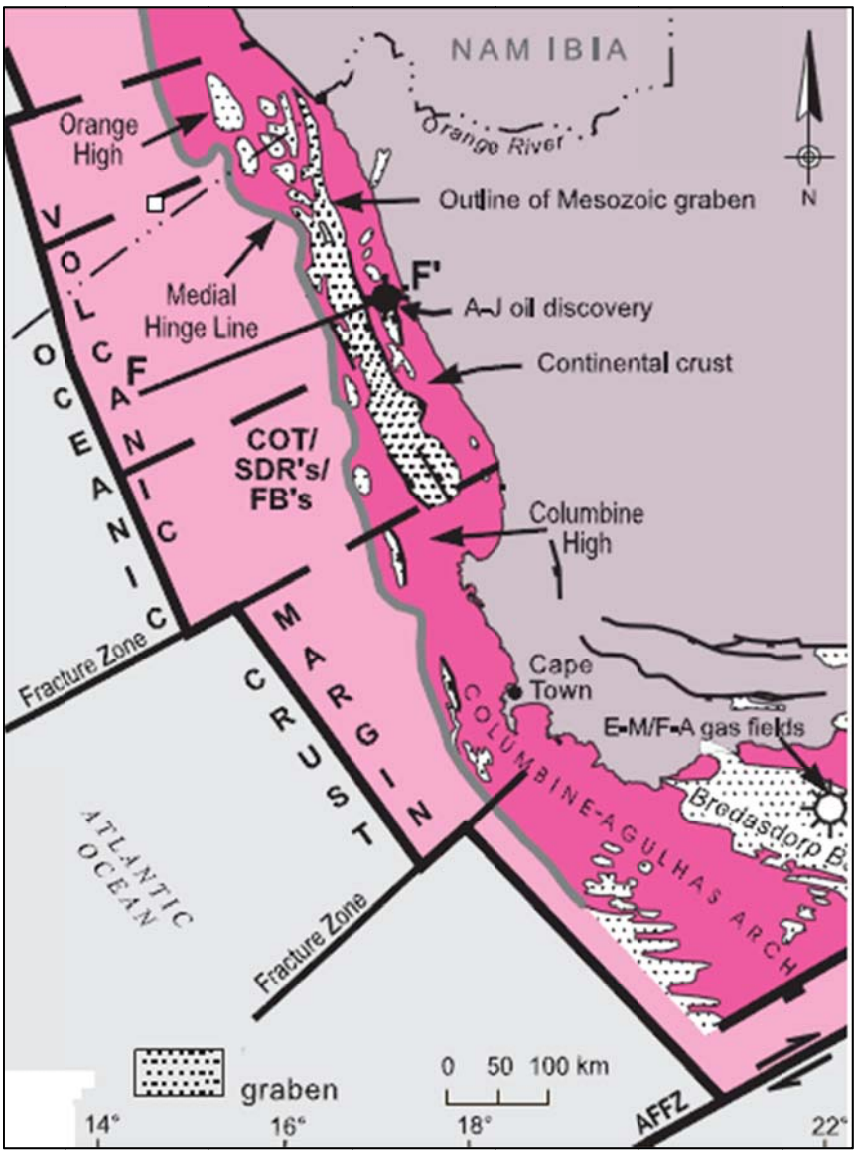

Figure 2.2: Graben system of the Orange Basin and the medial hinge line modified from (Broad et al., 2006).

2.2.2 Early Drift Phase

The early drift phase/transitional succession, 6At to 13At, consists of Aeolian marine sandstones and shales, red continental sediments with inter-bedded with lavas which was deposited from the late Hauterivian to the early Aptian. These Aeolian sandstones form the reservoir of the Kudu gas field offshore Namibia. During the Aptian period, drowning of the margin occurred resulting in the deposition of organic rich shales producing a source rock interval. This major marine flooding period is established to have occurred at 112Ma (Broad et al., 2006).

2.2.3 Drift Phase

The start of the drift phase is marked with the major margin flooding event at 112Ma marked the onset of passive margin drifting and subsidence and the development of a shelf edge and open marine conditions differentiating the early drift phase as ramp like without a well-developed shelf edge which formed during the drift phase. The Orange river and to a lesser extent the Oliphants river contributed to most of the sediment input into the basin, forming a sedimentary wedge during the drift phase, made up of a thick succession of siliciclastic sediments. During the Albian to Cenomanian, fluvio-deltaic sandstones were deposited which are the main gas reservoirs in the Ubhubesi gas field, with aggradational sequences forming above these followed by collapsing of the shelf edge by extensional faulting and large scale slumping(Broad et al., 2006).

2.2.4 Tertiary Phase

Cenozoic sediments were deposited as a well-developed wedge of siliciclastics increasing in thickness from, 200m thickness on the shelf to 1500m thickness basin ward. These formed by organic and chemical sedimentation with little continental sediment input except with the rise and fall of sea levels (Broad et al., 2006). Figure 2.3 displays a cross section where each rift sequence can be identified from basement to the sea floor.

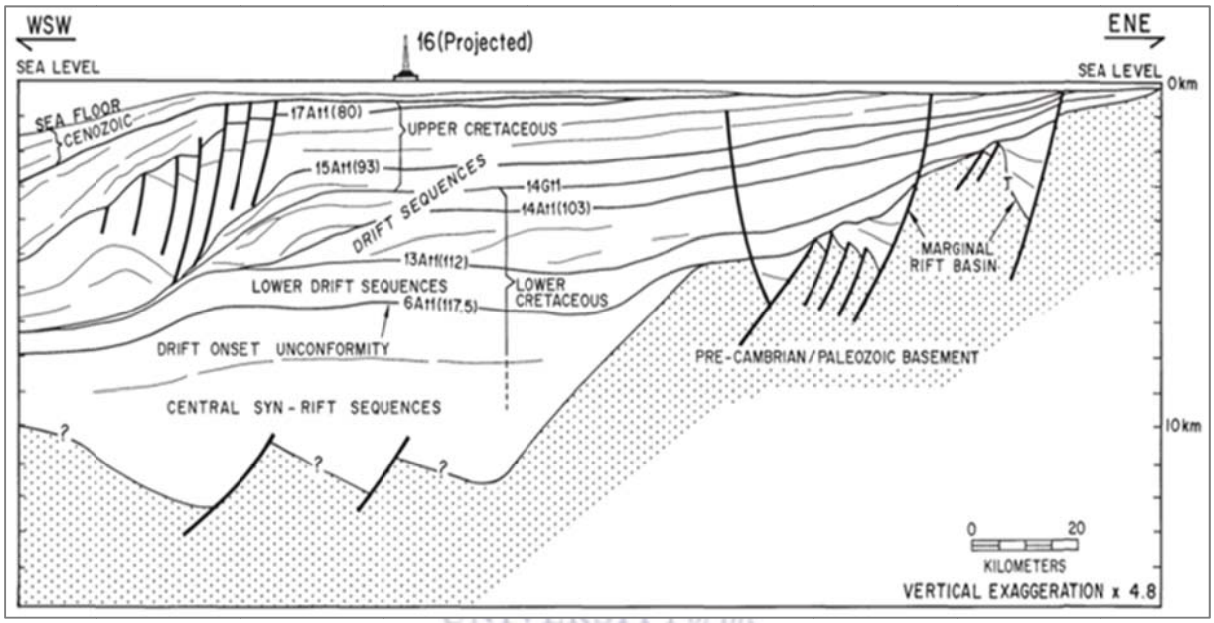

Figure 2.3: Cross section displaying the post rift sequences from basement to the top of sea floor, modified from (Brown et al., 1995).

2.3 Tectonic setting

'The break-up of Gondwana land', Watkeys 2006 article, discusses the rift process by attempting to reverse continental drift and the 5 stages which resulted in the current continental positions. Stage 4 (135-130Ma) discusses the separation of South America from Africa 115Ma to 130Ma which is related to the arrival of the Tristan da Cunha plume beneath the rift (Watkeys, 2006). Figure 2.4 displays the rifting which formed the Orange Basin.

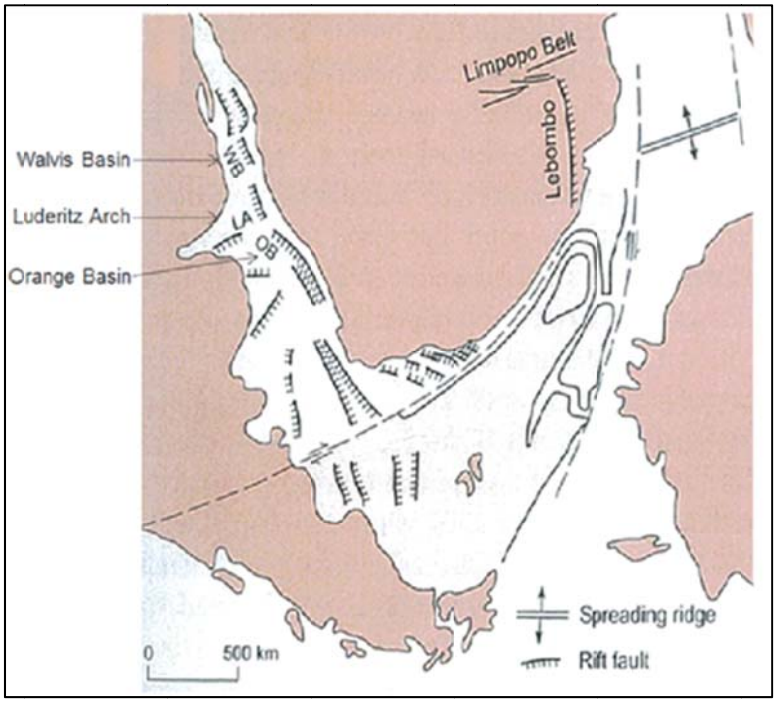

Figure 2.4: Displays the rift formation between African and South American continent and position of the Walvis and Orange Basins, modified from (Watkeys, 2006).

The margin off the west coast of South Africa is a divergent plate margin, which is underlain by synrift graben basins and the post-rift or passive margin Orange Basin (Brown et al., 1995). The Western offshore basin is defined by the Orange Basin which covers an area of approximately 130 000 km^2 and is characterised by the passive margin where deformation mechanisms were neither active nor completely dormant throughout the basin history (Hirsch et al. 2009).

Rifting occurred during the Late Jurassic period, during the separation of the African and south American plate post Gondwanaland breakup, where post-rift events were followed by infilling of rift basins by Lower Cretaceous and siliciclastic material (Brown et al., 1995).

The ancestral Orange River was the main contributor of sand rich sediments at high depositional rates with the Oliphant's drainage system contributing during the period 117.5-103Ma (Brown et al., 1995). In the northern central part of the Orange Basin, the sediment pile exceeds 7km with the thickest successions directly opposite the present day location of the Orange River mouth (Van der Spuy, 2003).

2.4 Sequence Stratigraphy

A depositional sequence is defined as a conformable succession of genetically related strata which is bounded at its top and its base by unconformities. The boundaries between the majority of depositional sequences are sub aerial and submarine type sequences which are defined by eustatic sea level changes. Sequences are defined by three depositional system tracts, low stand system tracts, transgressive system tracts or high stand system tracts. (Muntingh and Brown, 1991).

The sequence stratigraphy in figure 2.5 is fundamental to the understanding and prediction of petroleum play systems and the associated source rocks and reservoirs in the Orange Basin.

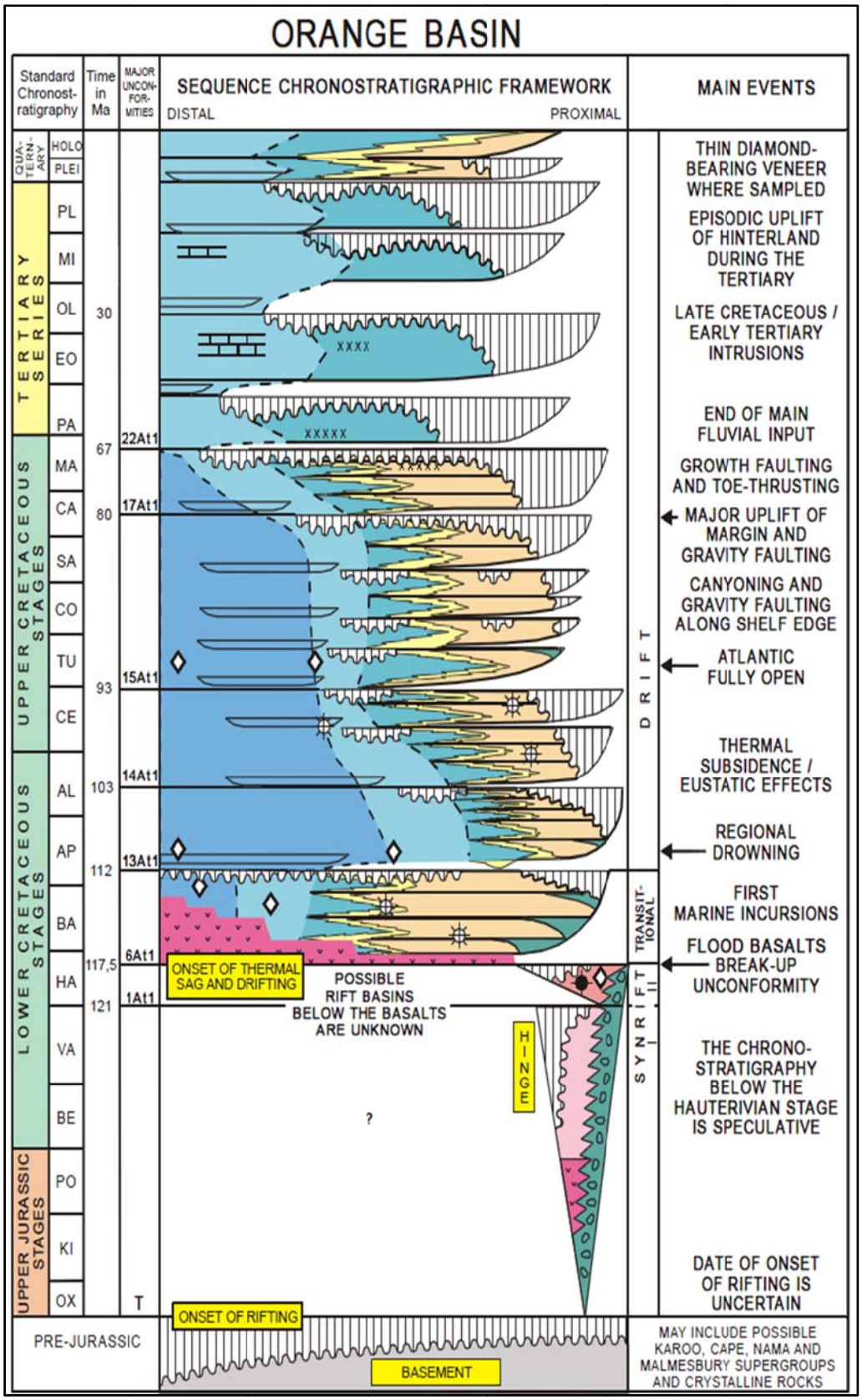

Figure 2.5: Sequence chrono-stratigraphic framework of the Orange Basin (PASA, 2015).

2.5 Petroleum system of the Orange Basin

A petroleum system exists if all the necessary geological elements are in place and processes occur for an accumulation of hydrocarbons to be present. Below, figure 2.6, gives a good overall profile of the petroleum system present in the Orange Basin.

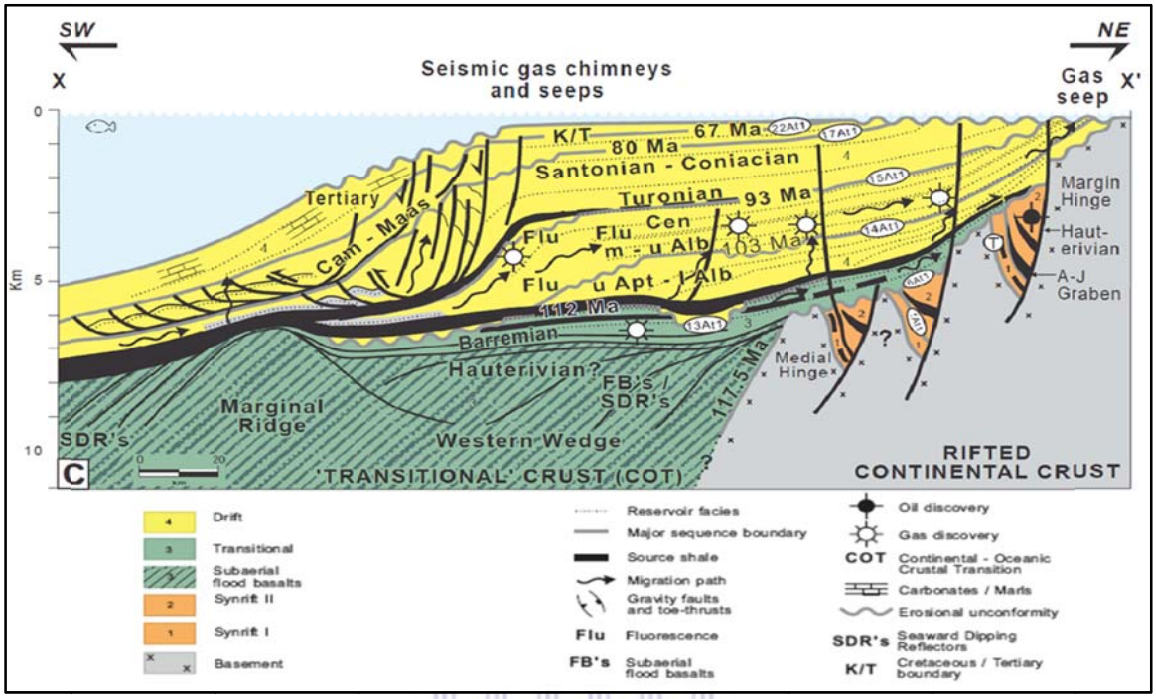

Figure 2.6: A cross profile displaying the petroleum system elements of the Orange Basin (Jungslager, 1999b).

2.5.1 Source Rocks

Source rocks are sedimentary deposits formed in anoxic environments which contain high percentages of organic matter. Shales contain 90% of all organic matter found in sediments; hence shales are generally found to be excellent source rocks and can act as seals depending on the position in the stratigraphic column in relation to reservoirs (Frank et al., 2008).

Aptian source rocks play a major role in the petroleum systems of the Orange basin with organic rich intervals having been intersected in other basins off the west coast of South Africa. Aptian source rocks for the study area are deemed proximal with Aptian sediments being continental to transitional in nature (Van der Spuy, 2003).

Source rocks are regionally developed above the Aptian unconformity (13At1) and ranges from dry gas to wet gas on the shelf with oil prone source rocks being found further west (Barton et al., 1993).

2.5.2 Reservoir Rock

Reservoir rocks are defined as a rock that's possesses both the porosity (Ø) and permeability (K) to contain and yield economic quantities of oil or gas in a suitable stratigraphic position. The fundamental property of a reservoir rock is its porosity; however its permeability determines its effectiveness as a reservoir. Porosity and permeability of a reservoir is at its peak when freshly deposited but will decrease significantly with compaction. Common reservoir rocks include sandstones and carbonates (North, 1985).

Reservoir sandstones occur throughout the Orange basin with reservoir rocks in the post rift sequence ranging from channel, fluvio-deltaic to marine sandstones (Barton et al., 1993).

2.5.3 Traps

Traps are an arrangement of strata that permits the accumulation of hydrocarbons in a reservoir that is in economic quantity. Two main classifications of traps exist and these are structural or stratigraphic. Structural traps require the secondary movement of strata to form post-depositional structures which include for e.g.; folding or faulting. Traps are otherwise classified as stratigraphic and do not require structure but are defined on the limits of the reservoir rock or i.e. lithological traps due to the presence of impermeable strata above and below the reservoir (North, 1985).

Combinations of these 2 classifications exist, and are termed structural-lithologic traps. Only the 2 main trap types have been described to avoid the ambiguities present in a very broad and complex classification scheme (North, 1985).

2.5.4 Seals

Seals are defined as relatively impermeable layers which are commonly either shales or evaporites. In the study area the regional seals are the shale source rocks found at 15At1 and above 13At1 and hence the trap style is termed stratigraphic, due to the presence of shale (the source rocks) above and below the reservoir.

3. Methodology

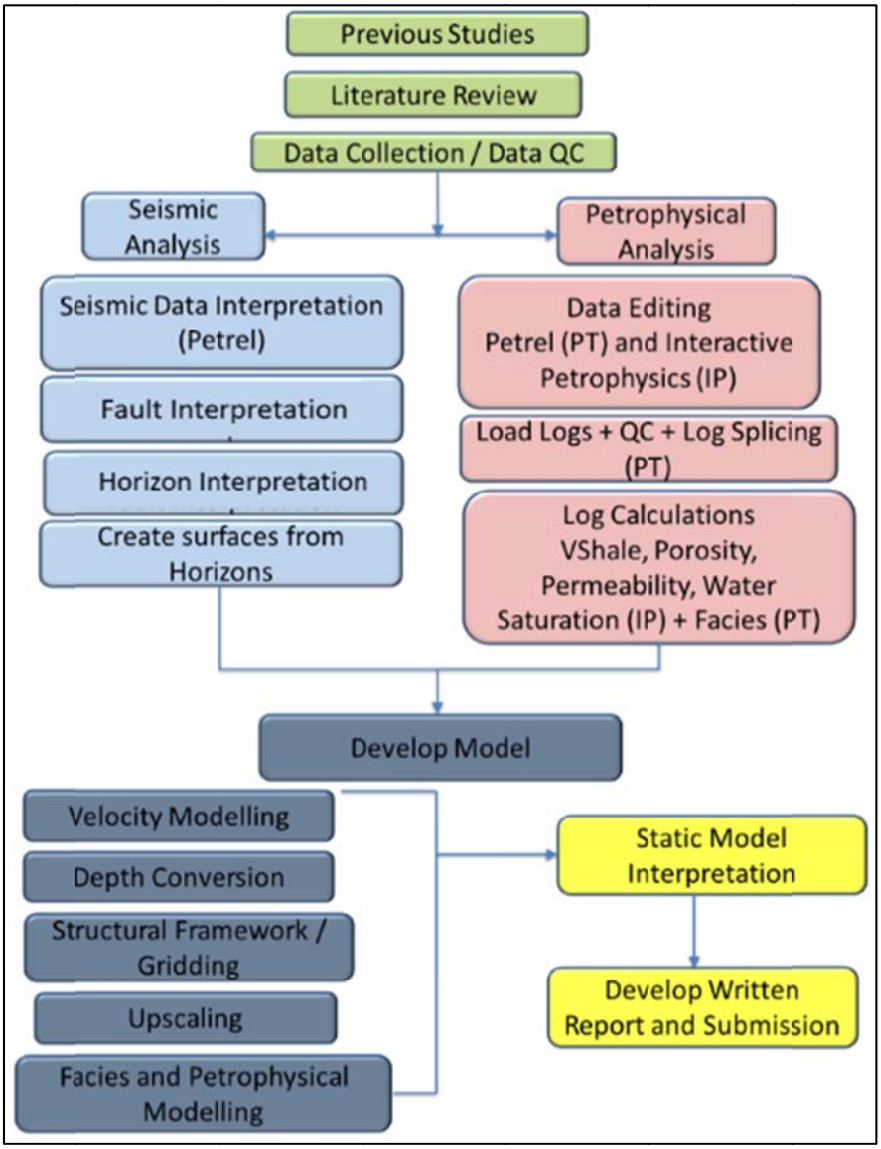

Figure 3.1: Flowchart of methodology.

The flow chart above (Fig 3.1) describes the multi-faceted approach taken in this study which combines literature reviews of the topic and previous studies. The next step is familiarisation of the seismic and petrophysical concepts which includes the software used and then the final interpretations and analysis to produce the 3-D static model.

This methodology section has been apportioned into seismic, petrophysical and modelling sections to distinguish the two disciplines being used for the product of this study which is the static models.

3.1 Data Collection

Data for the study was provided for this study by Petroleum Agency South Africa and acquired by the operators of block 1, Cairn India (80%) and Petro SA (20%).

Data used for this study includes the following:

3.1.1 Seismic Data (3-D Full Stack file):

Block1 3-D PSTM Final Full Stack file in segy format

3.1.2 Well Tops and Check shot data

Table 3.1: Well top data indicating depth and two way time.

Well name	Surface name	Depth	Twt (ms)
A-F1	Top of log	500	513
A-F1	16At1	867	813
A-F1	15At1	1186	1039.9
A-F1	14Jt1	1600	1303.6
A-F1	14Ht1	2140	1603
A-F1	14At1	2509	1801
A-F1	13At1	3385	2225.6
A-F1	6At1	3909	2384.4
A-F1	Bottom of log	3999.4	2490

3.1.3 Petrophysical Data (LAS files):

215 .las files were received, but only the 2 largest files were used as these merged all separate files.

3.1.4 Reports

Table 3.2: PASA project reports used for study.

No.	Report Name	Description
1	A-F1_WELL COMPLETION_POF5764	Well Completion Report
2	A-F1 LOG ANALYSIS AN INFORMAL REPORT_POF5010	Log Analysis Report
3	A-F1 CONVENTIONAL CORE ANALYSIS_POF7282	Conventional Core Analysis on Borehole A-F1
4	A-F1 GEOLOGICAL WELL COMPLETION REPORT(DATA PACK)_POF7766	A-F1 Geological Well Completion Report

3.1.5 Software

Software used for this study was Schlumberger's Petrel 2015 as well as Interactive Petrophysics V4.2. All seismic analysis and interpretation was performed in Petrel 2015.1 as well as data conditioning of log files. The facies/lithological log was done in petrel using the calculator to distinguish between sand and clay in the gamma ray logs. Log files were then imported into Interactive Petrophysics for creation and displaying of log curves as well as all calculations. Logs were then exported into a suitable file format for use in petrel. Up scaling of the logs and modelling was then performed in Petrel with the IP exported files and seismic interpretations.

3.2 Seismic analysis

3.2.1 Seismic Data Loading and Quality

The seismic cube was loaded into petrel and quality controlled to ensure a good interpretation could be carried out for the horizons as well as the major faults around the well area. This was the first 3-D data acquired in block 1 of the Orange Basin and covered an area of 1500km^2 and with only 1 well A-F1 located to the northern border of the cube.

Interpretation of the data as loaded was problematic due to high levels of noise with horizons and faults difficult to identify, hence various seismic volume attributes in the Petrel software needed to be applied to aid seismic interpretation.

3.2.2 Seismic volume attributes

Various attributes can be derived from the seismic signal to highlight given properties in the seismic dataset. The attributes need to be selected carefully and often specific workflows need to be followed when using more than one attribute to ensure which is highlighted to improve seismic interpretation. Workflows can be created to generate several attributes which assists the interpreter in data conditioning before interpretation begins. The volume attributes used in the study are discussed below.

3.2.2.1 Structural Smoothing

Smoothing of the signal is an extremely valuable operation especially for horizon picking and using 2D or 3-D auto tracking. Structural smoothing performs local averaging with a Gaussian weighted average which removes noise from the data. The attribute is best used of a realized version of the cube as it often needs to be used more than once to get a good decrease in the noise ratio. In figure 3.2 below faults and even stratigraphic features become much clearer once the attribute is applied Schlumberger (2014B).

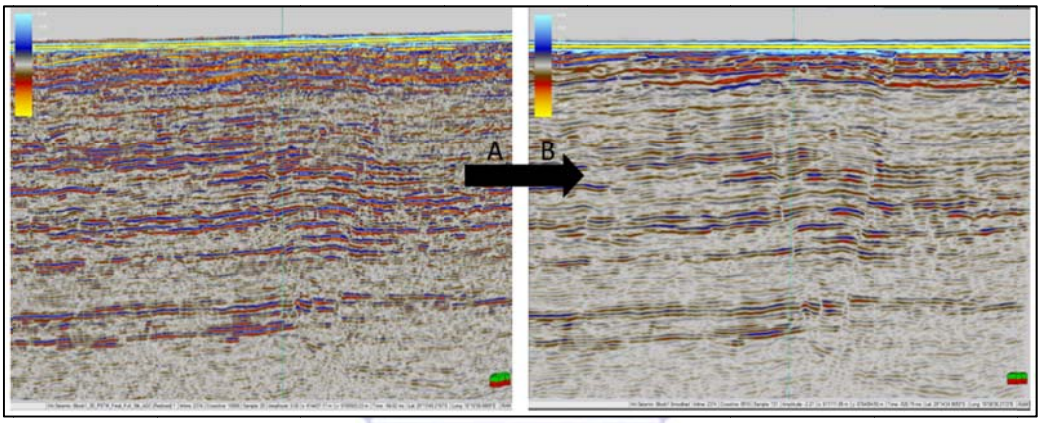

Figure 3.2: Displays original data cube (A) and structurally smoothed cube (B)

3.2.2.2 Variance

Variance, in figure 3.3, works by estimating trace to trace variances irrespective of low or high amplitude regions. It reveals discontinuities in seismic data which can discriminate between high and low continuity seismic reflection to indicate stratigraphy or structurally assist by identifying high variance and discontinuities which indicates fractures or faults Schlumberger (2014B).

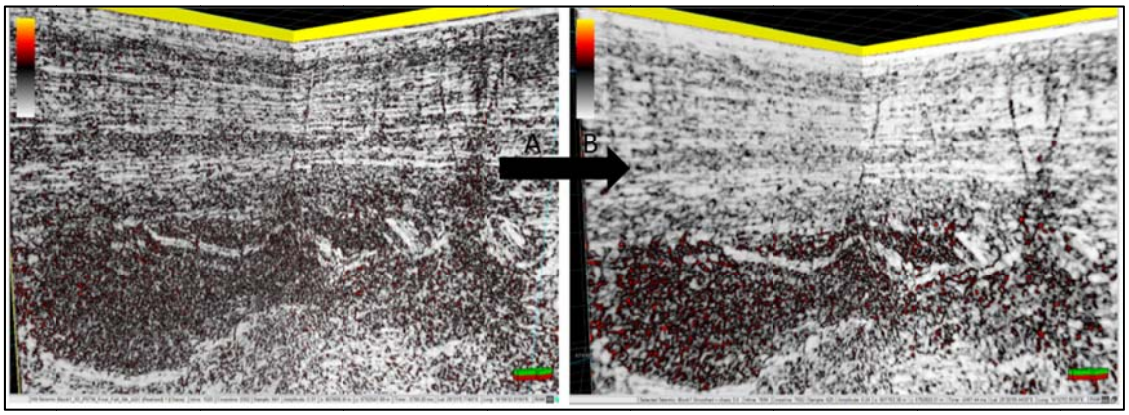

Figure 3.3: Demonstrates the importance of structural smoothing with (A) original data set with variance applied and (B) variance applied to structural smoothed data set.

3.2.2.3 Chaos

Chaos measures the lack of organization in the dip and azimuth estimation method.

Chaos is useful for mapping mainly structure by mapping the patterns of seismic signal from the statistical analysis of dip/azimuth to assist in fault and fracture identification as seen in figure 3.4, Schlumberger (2014B).

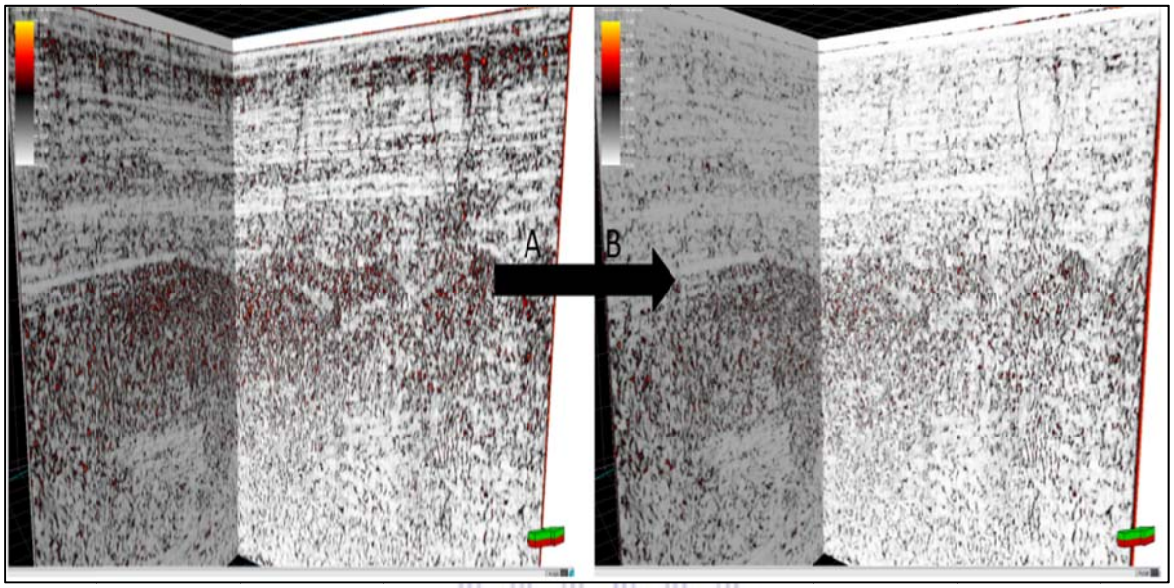

Fig 3.4: Chaos applied to (A) original data set and (B) structurally smoothed data set

3.2.2.4 Ant Tracking

Ant tracking is a patented fault enhancing attribute based on the principles of swarm intelligence. The ant tracking algorithm is cpu intensive and best tested on small cropped volumes to get the parameters set correctly. In general if unfamiliar to using this attribute, it is recommended a workflow, as per figure 3.5, be followed to generate good results to enhance stratigraphic and fault presence (Othman et al. 2016).

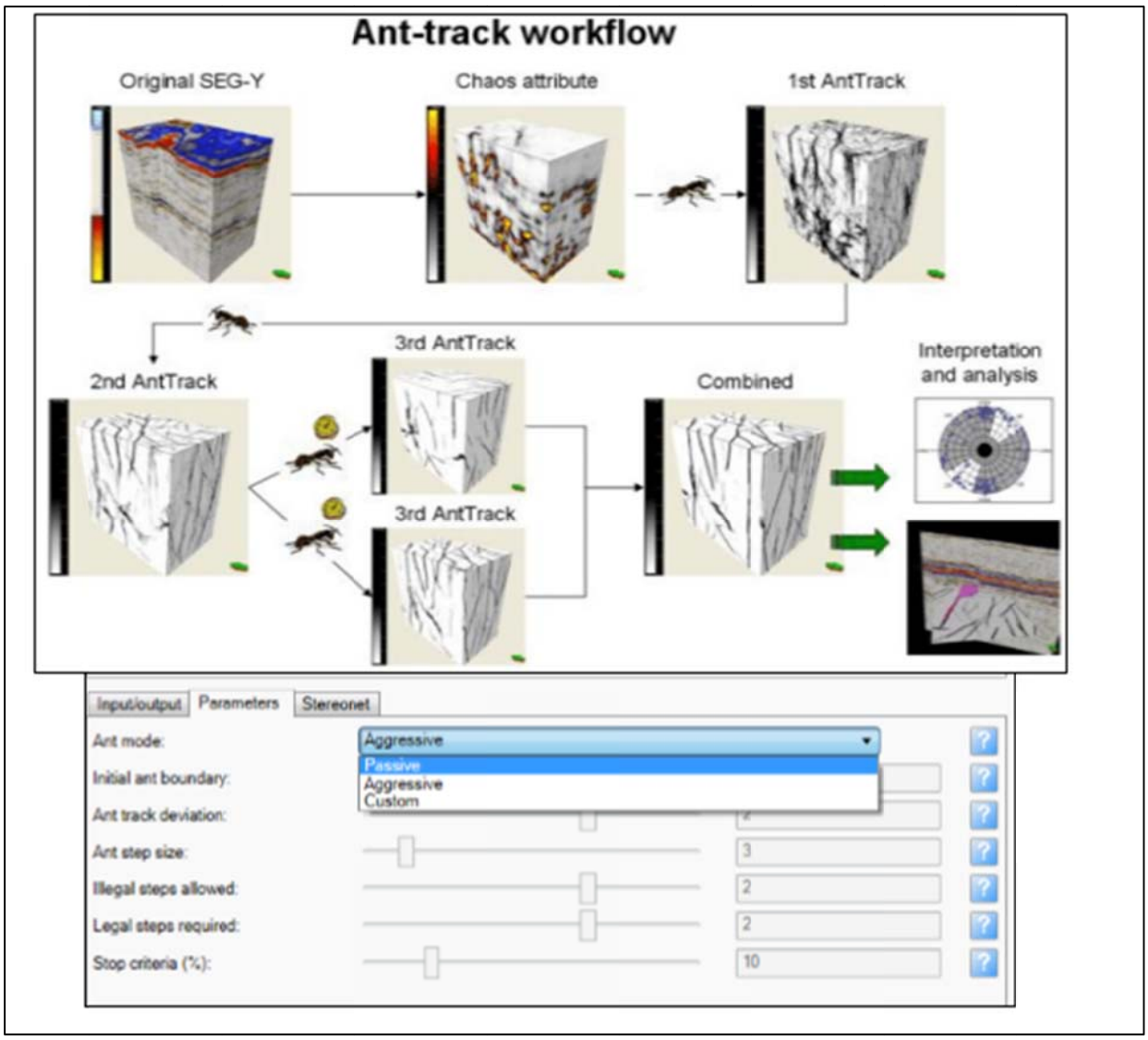

Figure 3.5: Ant tracking workflow illustrating multiple steps and settings, modified from (Othman et al. 2016).

3.2.3 Seismic well tie and time-depth relationship

Seismic well tie, involves the creation of the time depth relationship. This is crucial for the accuracy of interpretations and eventual modelling. The seismic data needs to be positioned in the correct depth as can be seen in figure 3.6 with check shots aligning with well tops. This is achieved using checkshot data as this represents a direct measurement of travel time between the surface and any given depth. The sonic log is calibrated with the checkshot data and any discrepancy between the two logs can indicate a drift in the sonic log. The time depth curve of both logs was evaluated and residual drift in the sonic log corrected. A synthetic seismogram was then generated and checked against the seismic trace to adjust the seismic surface for shift and check alignment of well tops.

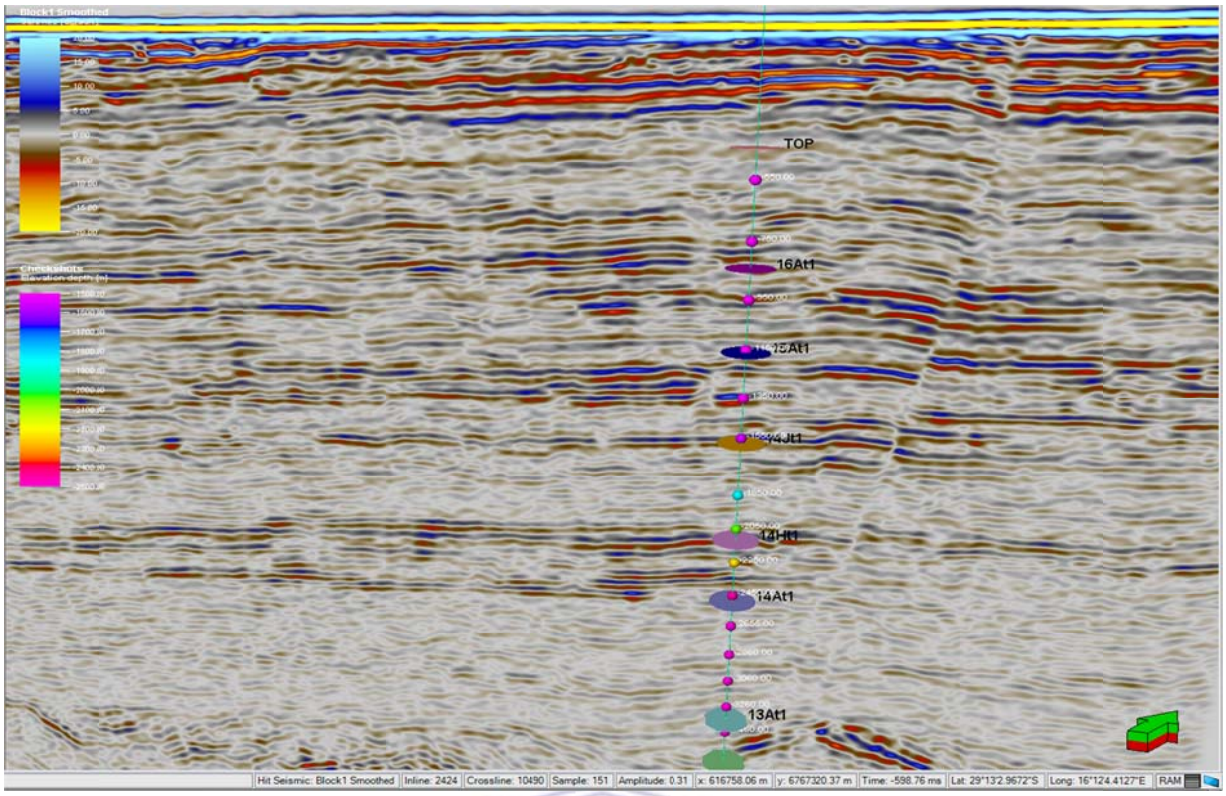

Figure 3.6: Displays check shots and well tops along the well trace in the X-Line.

3.2.3.1 Synthetic Seismogram and Wavelet Generation

Synthetic seismograms are the links between the well depth data and the seismic in time. To generate a synthetic seismogram the following steps are require; time convert well with checkshot or sonic log for a time-depth relationship (TDR) (Appendix A - 09), calculate acoustic impedance from density or sonic logs, generate a wavelet and then generate the synthetic seismogram from using the log, seismic wavelet and calculated acoustic impedance and reflection coefficients (Schlumberger, 2014).

3.2.4 Horizon Interpretation

Horizon interpretation in figure 3.7 was achieved using a combination of manual and 3-D auto tracking. Manual interpretation was used in low amplitude areas with 3-D auto tracking for high amplitudes, which allowed for horizon mapping outwards in all directions from the seed points.

Noise in the seismic signal disrupts the auto tracking procedure by creating false horizon seed points. Structural smoothing of the data greatly assisted in easing the interpretation in the inline and crossline of the seismic data cube. Horizon interpretation is a crucial step and care needs to be taken as the bulk of the seismic analysis workload is in this section. Horizons once interpreted are ready to be converted to surfaces.

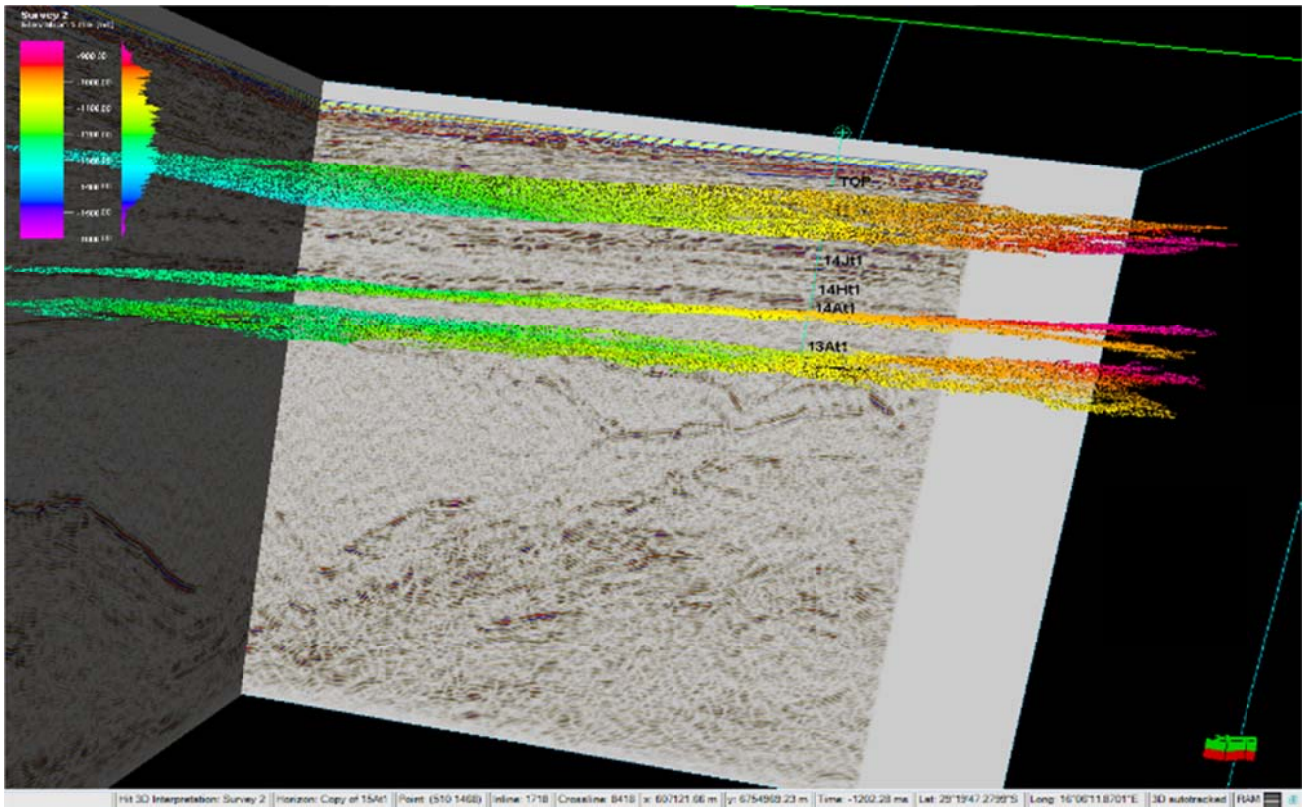

Figure 3.7: Displays horizons tracked and interpreted in the seismic cube.

3.2.5 Fault Interpretation

Faults were interpreted on the inline and cross line manually as fault sticks and can clearly be seen in figure 3.7. Auto-tracking of faults is normally used for this function and then scrutinised, however due to the noise and the decision to only interpret faults near the well it was decided the manual method would be best in conjunction with the ant tracking attribute and chaos attribute. A clean faults operation in the software was performed on the fault interpretation to ensure one directional sticks based on dip and azimuth to ensure smooth operation when building the structural framework as seen in the figure below (Schlumberger, 2011). Faults are now prepared to proceed to the domain conversion process.

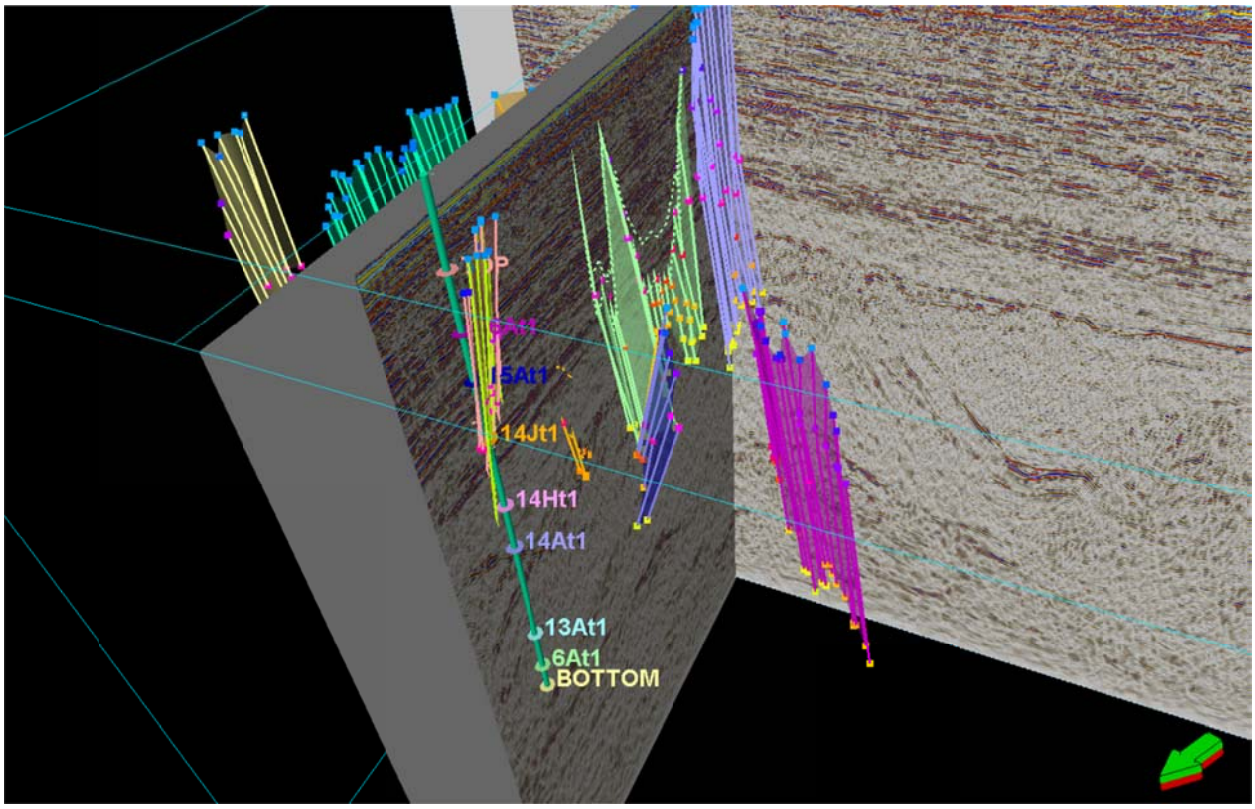

Figure 3.8: Fault sticks interpreted in the seismic cube in close proximity to well area.

3.2.6 Surface Creation

Stratigraphic surfaces need to be created from the horizons modelled to give high quality surfaces associated with the seismic data. These surfaces are gridded using the horizons as inputs and setting a boundary polygon to demarcate the surface area to be created. Surfaces are rough initially (figure 3.9 – Unaltered) but were smoothed using the smooth operation to improve the surface as the horizons when converted to surfaces have spikes from the interpretation section. Surfaces (figure 3.9 – Smoothed) are now prepared for domain conversion.

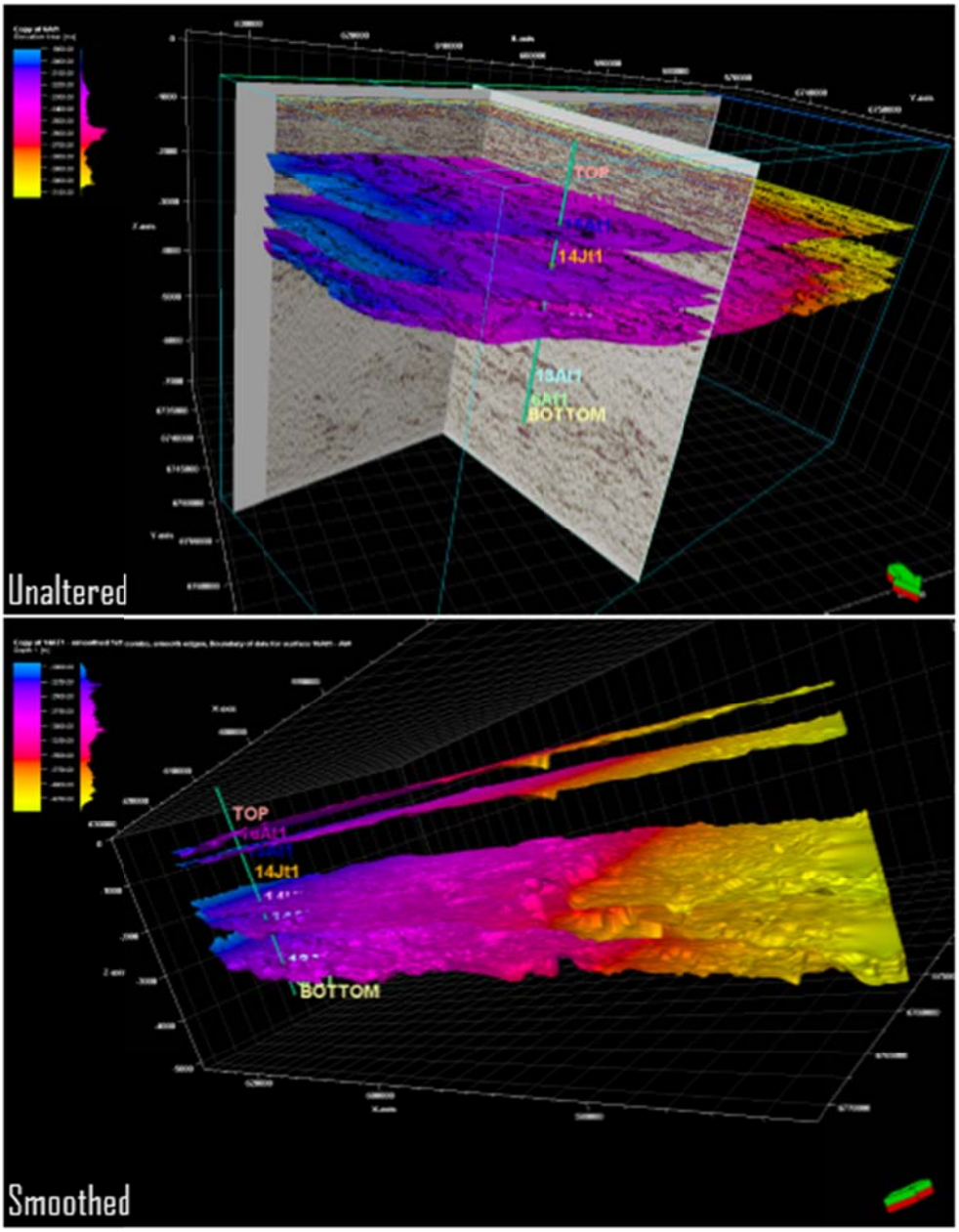

Figure 3.9: Surfaces as created from interpreted horizons, un-smoothed (above) and smoothed (below).

3.3 Petrophysical Analysis

3.3.1 Conventional Core analysis

Conventional core analysis involves the sampling of cores from specific zones of interest and have cores analysed to give information regarding target zones which are generally the reservoirs. Measurements of porosity, permeability and water gas and oil saturation is done to give indication of the presence of porosity and if the reservoirs contain and hydrocarbon in oil or gas form and if there is a permeability system to allow for the production of these hydrocarbons if present (Opuwari, 2010).

3.3.2 Log Data Quality Control

Log data loading was performed in Petrel in the well section window and viewed. The .las files contained multiple petrophysical logs of the same log type indicating tools had been run multiple times over different depths of the same borehole. Logs were arranged and checked for completeness and in most cases log splicing and despiking performed.

3.3.2.1 Log Splicing

Log splicing needs to be performed when multiple logs have been run and these need to be combined into one continuous log data set which can be viewed over the largest area of the well or specifically over the area of interest. Logs traces in track 2 and track 5 in figure 3.10 have been spliced to give the full log trace in track 1.

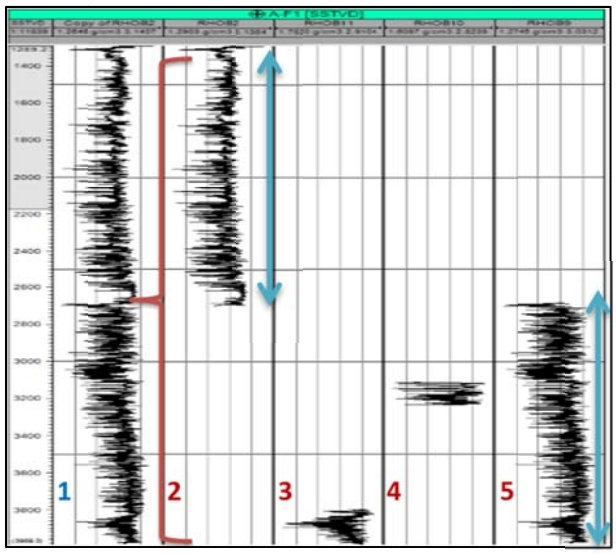

Figure 3.10: Logs in track 2 and track 5 were spliced to create the complete log in track 1.

3.3.2.2 Log De-spiking

Log de-spiking involves the removal of data spikes on the log curve. The spike can be attributed to a number of reasons but can included electrical noise from motors, other logging tools causing interference in a multi-log tool or electrical contacts touching the casing and even human error. Logs were manually de-spiked to avoid unnecessary alteration of the dataset by algorithms. In figure 3.11 is an example of spikes which were manually removed for this study.

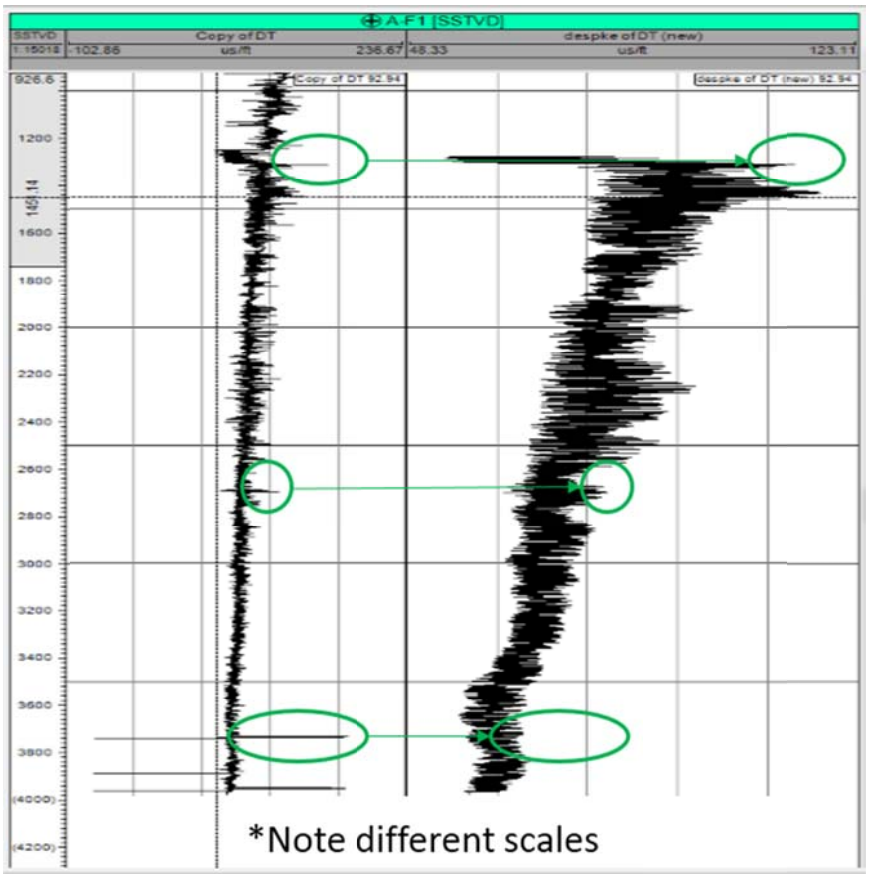

Figure 3.11 Original sonic log (left) and the manually despiked sonic log (right) with green circles displaying the exact same points in the log where the spike/s have been removed.

3.3.2.3 Environmental corrections

During logging, porosity and resistivity cannot be measured accurately due to factors affecting the response of the tool. It is affected by the hole size, mud weight bed thickness and depth of invasion and other factors in the logging environment and in the actual formation. These factors need to be accounted for and corrected before the evaluation of the logs can occur (Mustafa, 2012).

3.3.3 Log Interpretation

3.3.3.1 Identification of Lithology and Reservoirs

Using the gamma ray log as a guide, lithology and potential reservoir zones in the correct stratigraphic position can be recognized. A baseline needs to be identified using the gamma ray histogram plot. Maximum deflection to the left from the baseline indicates clean sandstone and maximum deflection to the right from the baseline indicates shale as in figure 3.12. Reservoirs are identified as thick sandstone units located between two impermeable shale sections.

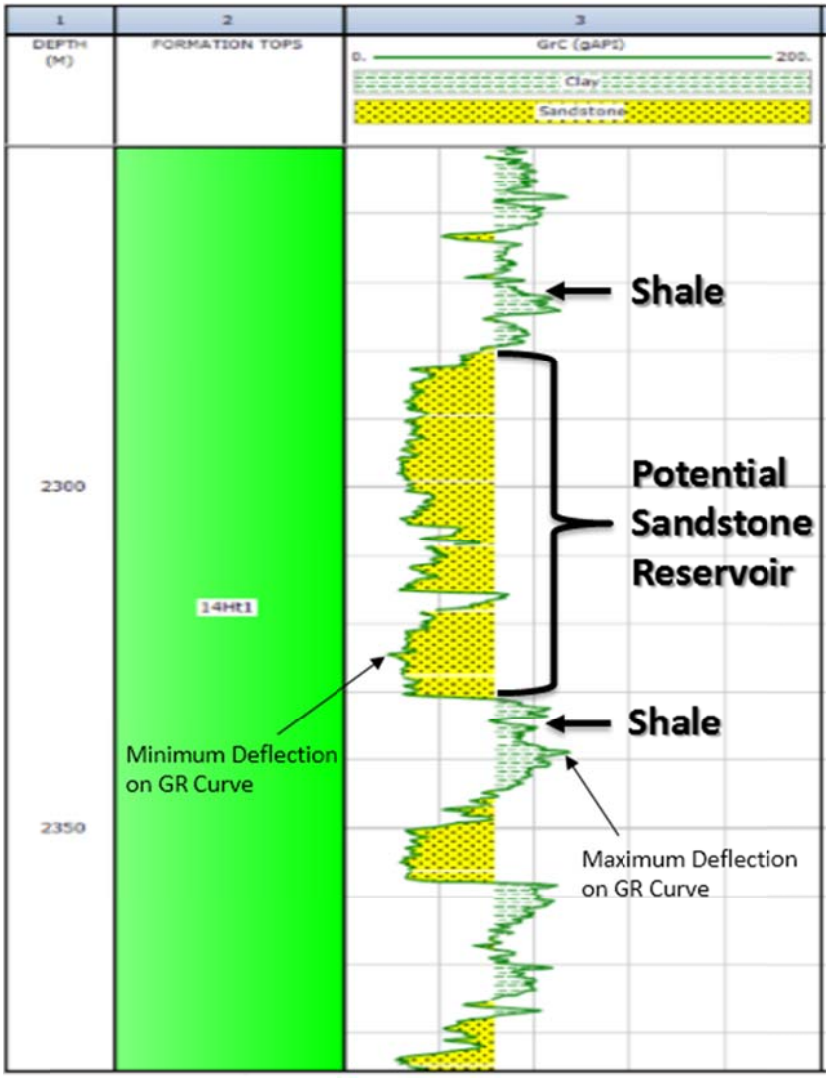

Figure 3.12: Log curve for gamma ray with shading indicating potential sandstone reservoirs and illustrating the maximum and minimum deflection.

3.3.3.2 Determining fluid saturation parameters from standalone picket plots

To determine tortuosity factor (a), cementation factor (m), water saturation (Sw) and formation water resistivity (Rw), a picket plot is used to plot porosity and against resistivity in water bearing intervals. Figure 3.13 below represent a typical picket plot for water saturation at 100% (dark blue line), 50% (light blue line), 30% (yellow line) and 15% (red line).

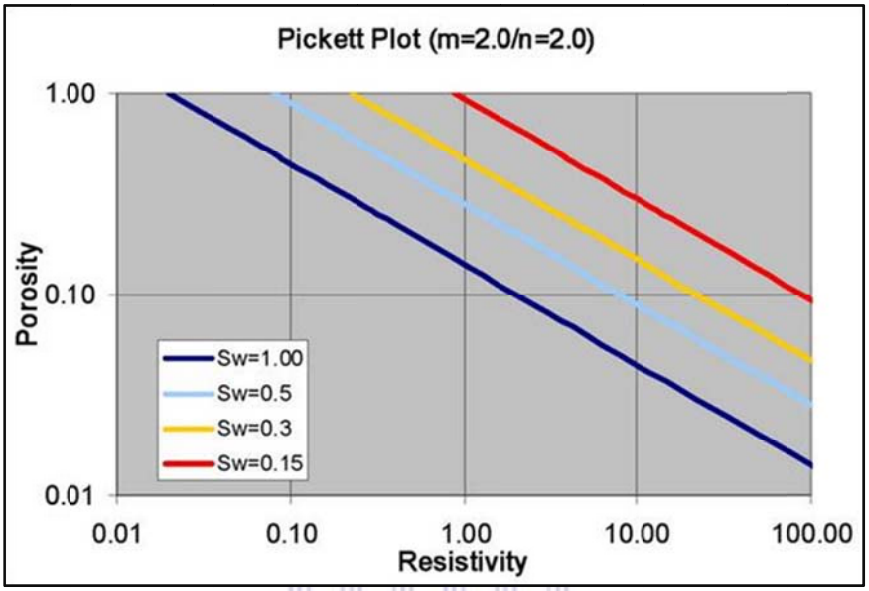

Figure 3.13: A typical water saturation picket plot with percentage lines (Crain, E.R. 2015c).

3.3.3.2.1 Fluid saturation parameters

Fluid saturation factors are discussed in the section below. These parameters each affect water saturation calculation and can deviate from the standard assumed values. In many cases the initial fluid saturation in unknown or incorrectly calculated and can result in miscalculation of reserves or the incorrect identification of pay zones resulting in loss of reserves (Bennion et al., 1996).

3.3.3.2.2 Water Saturation Exponent Value (n)

The water saturation exponent value can vary from formation to formation as it is a function of both pore framework geometry and formation wettability. A value of 2.0 is generally used, but due to the varying nature of formations this can result in overestimation and underestimation of water saturation. Increasing the (n) value increases water saturation and vice versa. Due to its influence on water saturation accurate determination of this value is important (Bennion et al., 1996).

3.3.3.2.3 Tortuosity factor (a)

According to Serra (1984), tortuosity is the crookedness of the pore pattern and is greatly affected by rock texture and structure, therefore the porosity and all factors affecting porosity, permeability and saturation. As per (Glover, 2002), permeability is highly dependent on tortuosity and tortuosity is controlled by a number of factors which include, grain size, grain shape, sorting, orientation, packing, cementation, fracture connectivity, clay content, bedding and diagenesis. Tortuosity is greatly affected by compaction, with compacted sands having a value of 1.0 and as low as 0.62 for poorly consolidated sands but with extreme compaction the value can exceed 1.0 (Bennion et al., 1996).

3.3.3.2.4 Cementation exponent (m)

The cementation factor is usually defined as 2.0 but this can vary depending on the degree on cementation as poorly cemented rocks can be less than 2.0 with highly cemented rock giving values as high as 3.0. Low cementation values result in a reduction in water saturation with higher cementation values increasing water saturation. Water saturation values can double if the cementation factor increases from 1.0 to 2.0 and the value can double again if the (m) is increases to 3.0.

3.3.3.2.5 Formation water resistivity (R_w)

Formation water resistivity is a critical exponent as the ionic composition of water affects the overall resistivity measured and hence will greatly affect the calculation of water saturation. When salts dissolve, Na, Cl, Mg, SO_4, K, Ca and other ions are released from their bonds and create conductive pathways (Crain, 2015b).

Pure water has near infinite resistivity, fresh water will report high resistivity readings and will decrease with salinity where highly saline brines which are very electrically conductive will give low resistivity measurements (Bennion et al., 1996).

3.3.3 Petrophysical Log Calculations

3.3.3.1 Conventional core analysis

Ground truthing of log data is critical to establish accuracy of any data collected using wireline logging tools. This determination of accuracy of formation evaluation is done via core analysis which involves the physical sampling of cores in the form of sidewall coring, conventional coring, plugs or cuttings from the formation and stored in its preserved state. Preserved cores are sent to the laboratory for routine core analysis to determine factors which include, porosity, permeability, fluid saturation (water, oil, gas) and grain density etc., (Opuwari, 2010).

3.3.3.2 Volume of Shale Determination and Cut-off

Due to shale's radioactive nature, the gamma ray log can be used to calculate shale in sandy reservoirs. On the gamma ray log, there are clear deflections on the log curve for shale and sandstone. To calculate for the volume of shale (V_{sh}) the gamma ray index needs to be determined. The gamma ray log has linear and non-linear responses as per figure 3.14. The linear response equation;

$$V_{sh} = I_{GR} = \frac{GR_{log} - GR_{min}}{GR_{max} - GR_{min}}$$

was used where,

I_{GR}= Gamma-Ray Index

GR_{log} *= Gamma-ray reading (for each zone),*

GR_{min} *(clean sand) is the minimum deflection*

GR_{max} *(shale) maximum deflection value.*

The minimum and maximum values used were obtained from the gamma histogram plots (figure 3.15) and are the highest and lowest points of deflection on the gamma ray log.

Non-linear response equations include,

$V_{shale} = 0.08(2\ 3.7^{*}IGR)$ Larinov (1969) for tertiary rocks,

$V_{shale} = 0.33\ x\ (2\ 2^{*}IGR - 1)$ Larinov (1969) for older rocks,

$V_{shale} = IGR/\ (3 - 2xIGR)$ Steiber (1970)

$V_{shale} = 0.33\ x\ (2\ 2^{*}IGR - 1)$ Clavier (1971) (Saputra, 2008).

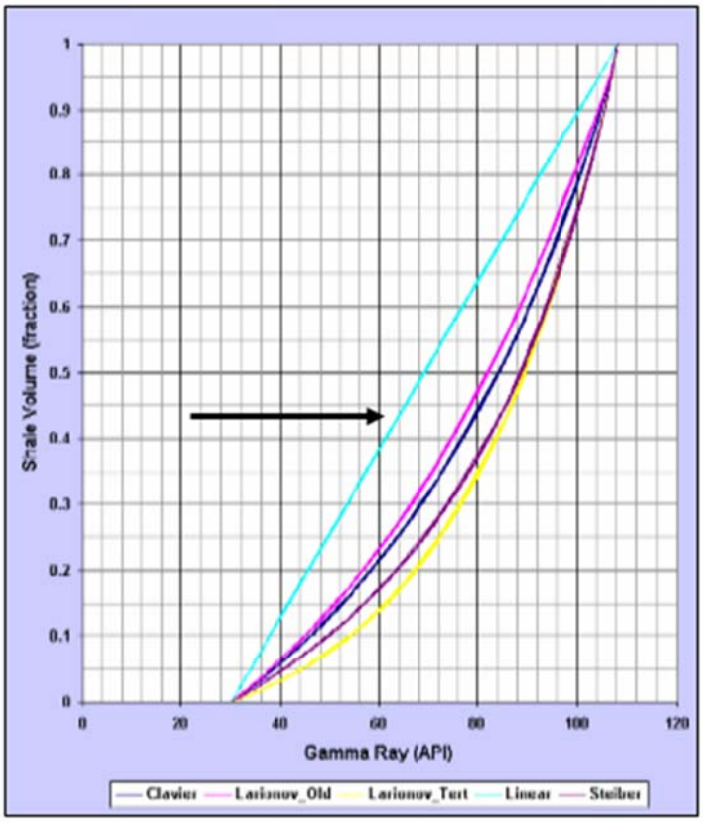

Figure 3.14: Gamma ray log displays higher linear response (black arrow) and non-linear responses (Saputra, 2008).

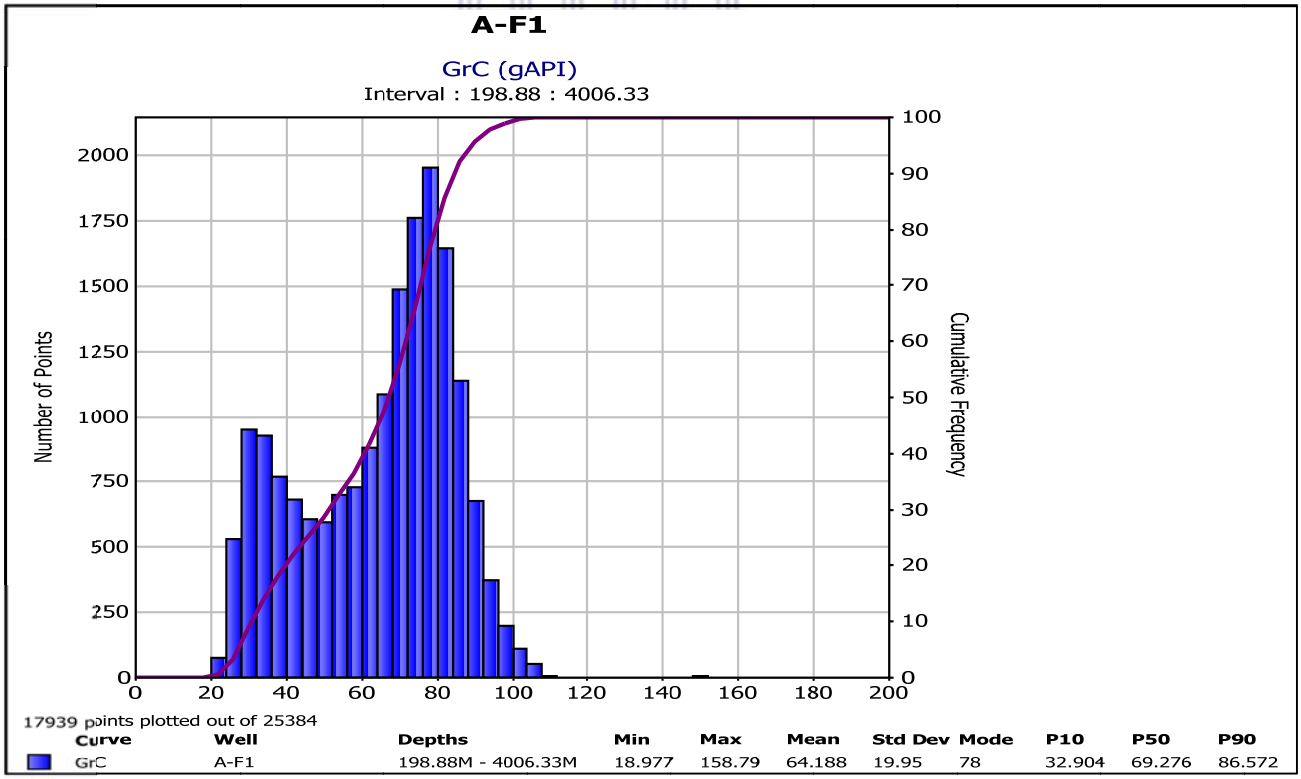

Figure 3.15: Histogram plot of gamma ray log for well A-F-1.

3.3.3.3 Core porosity

To determine core porosity, the cores once sampled are sent to a laboratory for further testing. The plugs are cleaned and pore fluids drained, porosity is determined from the grain volume and the bulk volume of the sample. For this study, the gas expansion method was used to measure the connected porosity (effective porosity), the sample is then broken down to get a grain volume and a measure of total porosity can be calculated. Petroleum reservoirs porosities range from 5-45% and is controlled by factors which affect porosity including cementation which occurs during diagenesis (Opuwari, 2010).

Other methods for measuring core porosity include, direct measurement, imbibition method, mercury injection, density methods, petrographic methods, computed tomography scanning, nuclear magnetic resonance and bulk volume measurement techniques. The gas expansion technique is based on Boyles Law for gas expansion,

$$P_1V_1 = P_2V_2 \quad \text{.....(1)}$$

If the bulk rock volume is defined as (V), volume of solids (Vs), the pore volume would be calculated using;

$$V_p = V - v_s \quad \text{.....(2)}$$

Porosity is calculated with formula;

$$\emptyset = \frac{V-Vs}{V} = \frac{Vp}{V} = \frac{Pore\ Volume}{Total\ Bulk\ Volume} \quad \text{.....(3)}$$

Any gas can be used but helium is most commonly used due to the small molecule size and its ability to penetrate small spaces. The method can be problematic in low permeability samples if enough time is not given for equilibrium to be achieved in the helium porosimeter and also time for the helium to diffuse into very small pore structures (Glover, 2002).

3.3.3.4 Porosity Determination and Cut-off

Porosity curves can be derived from various logs and their log curves. For this study porosity was derived from the sonic, density and neutron logs and plotted along with core porosity measurements on the same log track.

Three formulas were used to derive the porosity log curves as in track 4 of figure 3.16 below. These were calibrated against the measured core porosities of the core samples taken from the borehole. The sonic porosity log curve (dark blue curve) in figure 3.16 track 4, was the best fit to the trend of the core porosity data.

Using the density porosity log curve equation;

$$\emptyset = \frac{P_{ma} - P_b}{P_{ma} - P_f}$$

where,

P_b = bulk density of formation,

P_{ma} = density of rock matrix,

P_f = density of pore fluids,

to calculate porosity Ø.

The porosity f the formation can be derived from the bulk density if the mean density of the rock matrix and fluids is known. Factors which can affect bulk density measurements are oil, gas, fluid density and shale (Glover, 2002).

The neutron porosity curve can be read directly from the log for limestone formations in fresh water but needs to be corrected for other lithologies. Three effects need to be taken into account which need to be corrected for, namely hydrocarbon gas (underestimation of porosity), shale containing clays with bound water molecules (overestimation) and chlorine if present in formation fluids or mud filtrates; as chlorine is a good absorber of neutrons (overestimation). The corrected neutron porosity equation in a shaly formation would be;

$$\emptyset N_{cor} = \emptyset N_{log} - V_{sh} X \emptyset N_{sh}$$

where;

$\emptyset N_{cor}$ = corrected neutron porosity

$\emptyset N_{log}$ = neutron log reading

V_{sh} = Volume of shale

$\emptyset N_{sh}$ = neutron log of adjacent shale formation (Opuwari, 2010).

The sonic porosity log curve is mainly used to determine primary porosity as it does not react to secondary porosity features such as vugs or fractures. The Wyllie Time Average equation used for sonic porosity ($\emptyset_s$) is;

$$\emptyset_s = \frac{\Delta t - \Delta t_{ma}}{\Delta t_p - \Delta t_{ma}}$$

where,

Δt = transit time in the formation of interest

Δt_{ma} = transit time through the rock matrix

Δt_p = transit time through the pore fluids

with specific values assigned for common lithologies and pore fluids (Glover, 2002).

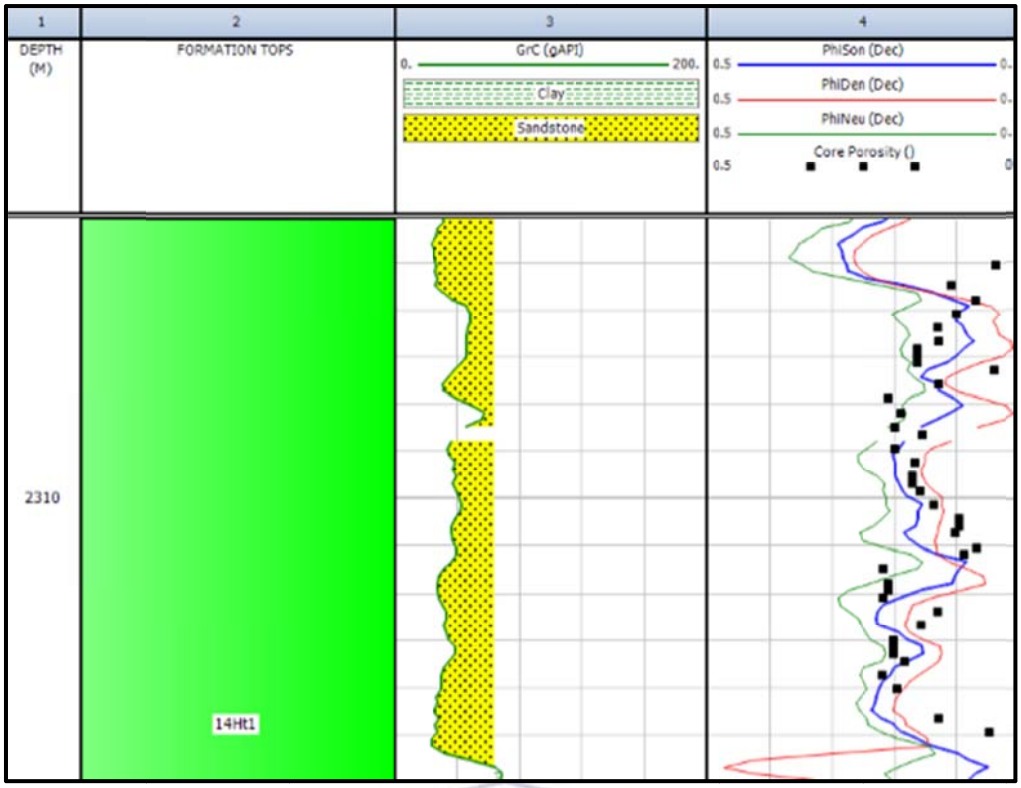

Figure 3.16: Porosity logs and core porosity points plotted in track 4 with best fit sonic porosity log (PhiSon) closest to the core porosity trend.

3.3.3.5 Water saturation Determination and Cut-off

Water saturation (Sw) models can be determined using different models which can be categorised into clean sand models and shaly sand models, each with their own specific equations.

3.3.3.5.1 Archie's Model

Archie (1942) model is specifically used for clean sands; a porous media having a non-conductive matrix (silica) as a function of the porosity and the conductivity of the saturating fluid. The model assumes the only conductive material in the formation is the electrically conductive fluid. Fluid salinity acts as the conductive path of the current through the formation and thus is not suited for formations with low salinity fluids or shaly sands.

Shaly sand models can be divided into two categories, volume of shale models and cation exchange capacity models. For this study, only two volume of shale models will be considered, Simandoux (1963) and Indonesia (1971).

3.3.3.5.2 Simandoux Model

The simandoux model equation is as below, however, there are many modified variations used;

$$Sw = aRw / 2\Phi^{m} - (V_{sh}/R_{sh} + \sqrt{(V_{sh}/R_{sh})^2 + 4/F * R_w * Rt})$$

Where;

Sw = Water Saturation

a= Equation Coefficient

Rw = Resistivity of water

Rsh = Resistivity of shale

Vsh = Volume of shale

F = Formation Resistivity factor

Rt = True formation resistivity from corrected deep resistivity log.

Φ = Effective Porosity, fraction

m= Cementation exponent

3.3.3.5.3 Indonesia Model

The Poupon-Leveaux (Indonesia) model was developed in Indonesia by field observation with field data in water bearing shaly sands. Again, there are different variations or modified versions of this equation. The equation used for the Indonesia model is;

$$1/\sqrt{Rt} = \sqrt{\Phi e^{m}/ a*Rw} + Vcl\ (^{1-Vcl/2}/\sqrt{Rcl}) * Swn^{/2}$$

Where;

Rt = Resistivity curve from deep log reading

Rcl = Resistivity of wet clay

Φe = Effective porosity

Sw= Water saturation, fraction

Vcl = Volume of shale, fraction

Rw= Formation water resistivity

m=Cementation exponent

a=Tortuosity factor

n= Saturation exponent

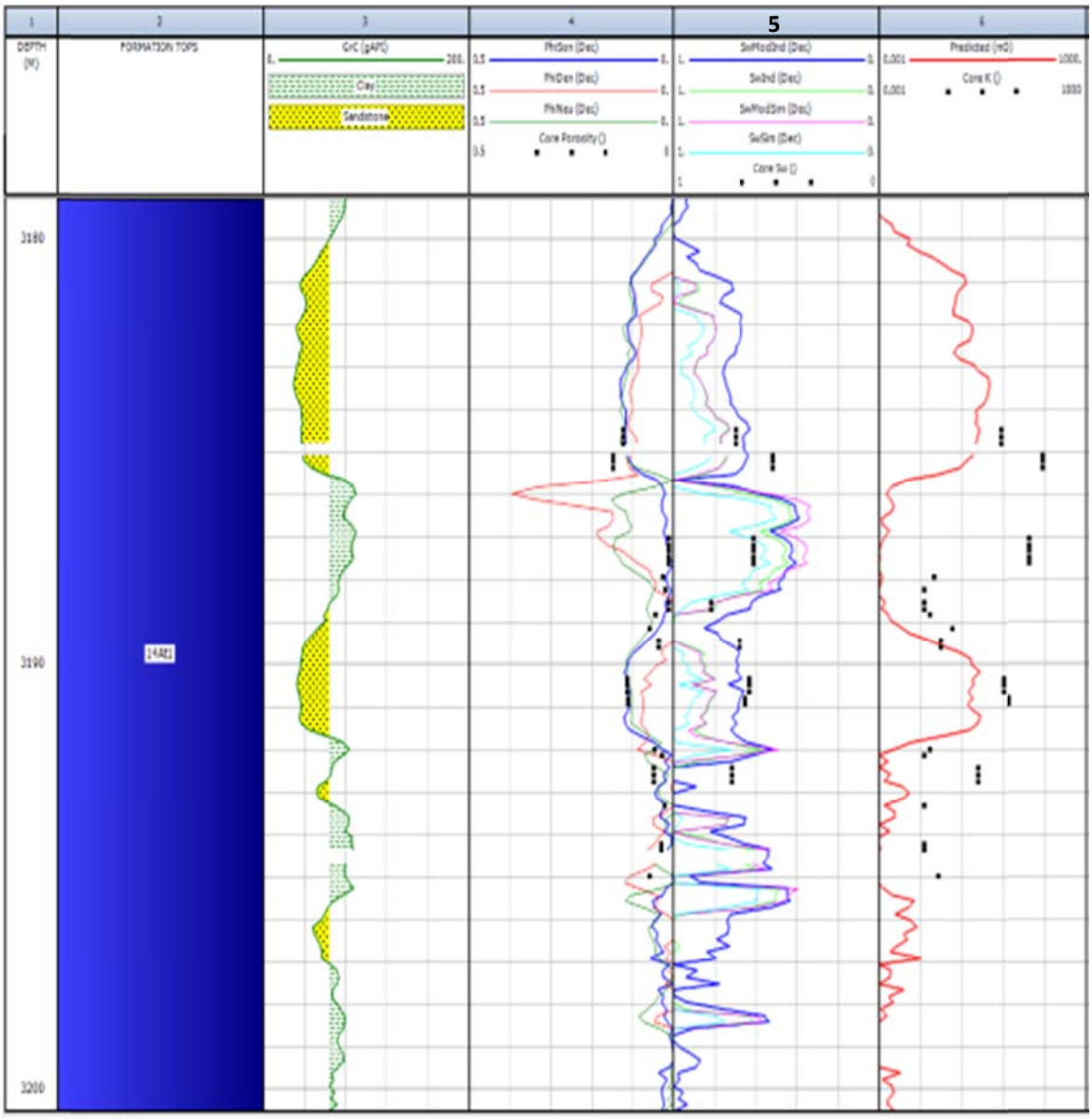

Figure 3.17: Track 5 above, displays the different Sw curves and the fit to the core porosity.

Four porosity models (curves) and lab measured core porosity (points) were plotted in track 5 in figure 3.17 above to determine best fit. These were Simandoux (light blue curve), Modified Simandoux (pink curve), Indonesia (light green curve) and Modified Indonesia (dark blue curve). Modified Indonesia represented the best fit to the measured core porosity when plotted in a water saturated zone of well A-F1.

3.3.3.6 Porosity vs Permeability Relationship

3.3.4.6.1 Core permeability

Multiple variable regressions were used to predict permeability in this study. Predicted permeability (predicted K) was estimated from the regression equation obtained from the porosity versus permeability cross plot in figure 3.19 and the function and correlation coefficient as per table 3.3. In figure 3.18 below, the porosity permeability plot relates to a mixture of crystalline cemented sandstone and clean sandstones. This agrees with the depositional history where during the drift phase, thick successions of siliciclastic sediments were deposited.

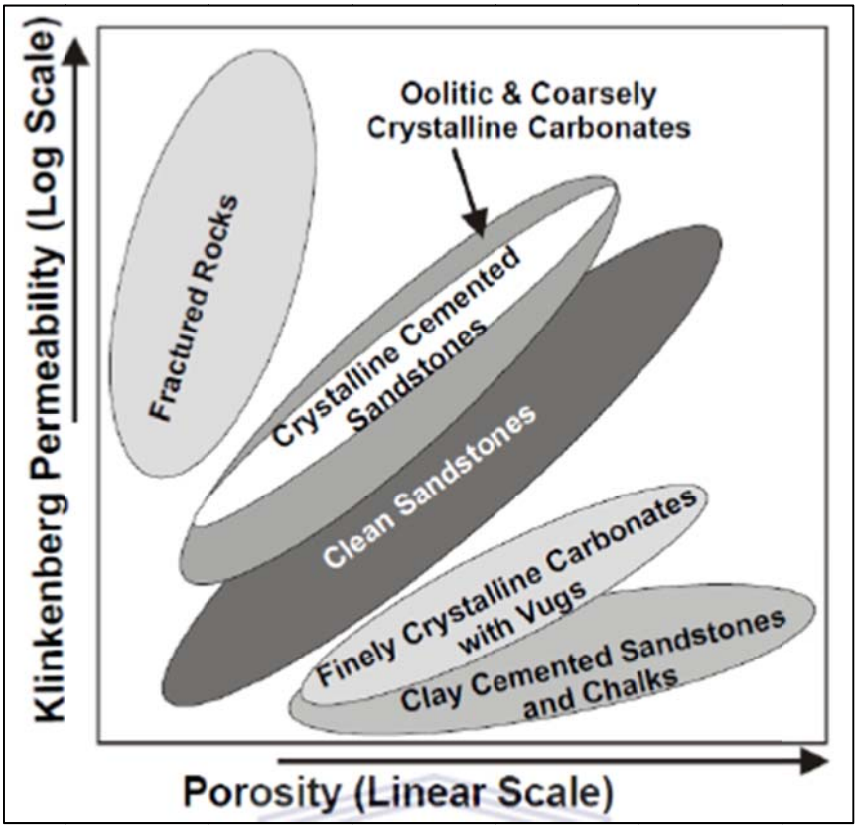

Figure 3.18: Porosity vs Permeability cross plot (Glover, 2009).

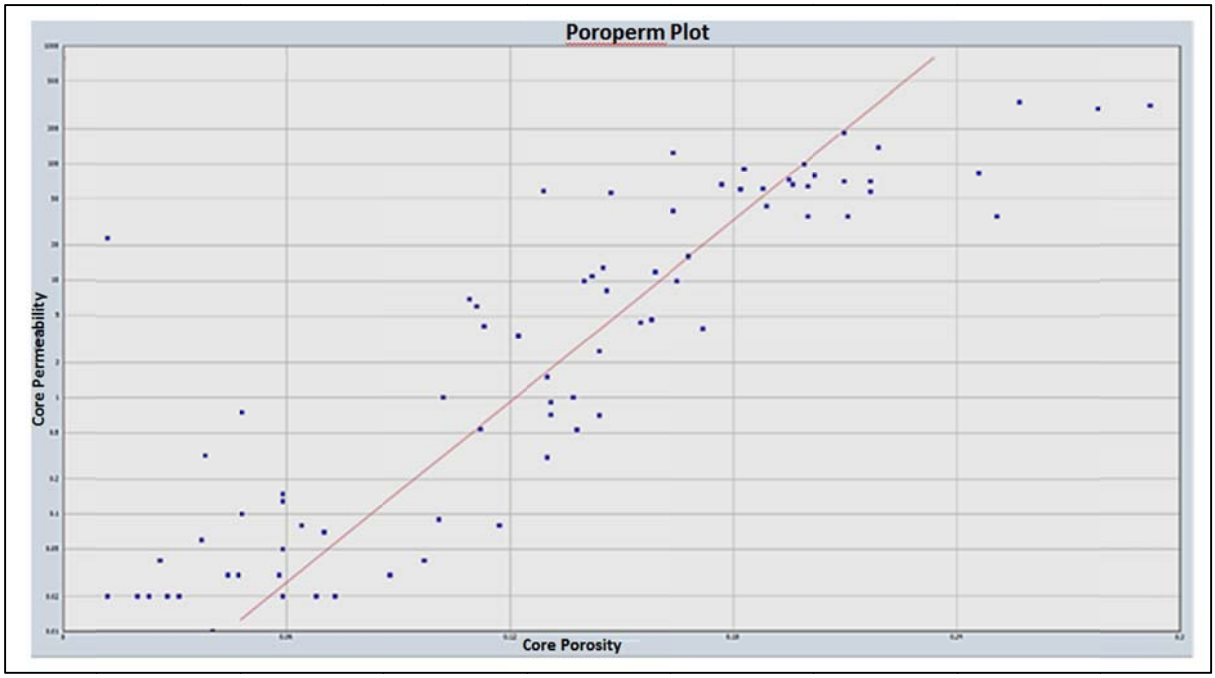

Figure 3.19: Porosity Permeability Plot for Well A-F1 (Appendix A)

Table 3.3: Established porosity-permeability functions for well from poroperm plot.

Well	Porosity-Permeability functions	Correlation Coefficient (R^2)
A-F1	Log (K) = -3.12889 +25.7792 *Core Porosity	0.913524

3.3.4.7 Net-Pay determination

The overall interval in which pay volumes occur is also referred to as the gross pay (entire thickness of the reservoir zones) and includes the reservoir interval that contains zones in which hydrocarbon can be produced and zones where hydrocarbon is not probable.

Net-pay is defined as the interval of rock or reservoir that can produce hydrocarbon in a commercially/economically accepted manner and has high storage capacity (porosity), good mobility (permeability) and good hydrocarbon saturation.

3.4 Modelling

3.4.1 Velocity Modelling

The definition of velocity model is, '*a model that describes the complete sequence of velocities and corrections in a geological section*' (Schlumberger, 2011).

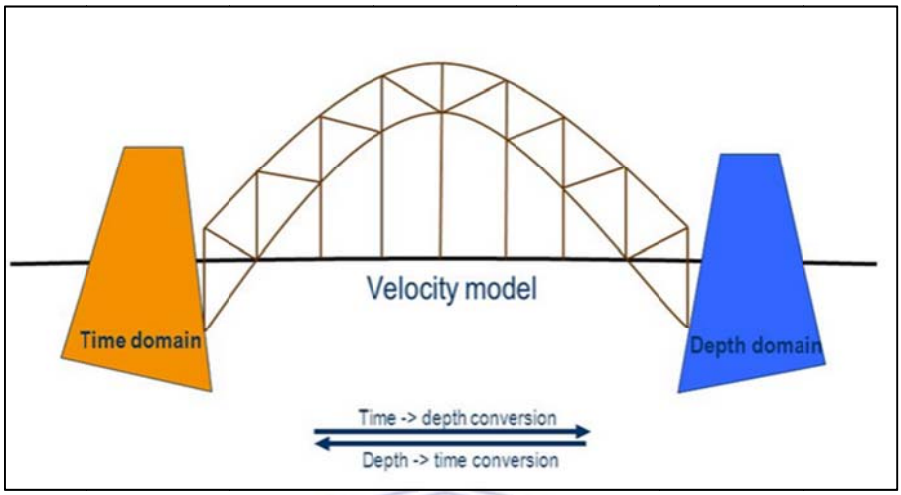

Figure 3.20: Depiction of the time and depth domain relationship, (Schlumberger, 2011).

The velocity model is the link between time to depth conversion or depth to time conversion as depicted in figure 3.20. Checkshot data is a direct means to measure the time it takes between the surface and given depth to determine the time depth relationship (TDR) at the well location. It is the ground truthing data which records the seismic source at the surface using geophones in the well borehole and is a measured travel time through the sediments (Schlumberger, 2011).

3.4.1.1 Preparation for Velocity modelling:

-Preparation of well top data - establishing confidence in well tops for TDR

-Checkshot calibration of sonic logs – conversion of sonic log to a time-depth curve, correct for drift using the checkshot time depth curve and save corrected sonic log.

- Well calibration using the correct sonic log

- Create seismic well time depth relationship (TDR)

-Estimate and correct if necessary the error/offset in time surfaces to the well tops in 3-D window

3.4.1.2 Steps in creating Velocity model

Input data required is, a set of surfaces, zone definition for velocity model, input parameters which would be a surface and data used for correction like the well tops.

An analytical velocity function needs to be selected (e.g. linear velocity function or an averaged velocity seismic cube can be used). One of two possible linear functions was used for this study which should give the same result but are associated with differing reference levels. Compaction increases with depth which increases density which in turn increases acoustic velocity. The degree of compaction can also change due to change in lithologies which will change acoustic impedance and will result in changes in the sonic velocity, which these velocity functions are used to model.

The linear velocity function used was;

$$\boldsymbol{V = V0 + K * Z}$$

Where,

V = V_{int} (instantaneous velocity)

K = Velocity gradient

V0 = reference velocity

Z = depth

Once this is completed, interval velocities need to be determined and depth errors need to be corrected using the TDR which can be the check shot data (Schlumberger, 2014).

The depth vs interval velocity chart is attached in Appendix A, item 9.

3.4.2 Domain conversion

Domain conversion is when an object is converted from one domain to another which is usually two way time to depth or vice versa if needed. Domain conversion can only be done once the velocity model has been created and can be used to among others, convert horizon interpretations, surfaces, fault interpretations, well tops, seismic data and 3-D grids. An entire 3-D model can be domain converted from two way time to depth. For this study all items were created/interpreted in two way time and then individually domain converted to depth (Schlumberger, 2014).

One needs to ensure the correct velocity model is active, in the event more than one was created, and then single object conversion can be done by converting the active velocity model. Once this has been completed successfully, the object will have two versions, one in TWT (two-way time and one in Z (depth). Another method is to do batch conversions where several objects can be converted at the same time using the 'general depth conversion tab'.

3.4.3 Modelling Framework

The 3-D grid model was built using the interpreted horizons with the top and bottom horizon being used to create the top, bottom and mid-section of the 3-D grid (figure 3.21).

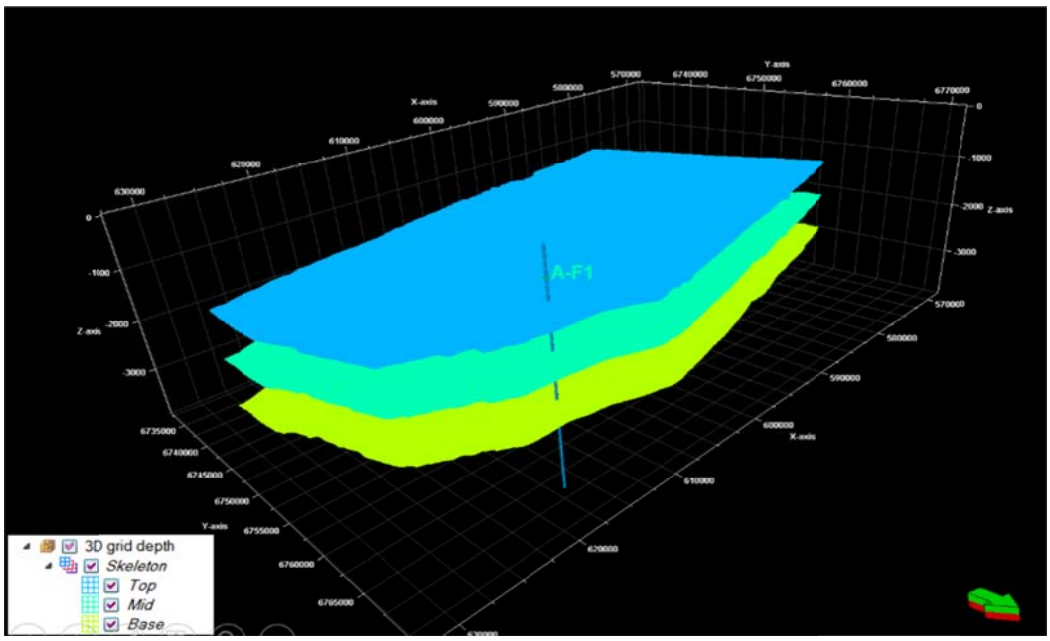

Figure 3.21: 3-D grid model constructed for population of seismic surfaces and faults.

Once the 3-D grid is created the structural grid was built and is populated with the fault interpretations and the horizon interpretations as in figure 3.22 displaying one horizon (black shaded area cutting through the faults) and the fault interpretations.

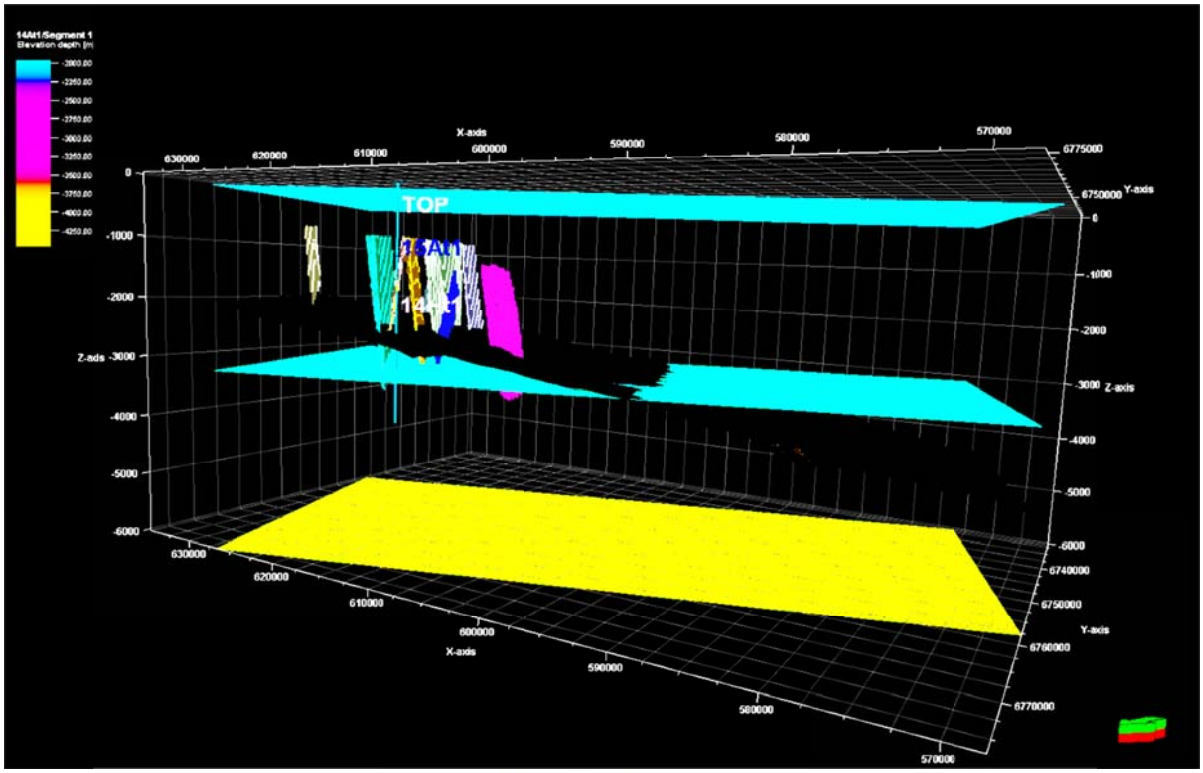

Figure 3.22: 3-D structural grid model displaying faults and one horizon in black.

Depth converted and smoothed surfaces for horizons are then are then imported into the model and edges created. In figure 3.23 the surface being displayed is 14Ht1, with the horizons above it being 15Ht1 and the top horizon not being displayed. This model with the edges and grid intersections included gives a nice stratigraphic position of the horizons in relation to position and thicknesses.

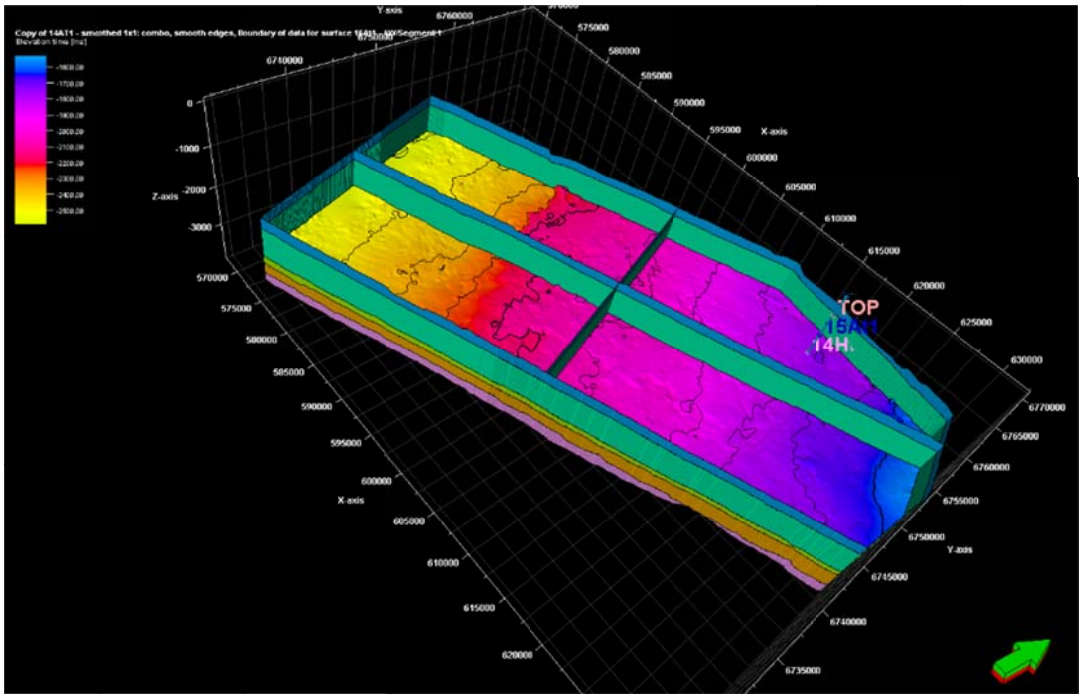

Figure 3.23: 3-D model displaying horizon 14Ht1.

Zone horizons were then created whereby the horizon thicknesses are divided into multiple zones. These zones can be selected when populating the model using the upscaled logs. In figure 3.2.4 one can clearly see all 5 zones (inset, bottom left) which have been created as well as main image displaying zones 1, 2, 3 with their respective layers.

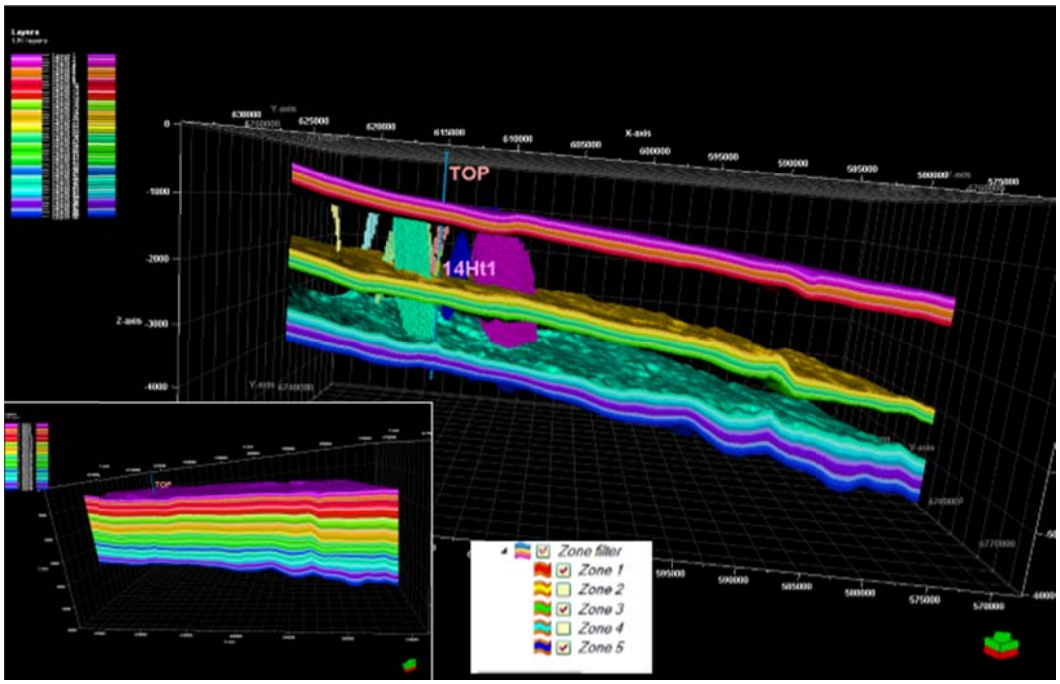

Figure 3.24: 3-D model displaying all horizon zones (inset) and 3 horizon zones (main).

The option for populating the model used for this study is to build a regions fault block model. Regions fault blocks model divides the horizon thickness into cells. These cells are then populated using variograms to stochastically model the log data. The regions fault block model in figure 3.25 displays three of the 5 regions which can be populated, with the middle region being the focus of study which is horizon 14Ht1.

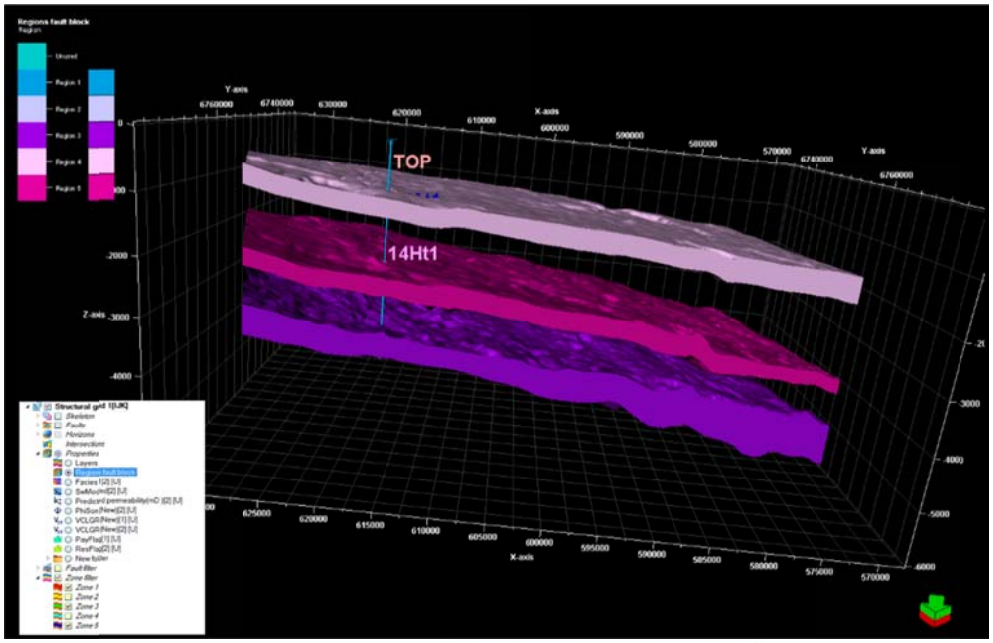

Figure 3.25: Displays 3 of the 5 regions of the regions fault block model.

3.4.5 Up scaling

Up scaling is a critical process in spatial prediction, as the only petrophysical data available is from the log data in the well bore which has to be extrapolated in all directions away from the well bore. In the up scaling process, the cells which pass thru the well trace in the seismic cube can be assigned a value from the petrophysical log traces using an algorithm. These values can then be geo-statistically modelled using stochastic or deterministic algorithms with facies being used as a bias factor.

The stochastic method was used for this study and the algorithm applies was random sequential gaussian algorithm. Sequential gaussian simulations can be made to honour the log data, the trends as well as the spatial correlation (variogram) and generate 3-D realizations. Sequential simulation uses kriged values as data and reproduces the covariance between all the simulated values (Statios, 2000).

4. Petrophysical Properties

4.1 Porosity

Total Porosity of a rock can be defined simply as the fraction of the bulk rock volume not occupied by solid matter and can be filled with gas or fluid. The fluid can be water or oil or a mixture of the two.

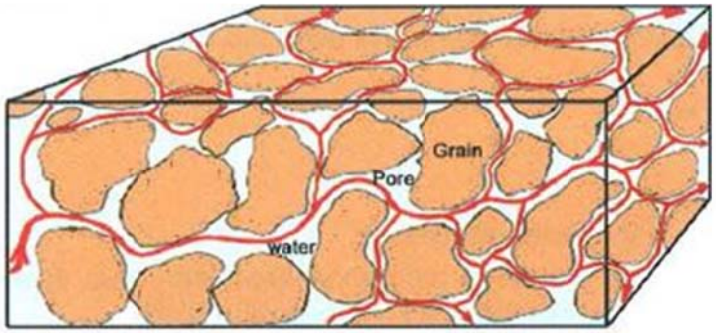

Figure 4.1: Pore space and connected pore space volume (Cogswell, 2014).

Many types of porosity exist with figure 4.1 illustrating the movement of fluids as displayed by the red lines via the connected or effective porosity. Table 4.1 defines the different types of porosities.

Table 4.1: Brief description of the types of porosity

Porosity Type	Description
Total Porosity	Ratio of bulk rock volume not occupied by solid matter
Connected Porosity	Ration of connected pore space volume to the total pore volume
Effective Porosity	The same as connected porosity as this is the "effective" porosity
Primary Porosity	Rock porosity resulting from original deposition
Secondary Porosity	Rock porosity resulting from diagenesis
Micro-Porosity	Porosity in small pores less than 2 micron in size – associated with clays
Inter-granular Porosity	Porosity present due to pore volume between grains
Intra-granular Porosity	Porosity due to voids present within the rock grains
Dissolution Porosity	Porosity resulting from dissolution of rock grains
Fracture Porosity	Porosity developing from fracturing in rocks
Vug Porosity	Porosity existing in carbonate rocks

4.1.2 Controls on Porosity

4.1.2.1 Grain Packing

Grain packing affects porosity by increasing or decreasing the pore volume space. Figure 4.2 depicts the highest theoretical porosity of 0.476 (46%) in a cubic of uniform grain size with rhombohedral packing giving a highest theoretical of 0.260 (26%). Random packing has a theoretical percentage of 0.399 (40%).

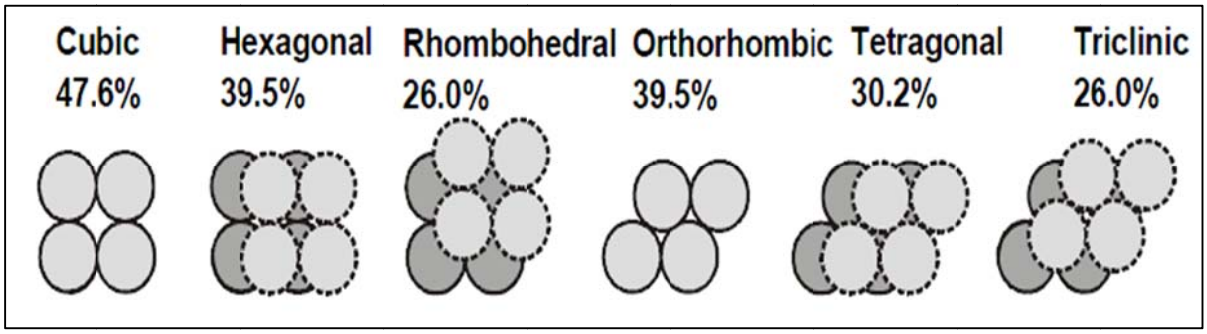

Figure 4.2: Grain packing and related porosities (Glover, 2005).

4.1.2.2 Grain Size

The effect of grain size or variations in grain size in un-compacted random packing will not decrease porosity below the known limit of 0.399. Smaller grain sizes will increase porosity due to the increase in frictional forces causing a decrease in porosity as grain size increases upwards of 100 micron.

4.1.2.3 Grain Shape

Grain shape studies have resulted in better porosities for angular and sub-spherical grains than for sphere shaped grains (Glover, 2005). The porosity scale in figure 4.3 does not take into account deformation of grains due to dissolution-recrystallization, fracturing or plastic flow. The processes which reduce porosity below the random packing porosity line (limit line) is termed compaction.

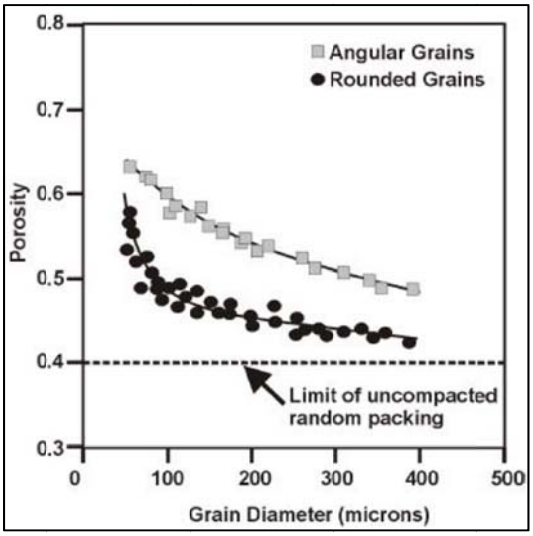

Figure 4.3: Grain Vs Porosity relationship and limit line (Glover, 2005).

4.1.2.4 Grain Size Distribution

Grain size distribution affects porosity negatively once more than one grain size is present. A mainly large grain matrix will have large interstitial spaces for smaller grains to occupy, hence reducing total porosity (Glover, 2005). A small grains matrix will have small but many interstitial pore spaces which when the volume of many small grains are replaced by a single large grain, the large grain will have essentially replaced many of the voids or potential pore spaces that were present within a uniform small grain matrix, thus, also reducing the porosity. The range of porosities can vary significantly in nature and the depositional environment and diagenesis will affect porosities. Figure 4.4 below gives a general range of expected porosities for different rock types.

Lithology	Porosity Range (%)
Unconsolidated sands	35-45
'Reservoir' Sandstones	15-35
Compact Sandstones	5-15
Shales	0-45
Clays	0-45
Massive Limestones	5-10
Vuggy Limestones	10-40
Dolomite	10-30
Chalk	5-40
Granite	<1
Basalt	<0.5
Gneiss	<2
Conglomerate	1-15

Figure 4.4: Range of porosities for various rock types (Glover, 2005).

4.2 Permeability

Permeability is a measure of ease at which a fluid will flow freely through a rocks interconnected pore space. Permeability is dependent on porosity or more specifically the effective porosity of a rock to allow for pathways for fluid to flow with the connectivity of the pore spaces influenced by grains size, grain shape, grain size distribution, capillary forces and wettability.

Generally, the higher the porosity the higher the permeability, smaller grain size reduces pore throat space which lowers permeability as well as increases surface area and frictional forces interacting between the fluid and the grains which also lowers permeability. Permeability can be measured on horizontally and vertically although the horizontal measurement as it is considered a measurement of the bedding which is the major contributor to fluid flow in a reservoir. Vertical measurements are affected by layering of beds and sedimentation and therefore generally a lower measurement.

Henri Darcy carried out laboratory experiments and developed a formula (figure 4.5), which is still valid for the oil industry today. The units of permeability is Darcy (D) but in geological applications, milidarcy (mD) is used where 100mD=1D. Fluid pressures can be calculated providing the density of the fluid is known and can be expressed as;

$$Q = \frac{k\,A\,(P_i - P_o)}{\mu\;L}$$

where:
- Q = the flow rate (cm^3/s or m^3/s)
- P_o = the outlet fluid pressure (dynes/cm^2 or Pa)
- P_i = the inlet fluid pressure (dynes/cm^2 or Pa)
- μ = the dynamic viscosity of the fluid (poise or Pa.s)
- L = the length of the tube (cm or m)
- k = the permeability of the sample (darcy or m^2)
- A = the area of the sample (cm^2 or m^2)

Figure 4.5: Darcy's Equation, modified from (Glover, 2005).

Reservoirs permeability's are classified based on a permeability value where, <10mD = Fair, 10-100mD = High, 100-1000mD Very High and >1000mD is Exceptional. Three types of permeability are used are, absolute, effective and relative permeability.

4.2.1 Relative Permeability

If a rock contains one fluid, the rock permeability is at its maximum and is termed absolute permeability. If two fluids are present, the fluid saturation of each fluid will determine the permeability of the two fluids present and are termed effective permeabilities and are always less than the absolute permeability.

Relative permeability is when the two effective permeabilities of the fluids are expressed as a fraction of the absolute permeability of the rock if either of those 2 fluids saturated the rock at 100%. Figure 4.6 below, displays how the relative permeabilities for Oil (Kro), water (Krw) and gas (Krg) would be defined.

$$K_{ro} = \frac{K_{eo}}{K} = \frac{\text{effective oil permeability}}{\text{base permeability}}$$

$$K_{rw} = \frac{K_{ew}}{K} = \frac{\text{effective water permeability}}{\text{base permeability}}$$

$$K_{rg} = \frac{K_{eg}}{K} = \frac{\text{effective gas permeability}}{\text{base permeability}}$$

Figure 4.6: Relative permeability equations, modified from (Glover, 2002)

4.3 Fluid Saturation

Fluid saturation is the fraction or percentage a fluid occupies the available pore spaces and is mathematically; 'fluid saturation = volume of fluid/total pore space' in rock. Electrical conductivity can give an indication of the fluid type or saturation of a fluid type in a rock as formation water contains salts which are conductive whereas hydrocarbons in formations are not conductive. Fluid saturation parameters have been described in chapter 3.

5. Wireline Logging

5.1 Overview

Geophysical wireline logs or well logs, is the term given to a set of geophysical parameters recorded and plotted along the depth of a borehole. Technological advancement has been swift since the first electrical logs were developed by Conrad Schlumberger and Henri Doll. These include measurements of electrical, radioactive, velocity and size. Examples of these in order would be spontaneous potential logs, gamma ray logs, sonic logs and caliper logs (Rider, 2002).

Wireline logs can be divided into 2 types, open-hole logging and cased-hole logging. Open hole logging measure the formations for electrical, nuclear and acoustic properties and are done before the well is cased. The cased hole logging involves magnetic, acoustic and nuclear properties. Various types of tools are used in wireline logging and these can also be divided into active and passive tools. Active tools measure the application of a stimuli to the formation and measures its response, i.e. an electrical signal is passed through the formation to measure conductivity of the formation. Passive tools measure an occurrence of a natural phenomenon in the formation; i.e. the radioactivity of the substrate which can be measure by the gamma ray tool and can give indication of lithology due to the presence of naturally occurring radiation from elements present in the rock.

It is also important to mention that a wireline log on its own only represents a specific set of parameter outputs from the tool. These logs are generally used in combination and analysed to give information on the condition of the area surrounding the borehole and these can include lithology, porosity and even the presence of hydrocarbons. Many factors can affect the quality of the logs, for example cable speed and the occurrence of washout and presence of mud in the invaded zone. Various logs are generally also created for these quality check parameters and should be scrutinized to evaluate the quality of all the wireline logs produce by the tools.

5.2 Wireline Logs

There are numerous wireline logging tools available and used in the process of logging. Below are table 5.1 and table 5.2, which are the logs which were available for this study with brief descriptions (Schlumberger, 2017b).

Table 5.1: Table of logs from well A-F1 dataset (classified logs).

Channel	Unit Quantity	Description	Unit of Measurement	Unit
ILD	Resistivity	Deep Induction Resistivity	ohm-meter	ohm.m
DT	Acoustic	Compressional Slowness	microsecond per meter	us/m
GR	API Gamma Ray	Gamma Ray	API gamma ray	gAPI
LLD	Resistivity	Laterolog Deep Resistivity	ohm-meter	ohm.m
ILM	Resistivity	Medium Induction Resistivity	ohm-meter	ohm.m
LLS	Resistivity	Laterolog Shallow Resistivity	ohm-meter	ohm.m
SFLU	Resistivity	SFL Resistivity	ohm-meter	ohm.m
MSFL	Resistivity	Micro-spherically-focused Resistivity	ohm-meter	ohm.m
MINV	Resistivity	Micro Inverse Resistivity	ohm-meter	ohm.m
MNOR	Resistivity	Micro Normal Resistivity	ohm-meter	ohm.m
DRHO	Density	Bulk Density Correction	gram per cubic centimetre	g/cm3
RHOB	Density	Bulk Density	gram per cubic centimetre	g/cm3
RHGX	Density	Grain Density from Cross plot Porosity		
SP	Spontaneous Potential	Spontaneous Potential	millivolt	mV
CILD	Conductivity	Calibrated Induction Deep Conductivity	millisiemens per meter	mS/m
NPHI	Porosity	Thermal Neutron Porosity	cubic meter per cubic meter	m3/m3
BS	Cylinder Diameter	Bit Size	inch	in
CAL	Cylinder Diameter	Caliper	inch	in
RCAL	Cylinder Diameter	Raw Caliper	inch	in
HD	Cylinder Diameter	Hole Diameter	inch	in
PEF	Photo Electric Effect	Photo Electric Effect	barns/electron	b/e

Table 5.2: Table of logs from well A-F1 dataset (unclassified logs).

Channel	Unit Quantity	Description	Unit of Measurement	Unit
AMPL	Electric Potential	Acoustic Amplitude	millivolt	mV
CBL	Electric Potential	Cement Bond Amplitude	millivolt	mV
CS	Velocity	Cable Speed	meter per minute	m/min
DPL	Density	Density Porosity Limestone	percent	%
FX FY FZ	Magnetic	Magnetic field strength X Axis Magnetic field strength Y Axis Magnetic field strength Z Axis	millitesla	mT
RI	Cylinder diameter	Radius of Invasion	millimetre	mm

More detailed descriptions for each log originating from the Schlumberger Curve Mnemonic Online Dictionary (Schlumberger, 2017a) are attached in the Appendix.

5.3 Wireline Log Tools

5.3.1 Nuclear Logs

Radioactivity is a fundamental property of all matter and radioactive logging tools measure the natural occurring radiation generated by the formation as with gamma ray logs, or the response to radiation generated by the tool as with neutron, density and litho-density logs (Glover, 2002).

5.3.1.1 Gamma Ray Log (GR)

Gamma ray logs measure the natural radioactive decay of potassium, thorium and uranium which are naturally occurring and concentrated in shales in sandstone reservoirs. Measuring the response in API (American Petroleum Institute), the gamma ray tool is able to areas of reservoirs which are clean sand, shaly sand and shale. The response for clean sand is 15-45 API with shale able to measure from 75-90 API with shaly sand siting in between these measurement boundaries. These measurements are scale dependant but usually 0-100API and 0-150 API are the chosen standards. The gamma ray log can be used for well to well correlation, identify bed boundaries; identify reservoir and non-reservoir formations and the volume of shale. A measure and corrected gamma ray plot is shown in figure5.1 below.

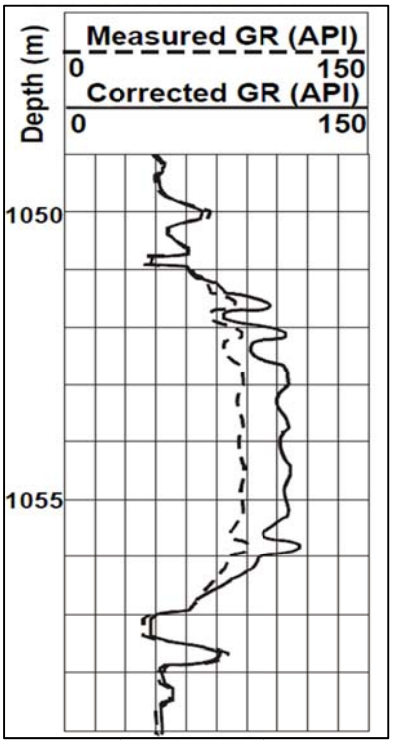

Figure 5.1: Gamma ray and corrected gamma ray log curves, modified from (Glover, 2005)

5.3.2Density Logs

5.3.2.1 Formation/Bulk Density Log (RHOB)

The density log measures the bulk density of a volume and this includes both the bulk material and any pore spaces and their content. It is useful for the determination of porosity as well as lithology and gas identification when the latter two are combined with the neutron tool. Typical values for density have been recorded, and are useful in determining lithology.

It is important to note that sandstones, limestones and dolomites all have bulk density ranges that overlap each other and that of shales as seen in figure 5.2 (Glover, 2005).

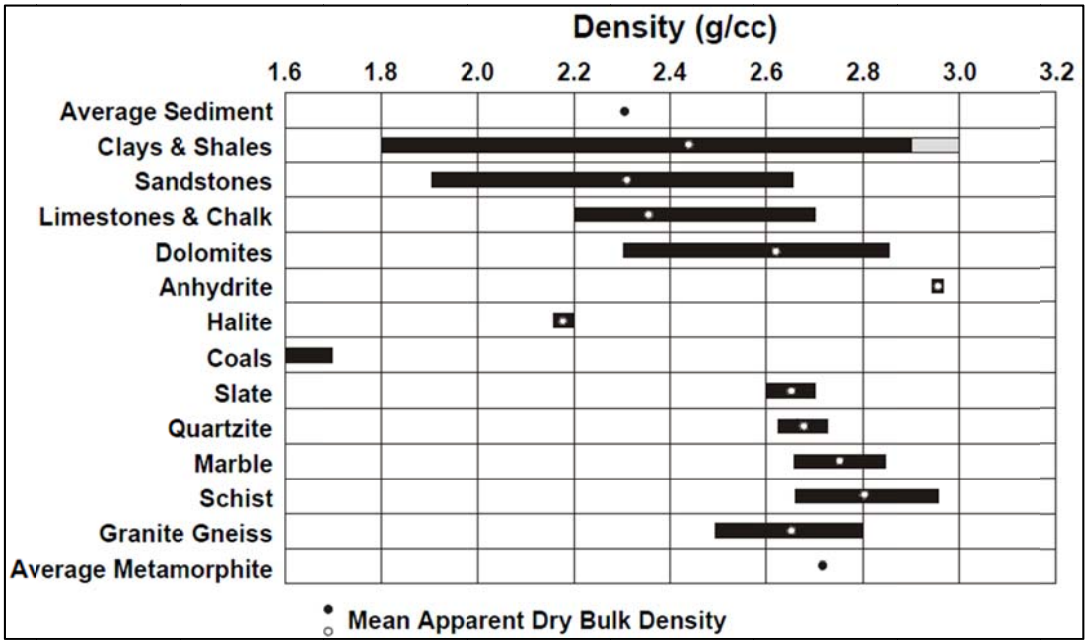

Figure 5.2: Density ranges of common lithologies modified from (Glover, 2005).

The porosity of a formation can be determined from the bulk density if the density of the rock matrix and fluid it contains is known using the following equation,

$$\emptyset = \frac{P_{ma} - P_b}{P_{ma} - P_f}$$

Where,
$\emptyset$ = porosity
P_{ma} =matrix density
P_b =density from log
P_f = fluid density of the mud filtrate

5.3.2.2 Acoustic/Sonic Log

The sonic log measures the travel time of a compressional wave through a formation at a set interval distance. The tool measures the time it takes for a wave to travel from the transmitter to the receivers after passing through the formation. Figure 5.3 shows an example of a single transmitter and dual receiver setup, which are both mounted on the tool. The travel time is affected by the rock type and compaction in the formation and measures the time taken for the acoustic signal to pass through the rock and can measure the attenuated amplitude of the signal to give information on the specific formation.

The information is useful for calibration of seismic data sets i.e. seismic ties for time-depth conversions, creation of synthetic seismograms, determination of porosity, identification of lithologies, stratigraphic correlation, identification of compacted areas as well as identification of source rocks.

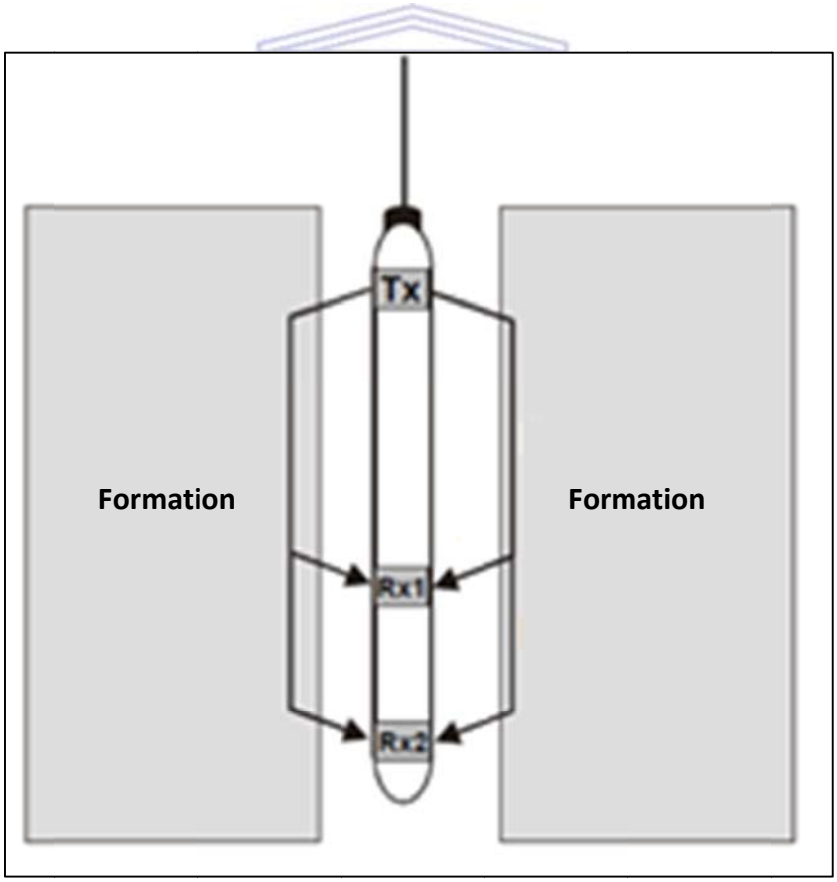

Figure 5.3: Sonic tool setup of a single transmitter (Tx) and dual receiver (Rx1; Rx2) (Glover, 2005).

5.3.3 Electrical Logs

Electrical logs were the first logs developed and essentially measure two electrical properties, potential and resistivity. Improvements in these logs have now included the use of electromagnetic coupling and induced alternating current which have produced different types of resistivity logs.

Electrical logs are useful in determining lithology, facies, correlation, overpressure, compaction , shale porosity and importantly, water saturation of a reservoir and hence STOOIP which is the stock tank original oil-in-place and refers to the original volume of oil in place before commencement of production.

5.3.3.1 Spontaneous Potential (SP)

The spontaneous potential log measure the spontaneous potential difference between and electrode in the borehole and another electrode at the surface. The spontaneous potential currents are created when two fluids with different salinities come into contact; in this case, the difference is the salinity of the borehole fluid/mud filtrate and the formation fluid/water. SP logs are useful to determine, permeable and impermeable formations as per figure 5.4, formation water resistivity, where shale is present in a formation and correlation. It is generally used in combination with the gamma ray log.

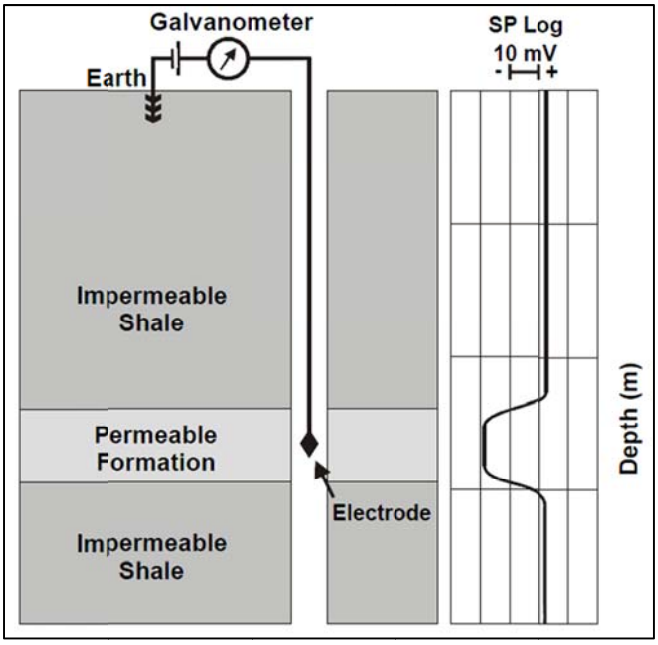

Figure 5.4: SP tool setup with an electrode at the surface and down the borehole (Glover, 2005).

5.3.4 Neutron Logs

Neutron logs are a good indicator of porosity and well as the presence of water in the formation due to its sensitivity to hydrogen atoms in a formation. The neutron tool emits high energy neutrons from it source from its source with is a reaction between either one source of alpha radiation ; radium, plutonium or americium reacting with beryllium-9 creating carbon -12 fast neutron and gamma rays. These fast neutrons when colliding with hydrogen nuclei lose energy much more efficiently due to the same particle sizes. The nuclei of silica and oxygen are larger and do not lose energy as efficiently when the collision occurs. The log hence relates to a formations hydrogen index which is an indication of the presence and volume formation water present and therefore relates directly to porosity if the solid minerals of the formation contain no hydrogen and if the pores are completely saturated with water.

5.3.4.1 Sidewall Neutron Porosity Tool (SNP)

The SNP too is designed to be used in open holes with the tool pressed against the sidewall of the borehole. The tool is not affected by the drilling mud, mud cake, chlorine in high salinity muds or formation fluids. The measurements are however affected by rough holes which can cause alignment issues with the source or detector and could cause erroneous readings.

5.3.4.2 Compensated Neutron Log tool (CNL)

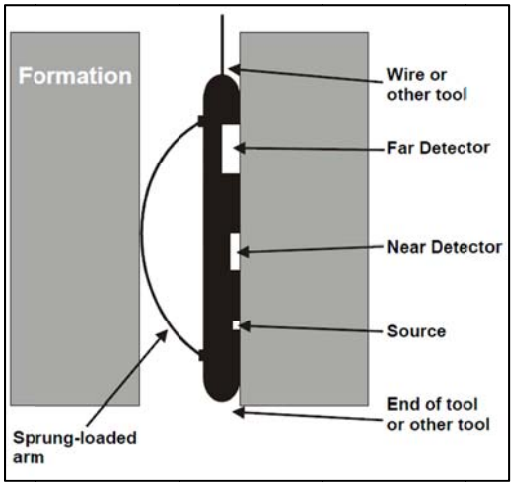

Figure 5.5: Example of CNL tool used by Schlumberger (Glover, 2005).

The CNL tool has a very strong neutron source ensuring the count rates are sufficient to negate any significant statistical errors due to fluctuations. The stronger source also allows for a deeper investigation of the formation and also allows for operation in cased holes. Drawbacks of the tool are that it is designed to be sensitive to thermal neutrons and is affected by the presence of chlorine in the formation fluids. Another drawback is its design in that it is pressed along the side of the borehole as in figure 5.5 and therefore only measures one side but is unaffected by the drilling mud. Figure 5.6 displays a typical CNL log.

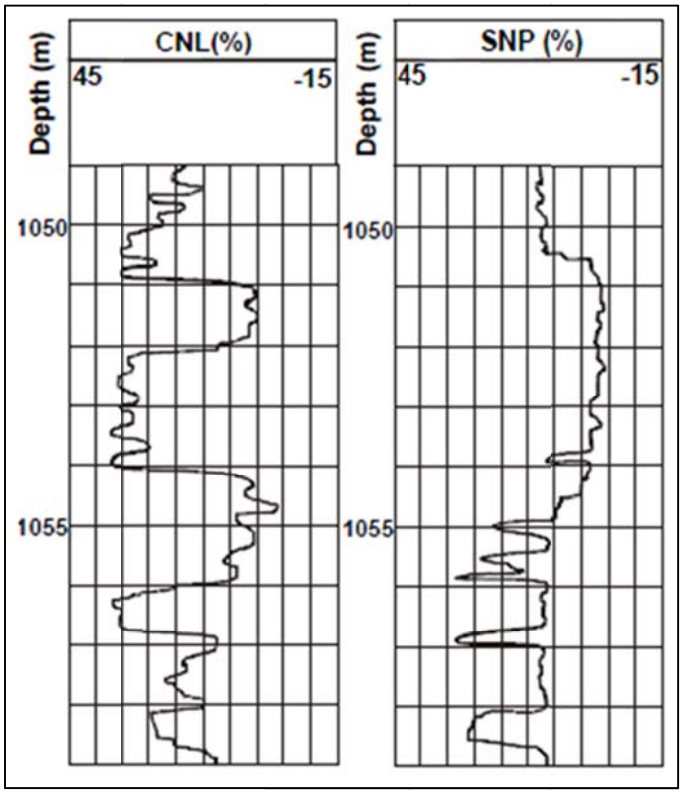

Figure 5.6: Typical logs for CNL and SNP tools modified from (Glover, 2005).

5.3.4.3 Factors affecting Neutron Porosity tools

Both SNP and CNL tools porosity curve response data and shown in figure 5.6, is given in limestone porosity units, as these tools are calibrated using high purity blocks of limestone with known porosity in test pits. Because of this method of calibration, any porosity readings in a different lithology will need to be corrected. The depth of penetration is dependent on the hydrogen index or hydrogen content. The more hydrogen present in the formation, meaning the more porous the rock the smaller the depth of investigation, with

lower porosity rocks having a greater depth of investigation as less hydrogen would be present. Shale also decreases the depth of investigation due to the presence of water on the clay crystals whereas the presence of gas can increase the depth of investigation due to the low density of hydrogen atoms present in gas as opposed to water or oil. The condition of the borehole is important, with roughness and washout causing poor readings (Glover, 2005).

5.3.5 Resistivity logs

Resistivity logs are based on Ohms Law which states that the current flowing from point A to point B (as in figure 5.7), through a conductor is proportional to the difference in electrical potential ΔE between those 2 points. The proportionality is the electrical conductance with the inverse of electrical conductance being the resistance which is measured in ohms.

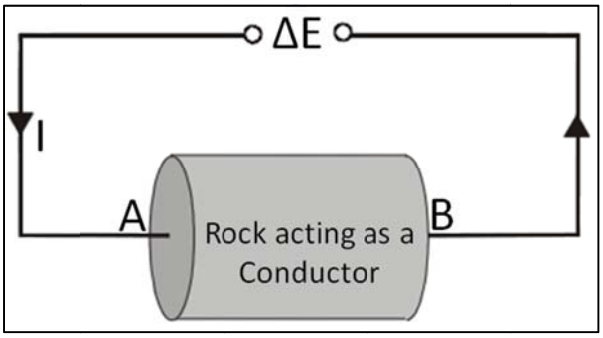

Figure 5.7: Diagram displaying measurement of electrical potential through a rock sample (Glover, 2005).

For a given electrical potential difference ΔE, if the resistance is high a small current will be measured, and if the resistance is low a higher current will be measured.

Resistance is hence, the ability of a material to resist the passage of a current passing through it for a given electrical potential difference. Three types of logs exist, namely induction resistivity logs, laterolog resistivity and micro-resistivity.

5.3.5.1 Laterologs

Laterolog tools use focusing or bucking currents into a planar disc shape and monitor the potential drop between an electrode on the tool and a distant electrode. The potential drop changes as the current and the formation resistivity changes and therefore the resistivity can be determined laterolog deep resistivity (LLD), is a measurement made several feet into

the formation whereas laterolog medium resistivity is a measure 2-3 feet into the formation with laterolog shallow resistivity (LLS) being a measurement less than 2 feet into the formation. LLD due to its depth is considered a measurement of the undisturbed formation with LLS measuring the formation where it contains fluids which are also comprised of mud filtrate due to the measurements close proximity to the borehole. Dual laterologs is the latest combination tool for laterologs deep resistivity (LLD) and laterolog shallow resistivity (LLS) (Glover2005).

5.3.6 Caliper Log

The caliper log measures variations (figure 5.8) in the borehole by using mechanical arms which push against the sidewalls. This is usually the first log run down the casing to correct measurements for the other logs. The log will show deviations from the drill bit diameter and can indicate areas of washout, caving and mud cake in the formation as seen in the log curve below.

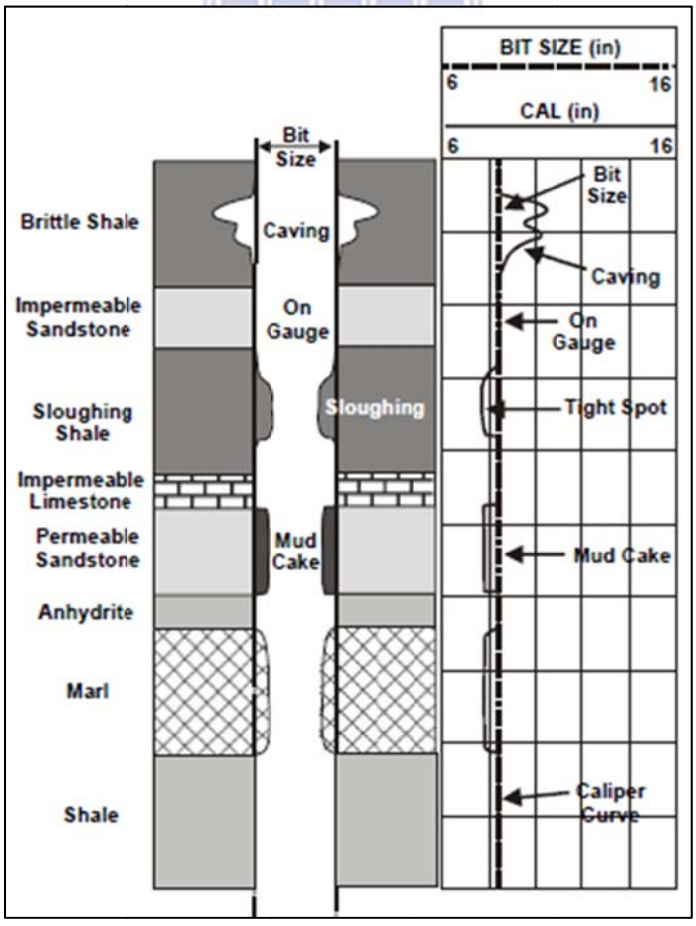

Fig 5.8: Varying scenarios for measurements down the borehole and related curves (Glover, 2005).

6. Results

6.1 Petrophysical Results

6.1.1 Lithological Interpretation

The three lithologies which were interpreted using the gamma ray plot is sand, siltstone and shale. Very minor inter-bedded siltstone (orange) was identified but as can be seen in figure 6.1, the majors were sand (yellow) and shale (green).

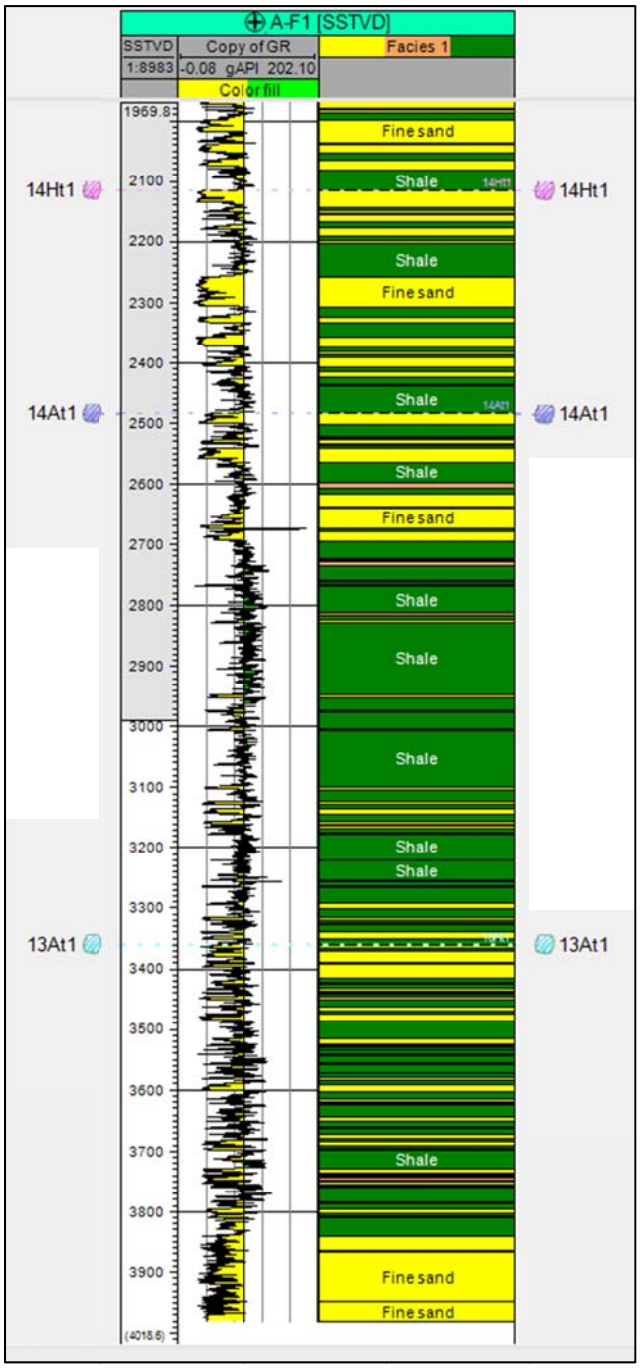

Figure 6.1: Lithologies defined in log as per analysis of gamma ray log.

6.1.2 Reservoir Zones (14Ht1)

Potential reservoirs identified are thick intervals of clean sandstone capped by an upper and lower shale sequence. Four reservoir zones were identified in 14Ht1 representing typical stratigraphic traps which were sandstone sequences capped on either side by a shale layer.

Sequence 14Ht1 was originally selected as the target reservoir zone with good thick sand strata identified with minor siltstone. Zones identified are as follows; 1-14Ht (2139.6-2162.7), 2-14Ht (2279.4-2330.8), 3-14Ht (2345.5-2358.4) and 4-14Ht (2377.3-2396.2) as per table 6.1 and side by side in figure 6.2 from left (shallowest) to right (deepest).

Table 6.1: Table of depths and thicknesses of potential reservoir zones identified for 14Ht1.

Reservoir	Top (m)	Bottom (m)	Thickness (m)
1-14Ht1	2139.6	2162.7	23.1
2-14Ht1	2279.4	2330.8	51.4
3-14Ht1	2345.5	2358.4	12.9
4-14Ht1	2377.3	2396.2	18.9
Total Reservoirs	2139.6	2396.2	106.3

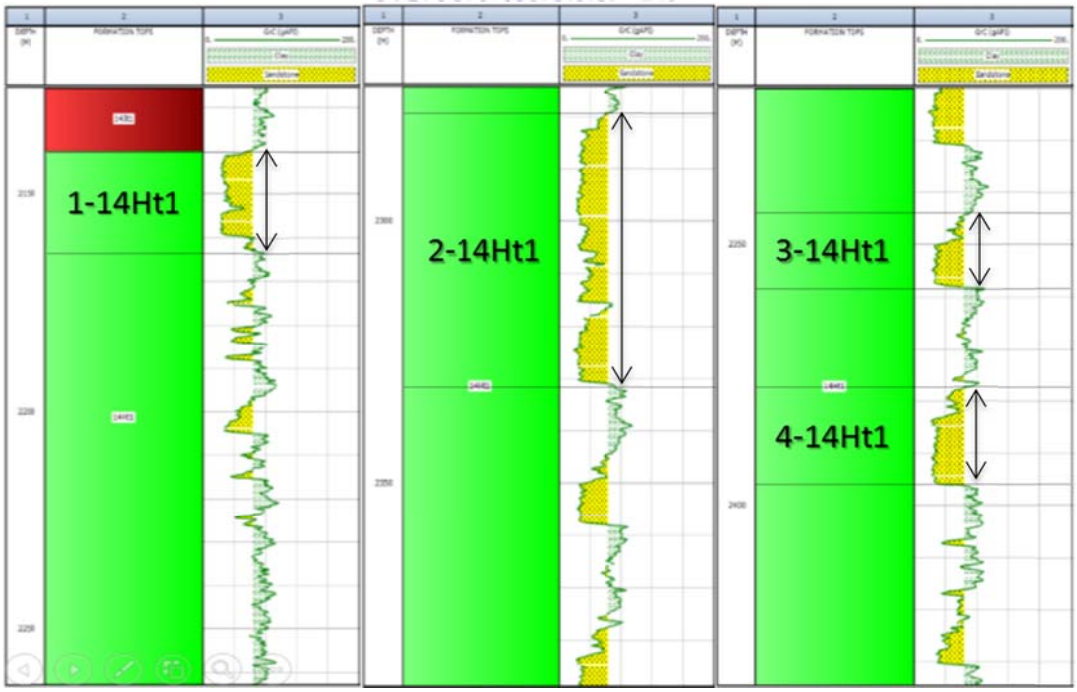

Figure 6.2: Side by side image of gamma ray logs and 4 zones identified (arrows depict extent of reservoir).

All four reservoir zones were selected based on stratigraphic features which show good thick clean sandstone reservoirs at a correct depth for hydrocarbon generation with good source rocks and good shale seals top and bottom (Figure 6.2).

6.1.3 Electrical properties determined from standalone picket plots

Fluid saturation has been discussed above in chapter 4 and the parameters in chapter 3.

The picket plot lines in figure 6.3 represent from left to right, 100% (red), 50%, 30% and 20% respectively. Fluid saturation parameters were calculated in a water bearing zone with depth between 2281.5m to 2331.4m in well A-F1.

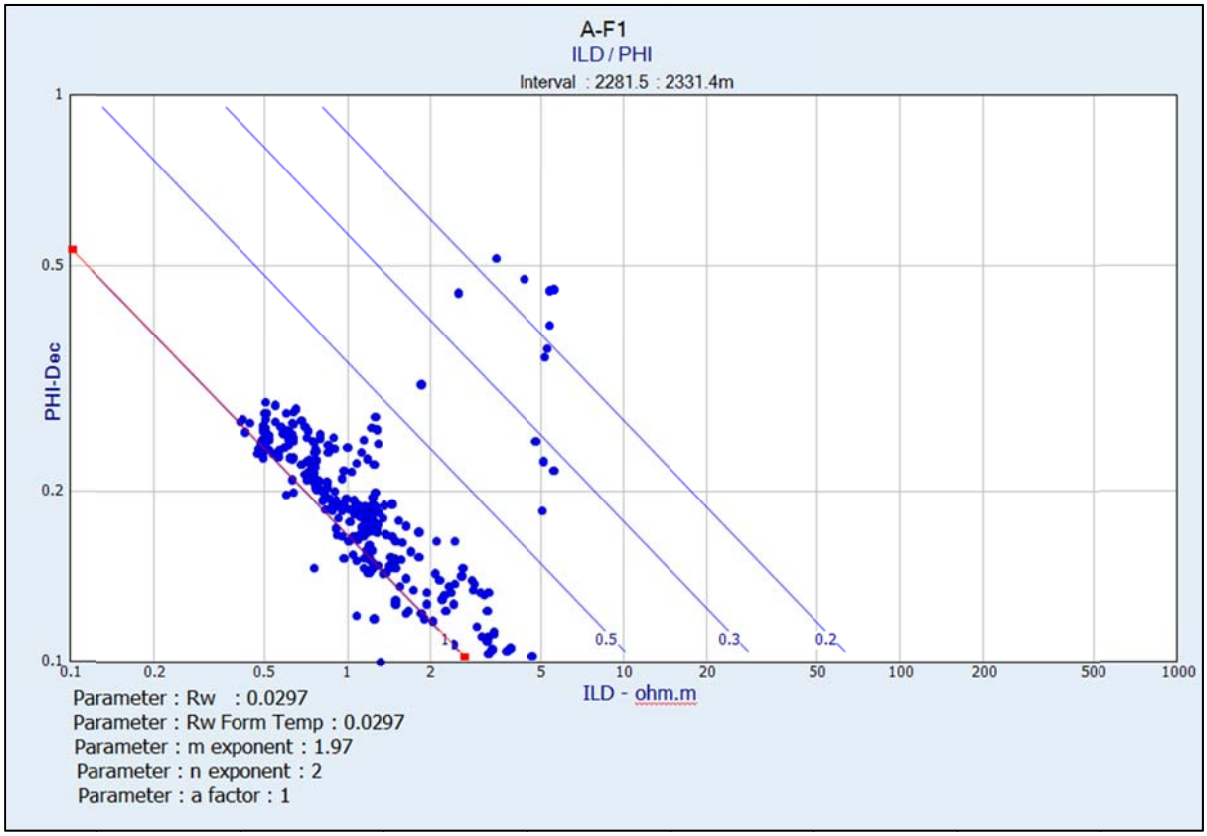

Fig 6.3: Picket plot representing water saturation % and calculated parameters for well A-F1

Table 6.2: Parameters as calculated for the picket plot above for well AF-1.

Top Depth (m)	Bottom Depth (m)	R_w	m	n	a
2281.5	2331.4	0.0297	1.97	2	1

As per table 6.2;

The saturation exponent for well A-F1 is 2.0.

The tortuosity factor for well A-F1 was calculated as 1.0.

The cementation exponent value for well A-F1 was 1.97 which indicates well cemented (Bennion et al., 1996).

The formation water resistivity for well A-F1 was calculated 0.0297.

6.1.4 Petrophysical analysis

6.1.4.1 Core data analysis

From the log analysis report it is firstly noted; due to well the being drilled overbalanced, this resulted in bad hole conditions. Overbalance refers to the amount of pressure in the wellbore exceeding the pressure of fluids required to prevent the reservoir fluids from entering the wellbore. High overbalance can cause sticking problems and result in poor borehole conditions, although this varies from one zone to another (Schlumberger, 2017b).

Four cores depths were sampled in well A-F1 and analysed as per core analysis results in Appendix A. Averaged figures for petrophysical parameters are condensed from log analysis report into table 6.3. Core 1 was drilled to investigate fluorescence; core 2-4 was drilled to investigate drilling breaks with core 3 being drilled to investigate a gas show. The hole condition for core 3 and core 4 is recorded as poor with the response of MSFL (micro resistivity log), BHC (borehole compensated sonic tool), LDT (litho-density tool) and CNL (compensated neutron log) being affected negatively (Bell, 1987).

Table 6.3: Laboratory core measurements as per log analysis report of A-F1 (Bell,1987).

Well A-F1 Cores (Depth)	Core 1 (1178m-1181.5m)	Core 2 (2305m-2321.8m)	Core 3 (2524m-2540m)	Core 4 (3184.5m-3194.9m)
Average Gamma Ray (API)	30	30	30-60	37-60
Average Porosity (%)	23	24	18	10
Permeability Range (mD)	42-367	none	none	none
Sonic Porosity (%)	35	none	none	none
Water Salinity (ppm NaCl)	50 000	50 000	41 000	41 000
Water Saturation (%)	80-100	100	55-70	100

6.1.4.2 Volume of Shale Cut-off

Volume of shale cut-off is used to determine the reservoir and non-reservoir interval. If Vsh cut-off value is determined, all rocks that have a volume of shale which is equal to or less than that value is considered part of the total reservoir volume and any rocks that have shale content higher than the determined cut off value is seen as non-reservoir (Opuwari, 2010).

The cut-off value for shale was determined to be 0.35. All rocks which contained 35 % and less hence is reservoir and all rocks containing more than 35% shale is considered non reservoir. The volume of shale cut-off value is presented in the volume of shale versus porosity plot in figure 6.4.

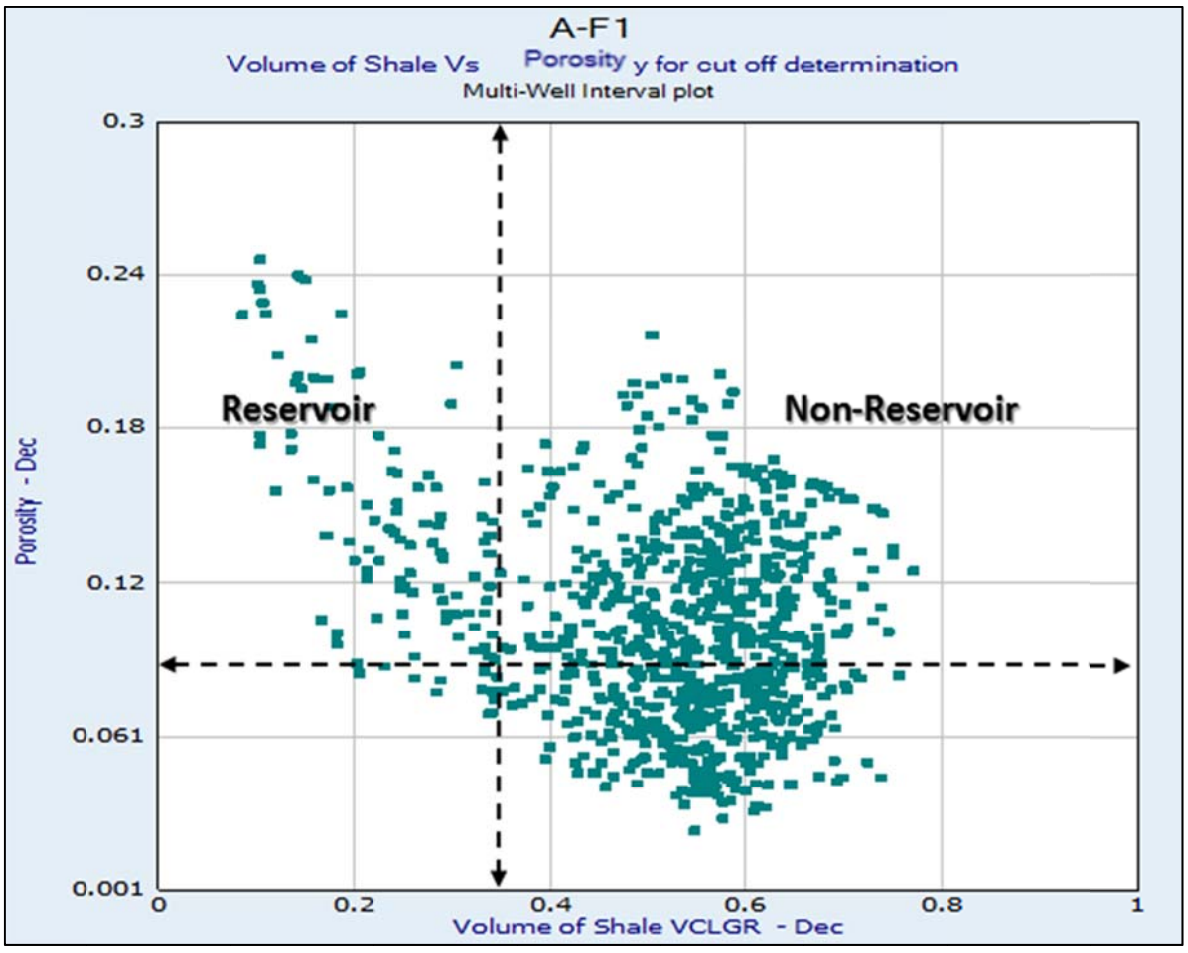

Figure 6.4: Volume of shale versus porosity plot.

6.1.4.3 Porosity and Permeability cut-off determination

Porosity cut-off is a parameter used to distinguish between formation rocks which are reservoirs and non-reservoirs and can greatly affect the dimensions of a reservoir, the estimations of reservoir volumes and hydrocarbon accumulations (Widarsono, 2011).

A cut-off of 0.08 (8%) was applied and a 0.1mD cut-off as per gas reservoirs. The dashed lines in figure 6.5 delineate points which are considered reservoir and non-reservoir analysis.

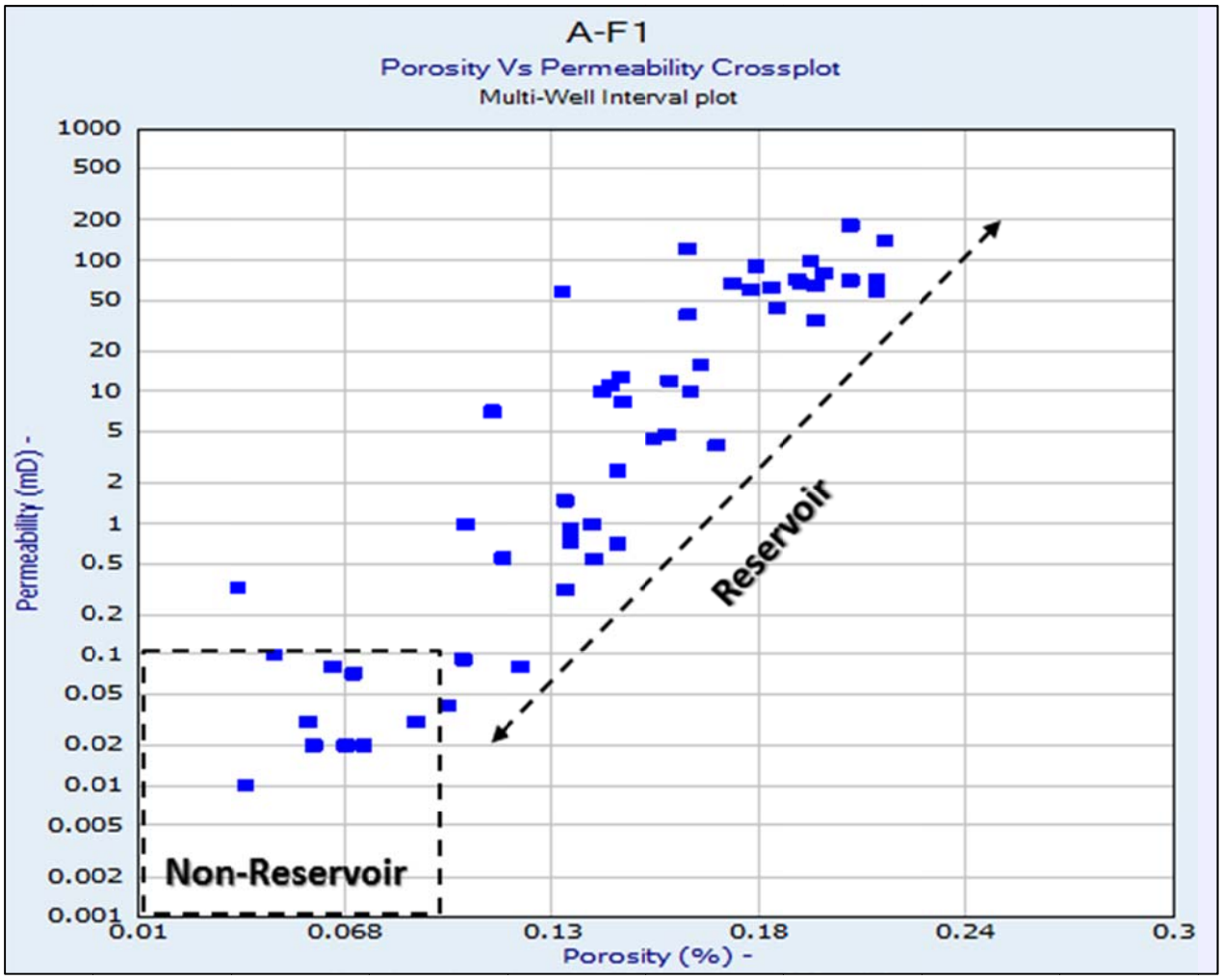

Figure 6.5: Porosity versus permeability cross plot for cut-off determination.

6.1.4.4 Water saturation cut-off

A water saturation value of 50% was used to differentiate between hydrocarbon bearing sandstones (pay) and water (wet) bearing intervals. Intervals that display a water saturation of 50% or less were assumed to be hydrocarbon bearing sandstones and greater than 50% were assumed to be non-productive intervals (Opuwari, 2010). The water saturation versus porosity cross plot presented below in figure 6.6 represents water saturation cut-off value differentiating between reservoir and non-reservoir and then the reservoir area into a wet (above 50% water saturation) and productive interval (below 50% water saturation).

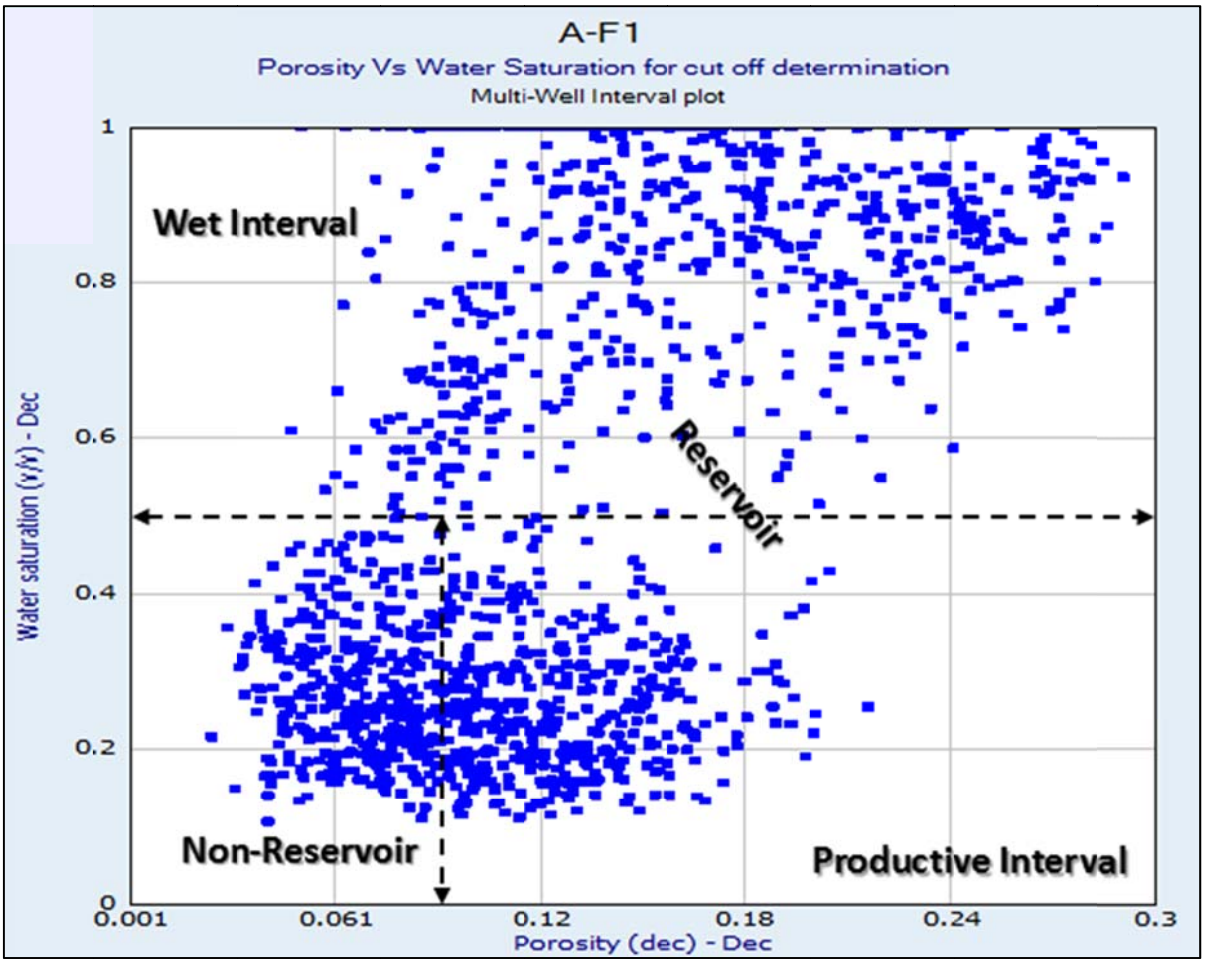

Figure 6.6: Porosity versus water saturation cross plot for cut-off determination.

6.1.4.5 Permeability Cut-off

For reservoirs, a cut-off of 1mD is applied for oil reservoirs and cut-off of 0.1mD is applied to gas reservoirs (Opuwari, 2010). The reservoir in this study is considered a gas reservoir and hence a 0.1mD cut-off was used. Permeability averaged/median values for the reservoirs are as follows, reservoir 1 = 3.2mD, reservoir 2 = 9.5mD, reservoir 3 = 2.3mD and reservoir 4 = 2.5mD. Predicted permeability curves are plotted in figures 6.7 – 6.9, track 6 (red squares).

Figure 6.7: Log curves plot displaying predicted permeability (track6), well A-F1, reservoir 1.

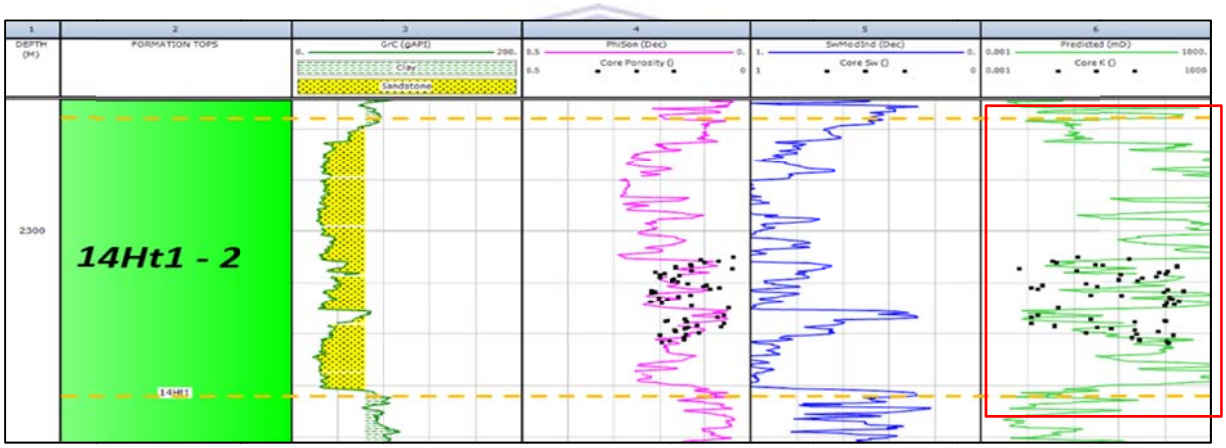

Figure 6.8: Log curves plot displaying predicted permeability with core permeability (track6), well A-F1, reservoir 2.

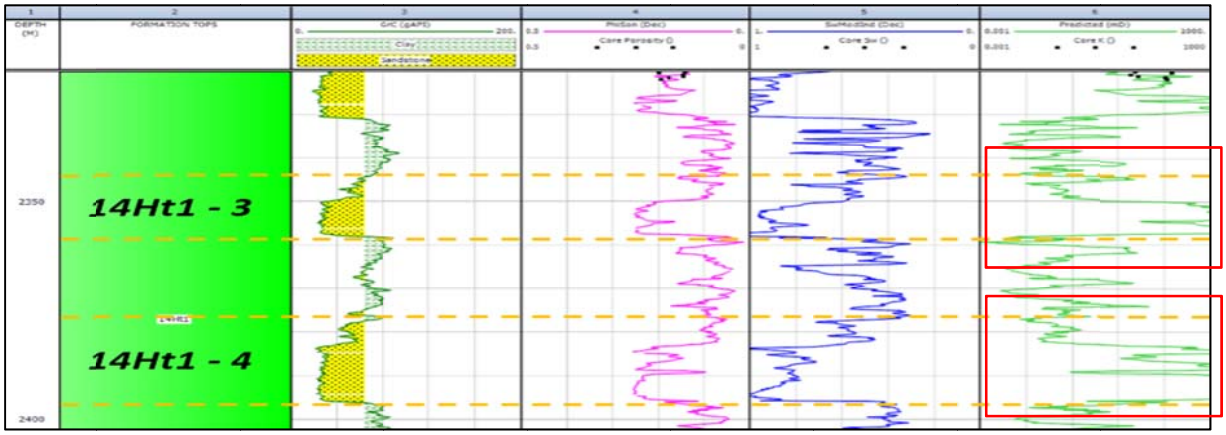

Figure 6.9: Log curves plot displaying predicted permeability (track6), well A-F1, reservoir zone 3&4.

6.1.4.6 Pay cut-off

To calculate net pay zones in the reservoir, cut off values is applied to the petrophysical dataset to define pay sand from non-pay sand. In table 6.4 below,

Table 6.4: Reservoir gross and net pay estimations colour coded per 14Ht1 reservoir zone.

Reservoir Name	Top (m)	Bottom (m)	Gross (m)	Net (m)	N/G	Av Phi (v/v)	Av Sw (v/v)	Av Vcl (v/v)
1-14Ht1	2139.6	2162.7	23.1	0.75	0.032	0.098	0.408	0.263
2-14Ht1	2279.4	2330.8	51.4	0.90	0.018	0.103	0.334	0.279
3-14Ht1	2345.5	2358.4	12.9	0.00	0	---	---	---
4-14Ht1	2377.3	2396.2	18.9	0.34	0.018	0.153	0.436	0.109
4 Reservoirs	2139.6	2396.2	106.3	1.99	0.019	0.11	0.384	0.244

Gross = the entire thickness of the reservoir zone (gross pay)

Net = the intervals of the reservoir that can produce hydrocarbons

N/G = the net/gross ratio the net pay thickness divided by the gross pay thickness

Ave Phi = Average Porosity for zone

Ave Sw = Average Water saturation for zone

Av = Averaged Water Saturation for zone

Cut-off values applied are, porosity equal to or greater than 8% (≥ 0.08), volume of shale less than or equal to 35% (≤ 0.35) and water saturation less than or equal to 50% (≤ 0.5) to identify net pay intervals with water saturation not being applied to identify gross reservoir interval. Permeability cut-off for oil reservoirs are normally set to 1.0mD and 0.1mD for gas. Gas shows were identified in the geological well completion report, thus 0.1mD was used as the cut-off.

The reservoir gross shows good potential with 106.3m thickness in total which range from 12.9m to 51.4m in thickness as presented in table 6.4 and can be seen in figure 6.10 below. Net pay potential was extremely poor with intervals not exceeding 1.0m in thickness resulting in a total net pay thickness of only 1.99m and a very low N/G ratio of 0.019. No net pay could be calculated for zone 3. The net pay reservoir flags are presented in figures 6.12-6.14 below with individual table's 6.4-6.6 for a detailed breakdown of pay zones.

Figure 6.10: Reservoir and pay flags for the four reservoir zones for 14Ht1.

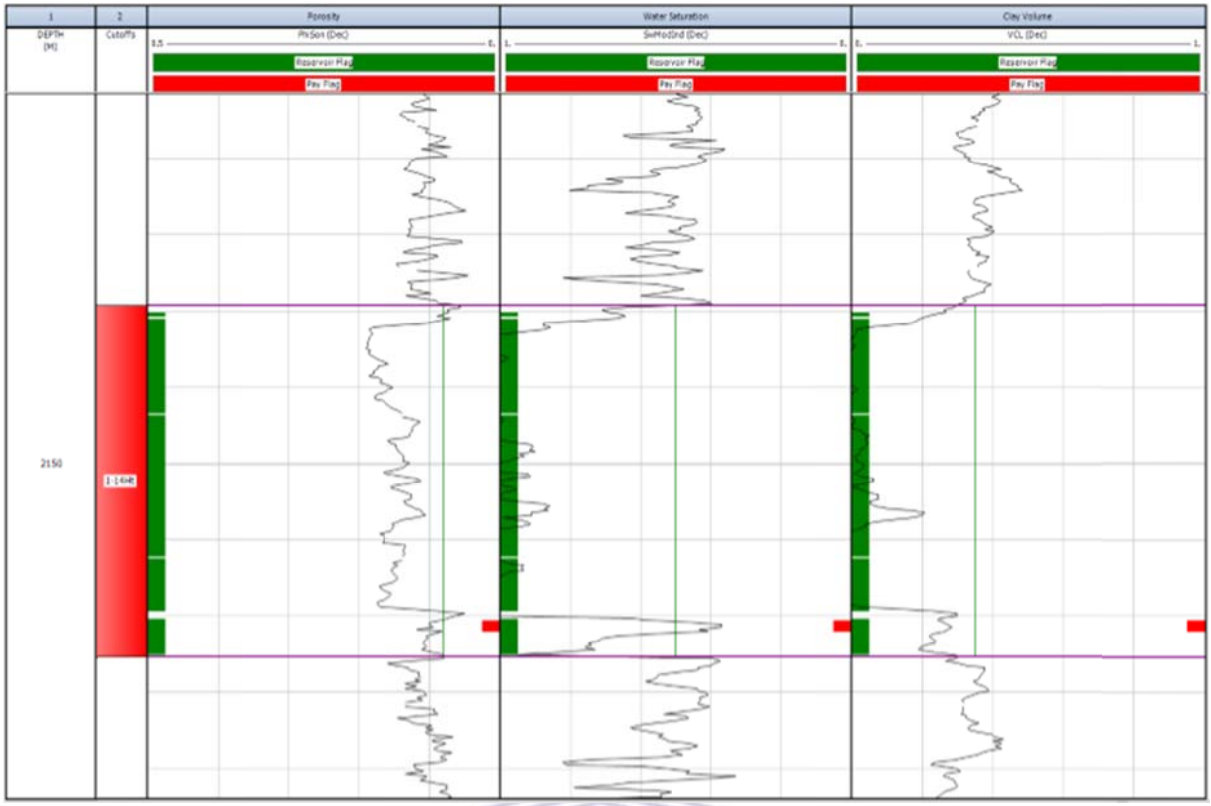

Figure 6.11: Reservoir and pay flag for well A-F1 reservoir 1-14Ht1.

Table 6.5: Net pay estimations for 1-14Ht1 reservoir.

Pay Interval Listing for Zone 1-14Ht1					
Top	Bottom	Net	PhiSon	SwModInd	VCL
(m)	(m)	(m)	(v/v)	(v/v)	(v/v)
2160.43	2161.03	0.75	0.0982	0.407	0.2628
	Average	0.75	0.0982	0.407	0.2628

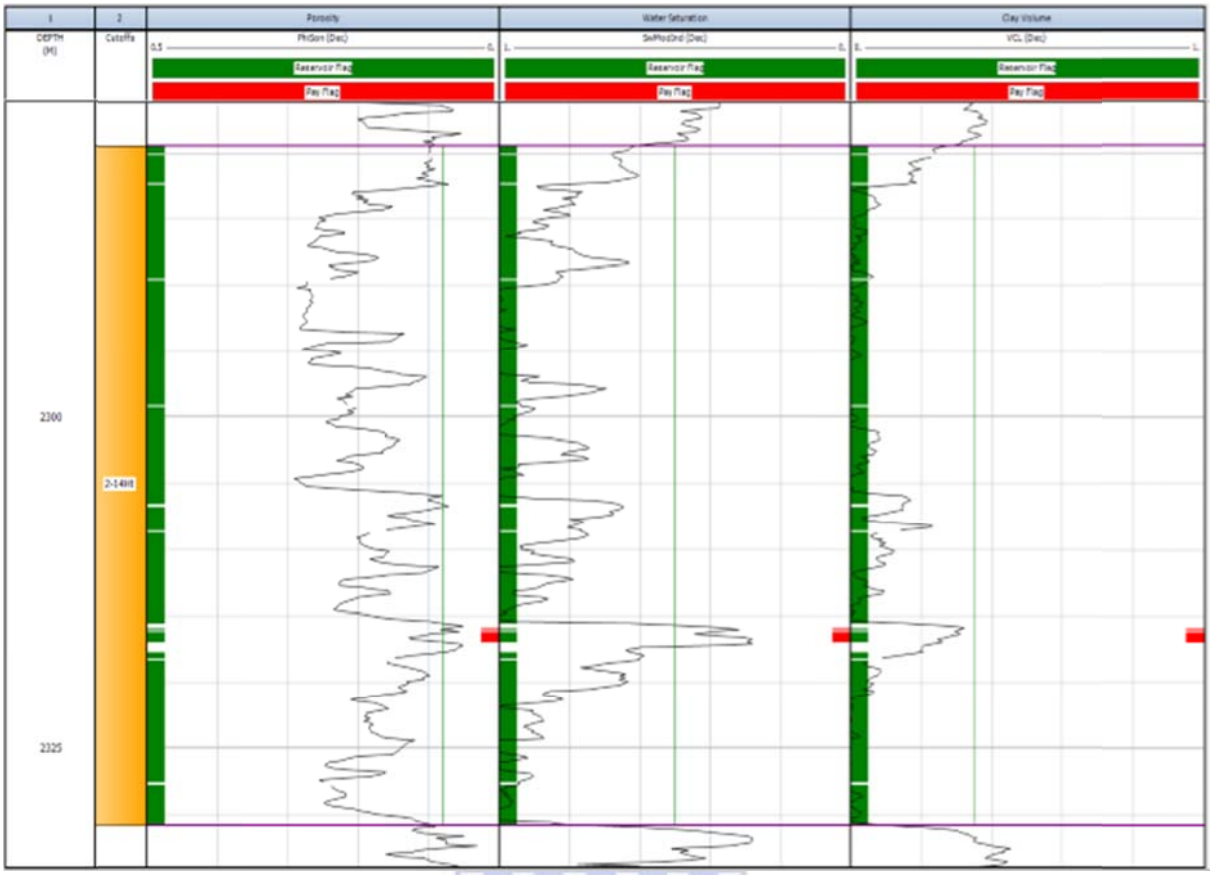

Figure 6.12: Reservoir and pay flags for well A-F1 reservoir 2-14Ht1.

Table 6.6: Net pay estimations for 2-14Ht1 reservoir.

Pay Interval Listing for Zone 2-14Ht1					
Top	Bottom	Net	PhiSon	SwModInd	VCL
(m)	(m)	(m)	(v/v)	(v/v)	(v/v)
2315.98	2315.98	0.15	0.0828	0.3178	0.3101
2316.28	2316.88	0.75	0.1075	0.3396	0.2725
	Average	0.45	0.0952	0.3287	0.2913

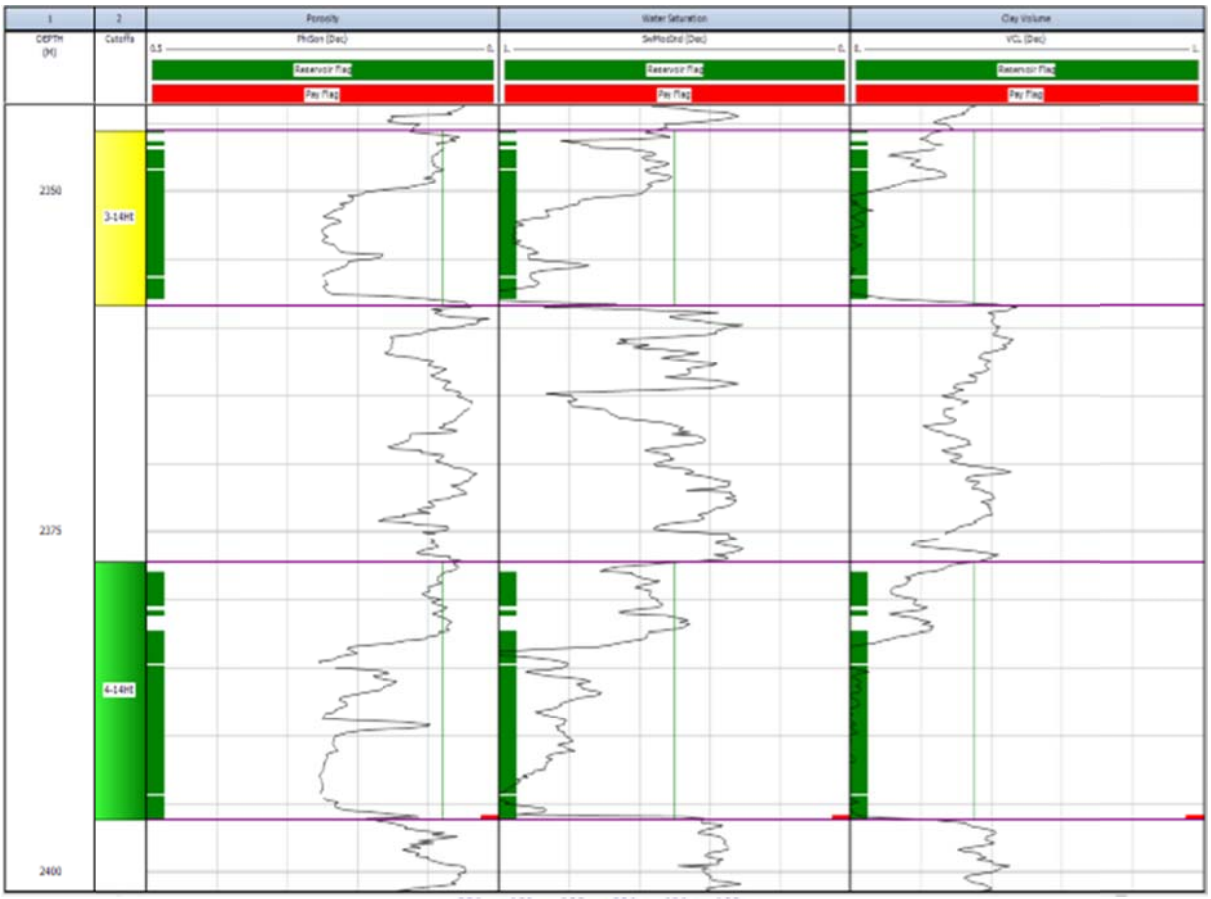

Figure 6.13: Reservoir and pay flag for well A-F1 reservoir 3-14Ht1 and reservoir 4-14Ht1, no pay intervals were identified for 3-14Ht1.

Table 6.7: Net pay estimations for 4-14Ht1 reservoir

Pay Interval Listing for Zone 4-14Ht1					
Top	Bottom	Net	PhiSon	SwModInd	VCL
(m)	(m)	(m)	(v/v)	(v/v)	(v/v)
2395.93	2396.08	0.3	0.1502	0.4462	0.0902
	Average	0.3	0.1502	0.4462	0.0902

6.2 Modelling Results

6.2.1 Facies Modelling

Litho-facies log was created using the gamma ray log and generated in petrel using the calculator to determine a baseline to differentiate between sand and shale responses. The baseline was calculated as a mean value of 64.118 in figure 3.15. Minor siltstone was manually interpreted as this was not accurately determined by a single figure variable input into the algorithm. The litho-facies log was upscaled and then modelled into region block 3 (14Ht1) with the result in figure 6.14 displaying sand (yellow), silty sand (brown) and shale (green).

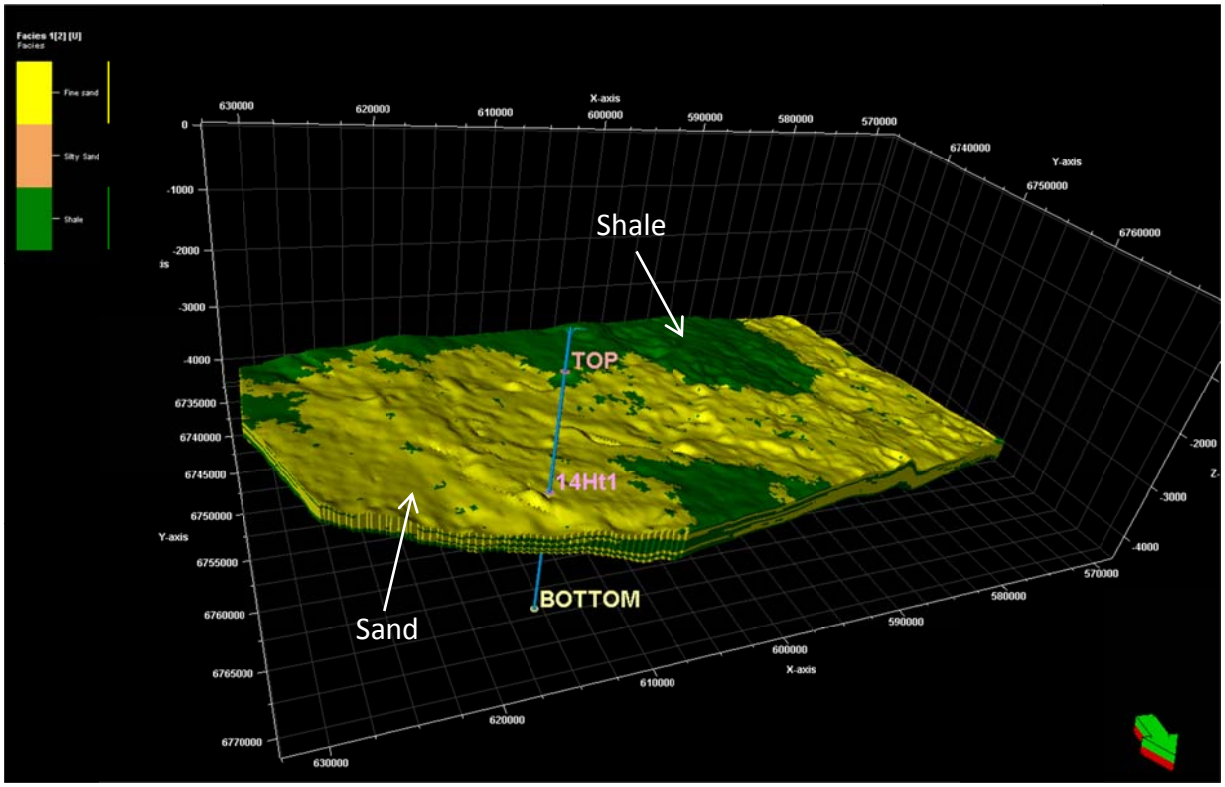

Figure 6.14: Litho-facies model for 14Ht1.

Litho-facies distribution indicates good sand volumes in the wellbore area with inter bedded shale which creates the stratigraphic trap required for the trap and seal mechanism of the petroleum system. Shale volume increases to the southern border of the cube and west. The increase of clay volumes is evident on the porosity and permeability models generated with good correlation between models.

6.2.2 Petrophysical Modelling

Petrel was used to generate stochastic models based on the sequential gaussian simulation (SGS) method, described in chapter 3, as it simulates continuous variables such as petrophysical properties using a spherical variogram. The petrophysical models for porosity, water saturation, permeability and volume of shale was created for Zone 3 block region model, 14Ht1. Realization simulations were run on all petrophysical models generated. Results and interpretation of the petrophysical models generated are shown below in figures 6.15 – 6.19.

6.2.2.1 Volume of Shale Model (14Ht1)

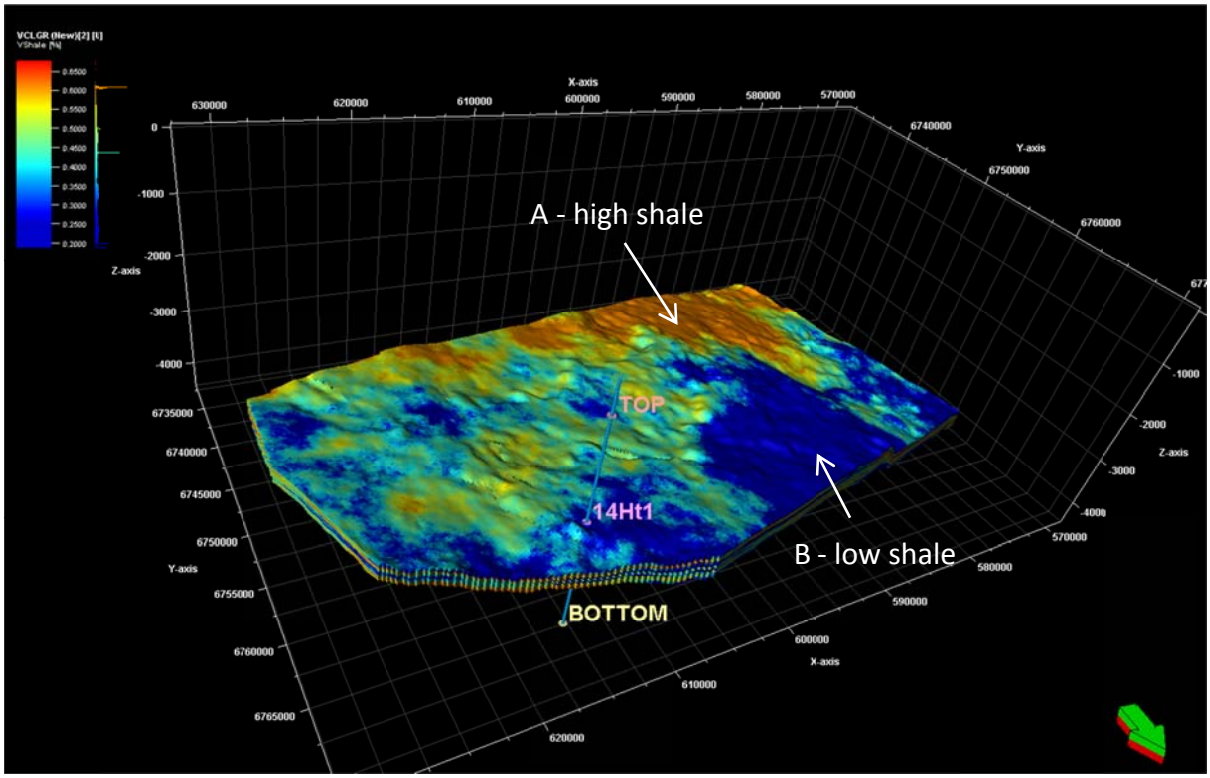

Figure 6.15: Volume of shale model for Well A-F1, 14Ht1.

Low estimated shale volumes (darkblue) around the borehole in figure 6.15, indicate good sandstone structure and the potential for good porosity and permeability in the sandstone reservoirs including good connectivity of pore spaces and low chances of compartmentalization of the reservoirs.

An increase of the shale volume (orange) to the south west (A) of the well position is clearly visible with good low shale volumes to the west (B). Average shale calculated for the gross

pay of the reservoir was 0.244 (24.4%) which ties in well with what is displayed at and around the well bore area in figure 6.15.

6.2.2.2 Porosity Model (14Ht1)

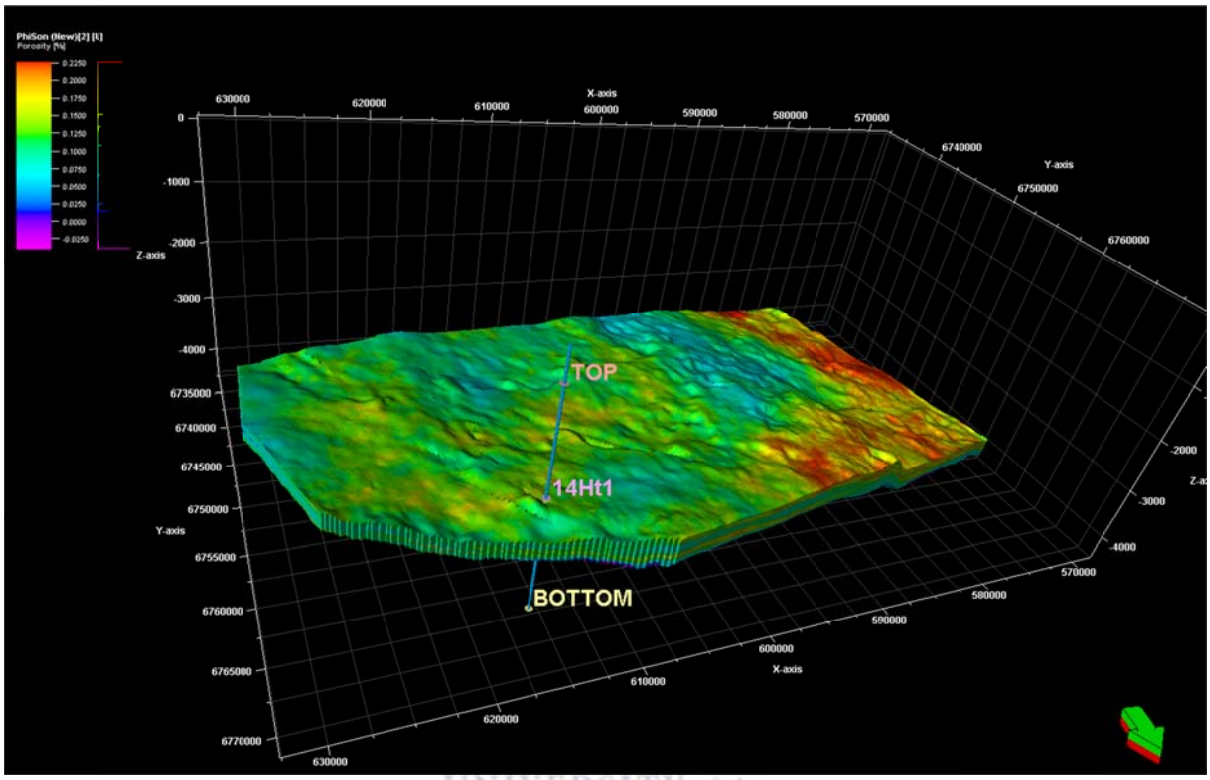

Figure 6.16: Porosity model for Well A-F1, 14Ht1.

In figure 6.16 above on the scale, the lowest porosities are indicated by the purple and the highest porosities by red. A porosity cut-off of 8% was used, with the averaged porosity calculated for 14Ht1 at 0.11 or 11% which correlates with the porosities displayed around the well area in the porosity model. The lowest reservoir zone, 4-14Ht1 recorded a good average porosity of 15.3% with 2-14Ht1 zone recording 10.3% and then decreasing to 9.8% for 1-14Ht1. Porosity increases toward the western border and is most likely due to higher sand to shale ratio. 14Ht1 overall exhibits very good porosity and is indicative of good clean sandstone reservoirs with very minor inter-bedded siltstone.

6.2.2.3 Permeability Model (14Ht1)

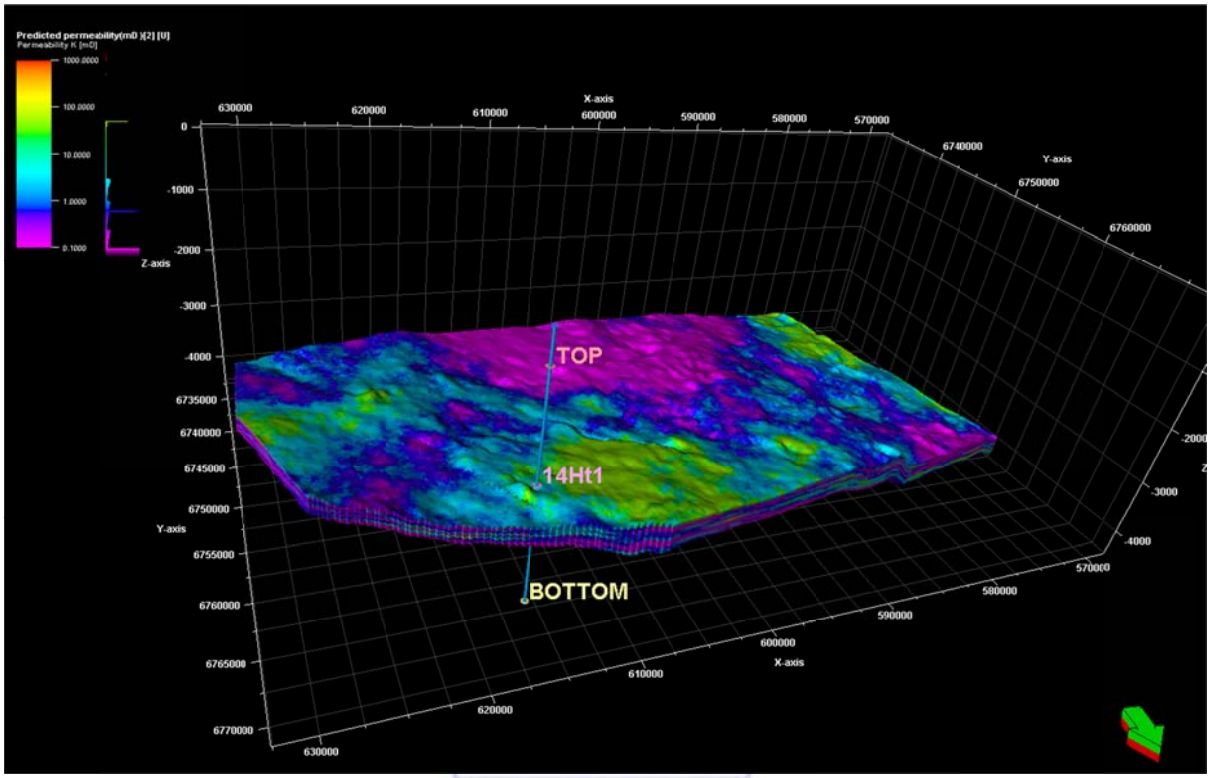

Figure 6.17: Permeability model for Well A-F1, 14Ht1.

The permeability model, figure 6.17, correlates well with the volume of shale model, figure 6.15, with very identical trends in terms of the volume of shale mirroring the permeability in the middle southern section of the model. Good permeability values are visible at the wellbore and around the well bore area. Permeability cut-off used was 0.1mD for a gas reservoir and this value is exceeded in the well bore area with modelled figures above 10mD modelled (green patch) around well area and to the west. Permeability for the reservoir zones as per the predicted log was between 2.3mD and 9.5mD as plotted in figures 6.7-6.9.

6.2.2.4 Water Saturation (14Ht1)

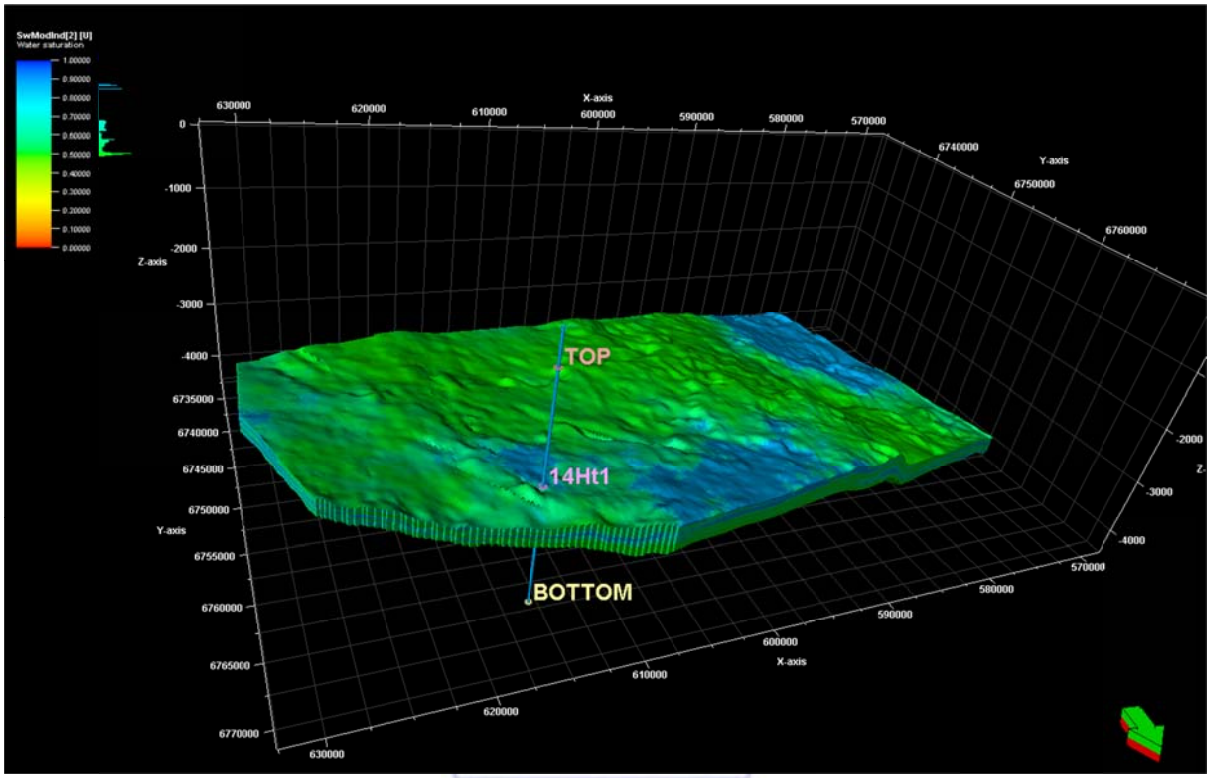

Figure 6.18: Water saturation model for Well A-F1, 14Ht1.

A water saturation cut-off of 50% was used to differentiate between wet interval and productive interval of the reservoir. The modelled water saturation log indicates high water saturation values using the mod Indonesia method described in chapter 3 (Figure 6.18). Very few areas are considered productive with almost the entire reservoir considered non-productive which agrees with the net pay calculation indicating extremely low amounts of hydrocarbon in the well. The geological report indicated sandstone reservoirs with water saturation of 73% up to 94% with poor gas shows which most likely refers to the 1.99m of pay thickness (Noble, 1987).

6.2.2.5 Gross Pay Model (14Ht1)

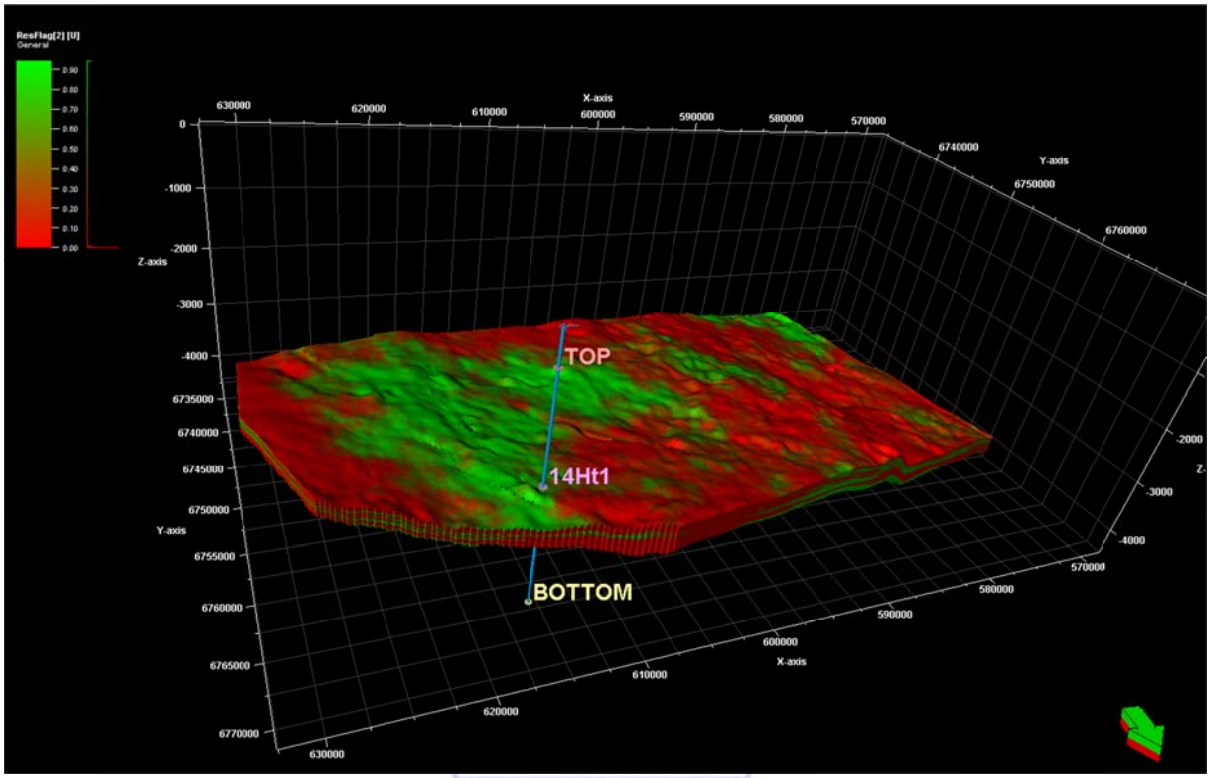

Figure 6.19: Gross pay reservoir model for Well A-F1, 14Ht1.

The gross pay or gross reservoir model in figure 6.19 shows good results in the well bore area but this decreases toward the west of the well bore and also is poor on the eastern and southern border and when compared to the other models explains the reason for this area being the target site for the well. The reservoir however as per the water saturation model in figure 6.18, shows the reservoir is water saturated. The net pay model was excluded from this study as the nett/gross ratio was extremely low at 0.019 with a gross pay figure of 106.3m to a net pay of 1.99m as determined in the pay cut-off section.

7. Conclusion and Recommendation

7.1 Conclusion

This project set out to characterize a reservoir in well A-F1 with 14Ht1 exhibiting good potential sandstone reservoirs for evaluation. The geological report was not examined in detail until after the modelling was concluded so as to not create a bias to the original report.

All the horizons were interpreted which include, top, 16At1, 15At1, 14Ht1, 14At1, 13At1, 6At1 and bottom. The only horizon which was not interpreted for was 14Jt1 as there was difficulty in mapping it and was excluded for quality reasons. Only once the seismic analysis was completed was 14Ht1 identified during the petrophysical analysis as having good reservoir potential and focussed in on as the target reservoir zones for this study.

Reservoir properties are good with well-developed sandstones, good porosity and permeability. However, the sandstones are water saturated with minor hydrocarbon shows of gas and hence the reservoir is completely uneconomical.

The geological well completion report classifies the well as a dry well with minor gas shows. It also states the stratigraphy is less marine influenced and cannot be related to the Kudu marine sediments. Low hydrocarbon accumulations or lack thereof, can be ascribed to regionally developed source rocks not being intersected or not being well developed. The well was terminated early due to poor prospectivity and even if lacustrine source rocks were present lower down the stratigraphic column as in other parts on the west coast of Africa, there are no indications of accumulations possibly due to poor migration pathways (Noble, 1987).

7.2 Recommendations

With the availability of 3-D seismic data, a high resolution 3-D and seismic inversion study should be performed to identify and compare the marine source rocks associated with the marine environment and less marine environment encountered in A-F1. This study will enhance distal exploration of block 1 to ensure a greater chance of success.

References:

Barton, K.R., Muntingh, A and Noble, R.D.P., (1993). Geophysical and Geological studies applied to hydrocarbon exploration on the West Coast Margin of South Africa.

Bell, C, (1987), Log Analysis of A-F1, An informal report, Soekor, Johannesburg

Bennion, D.B., Thomas, F.B. and Bietz, R.F. (1996). Determination of initial fluid saturations- A key factor in By-passed pay determination, 3-5.

Broad, D. S., Jungslager, E. H. A., McLachlan, I. R., & J, R. (2006). Offshore Mesozoic Basins. *Geology of South Africa*, (1996), 553–572.

Brown, L.F. Jr., Benson, J.M., Brink, G.J., Doherty, S., Jollands, A., Jungslager, E.H.A., Keenan, J.H.G., Muntingh, A. and Van Wyk, N.J.S (1996). Sequence stratigraphy in offshore South Africa divergent basins. An atlas on exploration for Cretaceous Lowstand traps by SOEKOR (Pty) Ltd A.A.P.G. Stud. Geol., 41, pp 184

Cogswell D. (2014): Borehole Wireline, http://borehole-wireline.com.au/2014/10/porosity-measurement/

Crain, E.R. (2015a), Crain's Petrophysical handbook: URL https://www.spec2000.net/14-Sws.htm

Crain, E.R. (2015b), Crain's Petrophysical handbook: URL https://www.spec2000.net/14-swrw.htm

Crain, E.R. (2015c), Crain's Petrophysical handbook: URL https://www.spec2000.net/14-swxplot.htm

Darling, T., (2005). In Well Logging and Formation Evaluation, First Edition, Gulf Professional Publishing, Burlington, 2005,

De Vera, J. Pablo Granado,P., McClay, K. (2009). Structural evolution of the Orange Basin gravity-driven system, offshore Namibia. Marine and Petroleum, Geology 27 (2010), pp 223–237

Frank, J., Cook, M., Graham M. (2008). Developments in petroleum geoscience, Hydrocarbon Exploration and Production, 2nd Edition

Glover P.W.J (2002): Formation Evaluation, MSc Petroleum Geology, Department of Geology and Petroleum Geology, University of Aberdeen, UK

Glover P.W.J (2005): GLG-66565 Petrophysics, MSc and PhD level, University Laval, Canada

Hirsch, K. K., Scheck-Wenderoth, M., van Wees, J.-D., Kuhlmann, G. (2009): Tectonic subsidence history and thermal evolution of the Orange Basin. - Marine and Petroleum Geology, Vol.27, issue 3, pp. 565-584.

Jungslager, E. H. A., (1999 a). Petroleum habitats of the Atlantic margin of South Africa. Special publications, Geological Society: Oil and Gas Habitats of the South Atlantic, pp. 153-168

Jungslager, E.H.A., (1999 b). New geological insight gained from geophysical imaging along South Africa's western margin, South African Geophysical Association, 6th Biannual Conference & Exhibition, 28th September – 01October 1999, Cape Town, Extended Abstract, paper 14.4

Ma, Y. Zee, 2011, Uncertainty analysis in reservoir characterization and management: How much should we know about what we don't know? , Uncertainty analysis and reservoir modelling: AAPG Memoir 96, p. 1 – 15

Mustafa, S. (2012) Interpretation, Basic Well Log Interpretation, Focus Energy Ltd.

Muntingh, A., Brown, L.F., (1991). Sequence Stratigraphy of Petroleum Plays, Post – Rift Cretaceous Rocks (Lower Aptian to Upper Maastrichtian), Orange Basin, Western Offshore, South Africa, AAPG, Volume XX, Chapter 4, pp 71 – 98

Noble, R.D.P, (1987), A-F1 Geological Well Completion Report, Soekor, South Africa

North, F.K. (1985), Petroleum Geology, Published by Allen and Unwin Inc., Winchester, Mass, USA

Opuwari, M. (2010). Petrophysical evaluation of the Albian age gas bearing sandstone reservoir of the O-M field, Orange Basin, South Africa, Ph.D. thesis, University of the Western Cape, South Africa.

Othman, Adel & Abdel Aziz Mohamed, Mohamed & Fathi Mohamed, Mohamed. (2016). Improving fault tracing detection applying 3-Dant tracking seismic attribute. IOSR Journal of Applied Geology and Geophysics (IOSR-JAGG), Volume 4, Issue 3 Ver. I (May. - Jun. 2016), PP 18-25. 4. 18-25.

Petroleum Agency South Africa 2008, Petroleum Exploration Information and Opportunities brochure

Petroleum Agency South Africa 2012, Petroleum Exploration Information and Opportunities brochure

Petroleum Agency South Africa 2012, Petroleum Exploration Potential of the Orange Basin

Rider, M.H (2002), The Geological Interpretation of Well logs; 2nd Edition, Rider-French Consulting Ltd, Whittles Publishing 2002.

Salomo, J. (2012). Seismic Stratigraphy of the Deep-Water Area in the Northern Orange Basin, Offshore South Africa. *AAPG Search & Discovery*, *10389*.

Saputra, I. (2008). Shale volume calculations. HRS Jakarta; CE8R2.

Schlumberger (2011): Petrel Geophysics Course, 2011 manual

Schlumberger (2014): Petrel Velocity Modelling Training and Exercise guide, 14th Edition

Schlumberger (2014B): Seismic Visualization and Interpretation, 14th Edition

Schlumberger (2016 A): Petrel Fundamentals Training and Exercise Guide, Version 2016

Schlumberger (2016 B): Petrel Geophysics Training and Exercise Guide, Version 2016

Schlumberger, 2017a, Schlumberger Curve Mnemonic Dictionary, http://www.apps.slb.com/cmd/

Schlumberger,2017b, Schlumberger Oil Field Glossary, http://www.glossary.oilfield.slb.com/

Serra, O. (1984). Fundamental of well logging Interpretation. Elsevier Science Publisher, V; 142.

Statios , (2000), Statios software services, Reservoir modelling with WinGslib free online course, Edmonton Canada http://www.statios.com/Resources/08-sgsim.pdf

Stegers, D (2012) Static Reservoir Modelling and Reserves Calculation, Amsterdam Petroleum Geoscience B.V, Amsterdam, The Netherlands

Van der Spuy, D., (2003): Aptian source rocks in some South African Cretaceous basins. In: Arthur, T.J., MacGregor, D.S & Cameron, N.R. (Eds.), Petroleum Geology of Africa: New Themes and Developing Technologies. Geol. Soc., London, Spec. Publ. The Geological Society of London.

Watkeys, M.K. (2006). Gondwana Break-Up: A South African Perspective. In: Johnson, M.R., Anhaeusser, C.R and Thomas, R.J. (Eds), The Geology of South Africa. Geological Society of South Africa, Johannesburg/Council for Geoscience, Pretoria, 531 – 537.

Widarsono, B. (2011, January). An Improvised Method for Determining Reservoir Rock Porosity Cut-off with Support of Laboratory Mercury Injection Data. Society of Petroleum Engineers.

Appendices

01 - Conventional core analysis on borehole A-F1 by Soekor core analysis section.

CORE1	Sample Depth (m)			Permeability (mD)	Residual Fluid Saturation		
	From	To	Gas Exp	Horizontal L	Sw (%)	So (%)	Sg (%)
	1178.00	1178.25	21.10	35.00	93.00	0.00	7.00
	1179.10	1179.25	25.10	35.00	92.00	0.00	8.00
	1179.93	1180.13	29.20	309.00	94.00	0.00	6.00
	1181.20	1181.51	25.70	337.00	92.00	3.00	5.00

CORE3	Sample Depth (m)			Permeability	Residual Fluid Saturation		
	From	To	Gas Exp	Horizontal L (mD)	Sw (%)	So (%)	Sg (%)
	2524.00	2524.39	24.60	83.00	67.00	0.00	33.00
	2525.19	2525.39	27.80	296.00	64.00	0.00	36.00
	2539.82	2540.08	5.90	0.15	61.00	0.00	39.00

CORE4	Sample Depth (m)			Permeability	Residual Fluid Saturation		
	From	To	Gas Exp	Horizontal L (mD)	Sw (%)	So (%)	Sg (%)
	3184.50	3184.77	12.20	3.40	70.00	0.00	30.00
	3185.14	3185.34	14.70	56.00	52.00	0.00	49.00
	3187.00	3187.60	1.20	23.00	61.00	0.00	13.00
	3188.00		2.60	0.04			
	3188.25		2.00	0.02			
	3188.50	3188.64	1.20	0.02	82.00	0.00	18.00
	3188.82		4.40	0.03			
	3189.07		5.90	0.13			
	3189.37		7.90	0.13			
	3189.44	3189.60	3.70	0.06	68.00	0.00	32.00
	3190.30	3190.57	11.30	4.10	63.00	0.00	37.00
	3190.82	3191.00	11.10	6.10	65.00	0.00	35.00
	3191.99		4.70	0.03			
	3192.16		2.80	0.02			
	3192.39		5.70	0.21			
	3192.50	3192.74	4.80	0.74	72.00	0.00	28.00
	3193.35		2.30	0.02			
	3194.27		3.10	0.02			
	3194.32		3.10	0.02			
	3194.93		5.90	0.05			

CORE2	Sample Depth (m)			Permeability	Residual Fluid Saturation		
	From	To	Gas Exp	Horizontal L (mD)	Sw (%)	So (%)	Sg (%)
	2305.04		3.80	0.32			
	2305.52		10.90	7.00			
	2305.80		7.00	0.07			
	2306.09		10.10	0.09			
	2306.44		13.10	0.91			
	2306.65		13.00	1.50			
	2306.90	2307.11	16.40	124.00			
	2307.22		4.00	0.01			
	2307.63		13.00	0.31			
	2307.95		21.00	70.00			
	2308.20		18.90	43.00			
	2308.41	2308.61	20.00	64.00			
	2308.66		15.50	4.40			
	2308.97		20.00	35.00			
	2309.22		16.80	16.00			
	2309.55	2309.74	17.20	3.90			
	2309.84		15.90	12.00			
	2310.19		13.80	0.53			
	2310.47	2310.63	9.70	0.04			
	2310.71		10.20	1.00			
	2310.96		6.80	0.02			
	2311.21		8.80	0.03			
	2311.46		21.70	70.00			
	2311.71		21.90	95.00			
	2311.80	2312.02	21.00	183.00			
	2312.10		21.70	57.00			
	2312.42		13.10	0.71			
	2312.66		15.80	4.70			
	2312.94		12.50	0.80			
	2313.03	2313.25	20.20	79.00			
	2313.46		18.30	90.00			
	2313.68		21.90	138.00			
	2314.08		19.60	66.00			
	2314.33		1725.00	101.00			
	2314.58		12.90	58.00			
	2314.86		4.80	0.10			
	2316.50		5.80	0.03			
	2316.88		7.30	0.02			
	2317.20		14.40	0.70			
	2317.45	2317.58	18.20	60.00			
	2317.59		18.80	61.00			
	2317.84		14.00	10.00			
	2318.09		5.90	0.02			
	2318.33		11.70	0.08			
	2318.74	2318.83	6.40	0.08			
	2318.89		13.70	1.00			
	2319.16		14.40	2.50			
	2319.44	2319.57	16.50	10.00			
	2319.58		16.40	39.00			
	2319.89		11.20	0.54			
	2320.17		14.20	11.00			
	2320.29	2320.49	19.90	99.00			
	2320.84		14.60	8.30			
	2321.27		14.50	13.00			
	2321.52		17.70	66.00			
	2321.79		19.50	73.00			

02 - Picket plot for water saturation in well A-F1 (corrected).

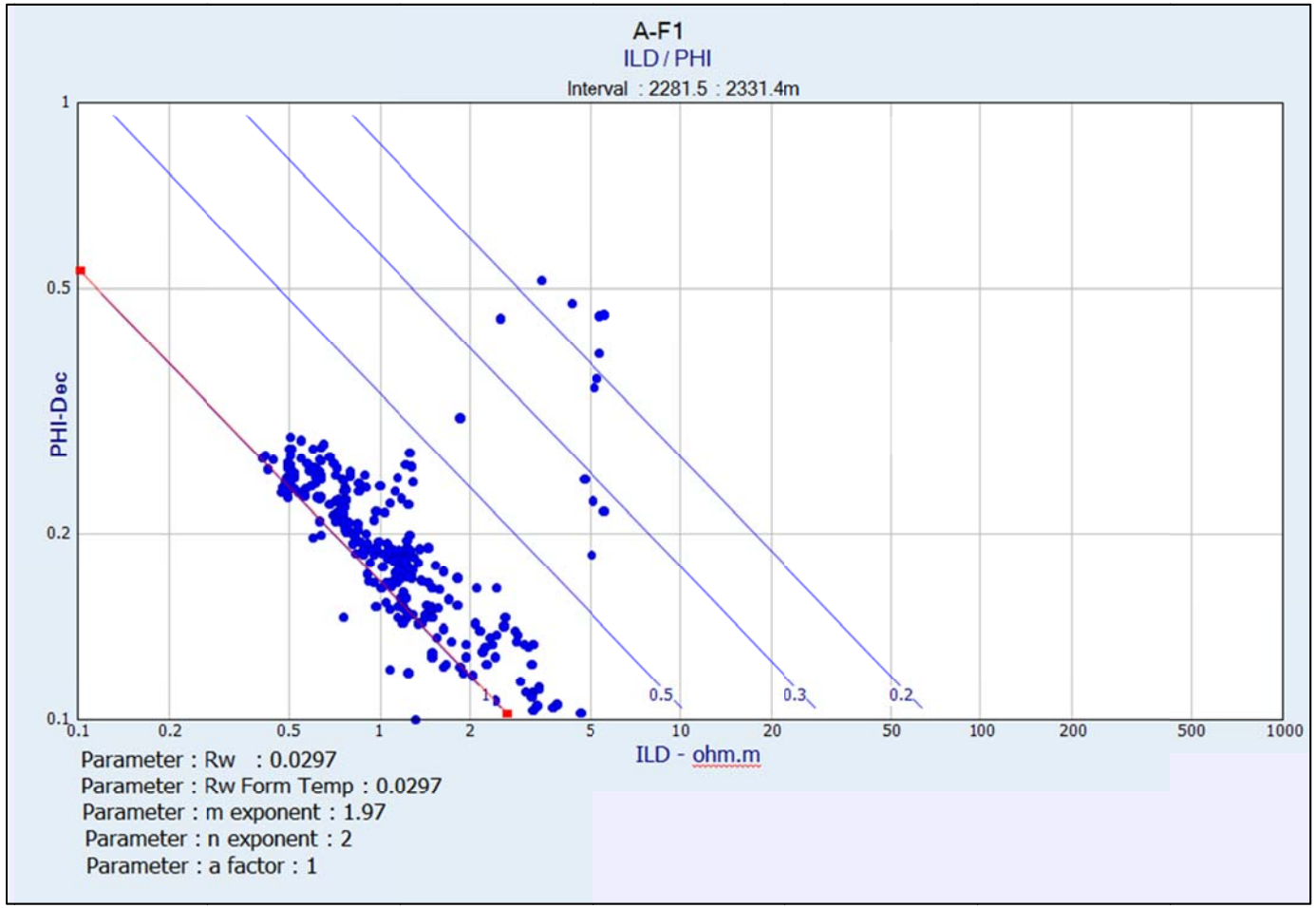

03 - Picket plot for water saturation in well A-F1 (un-corrected)

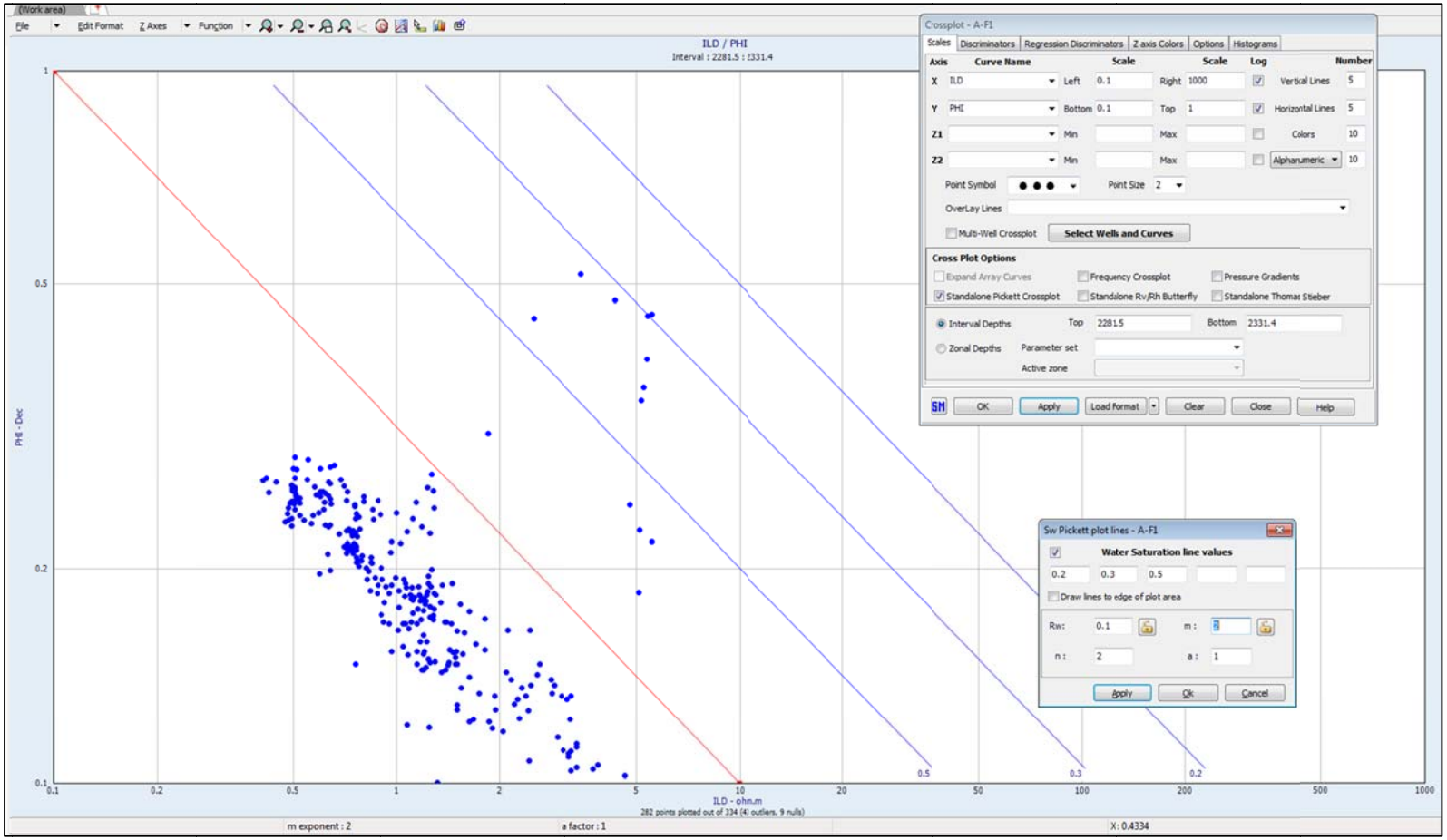

04 - PoroPerm Plot for well A-F1

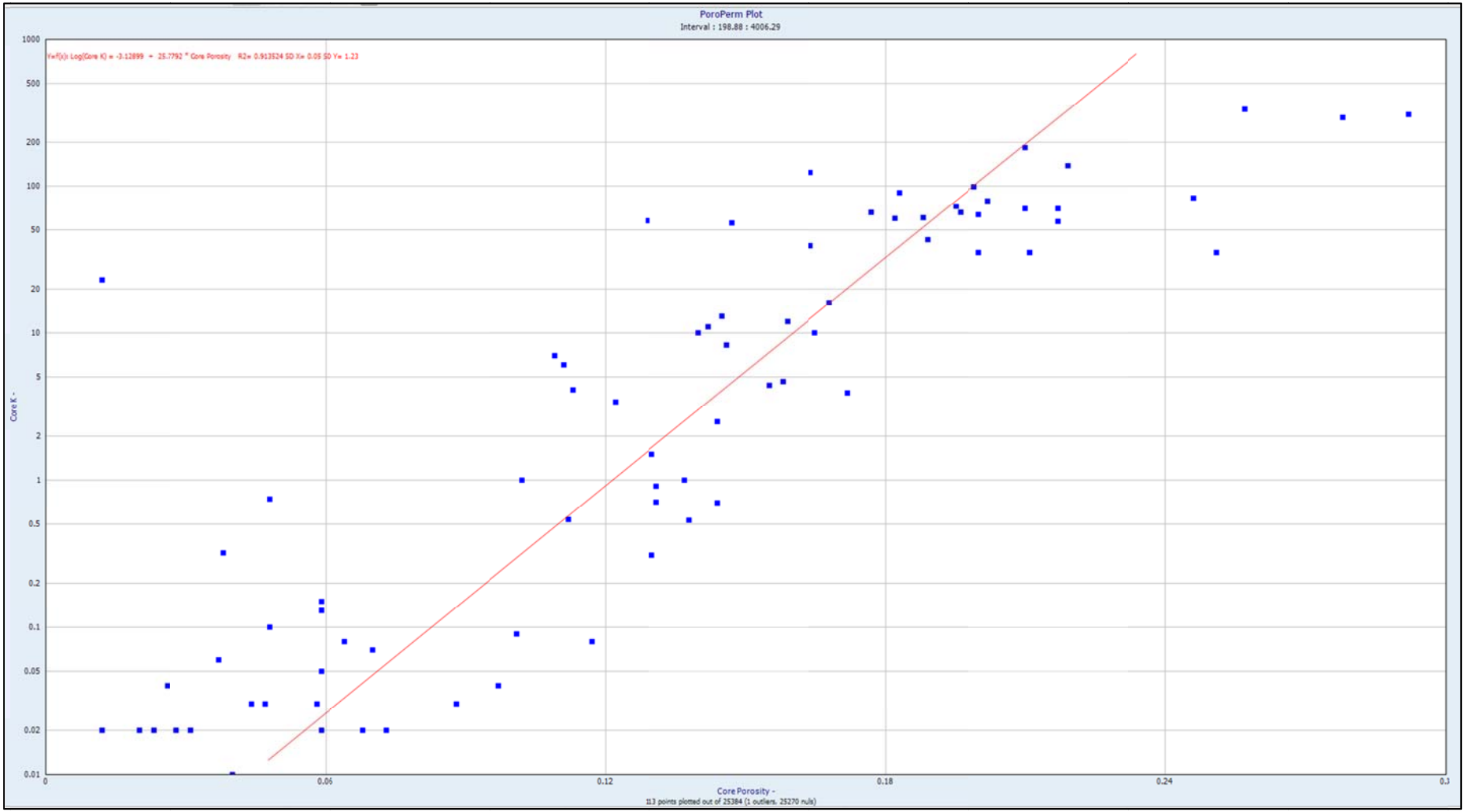

05 - Interactive Petrophysics Plot displaying Core measurements vs Porosity, Water Saturation and Permeability curves

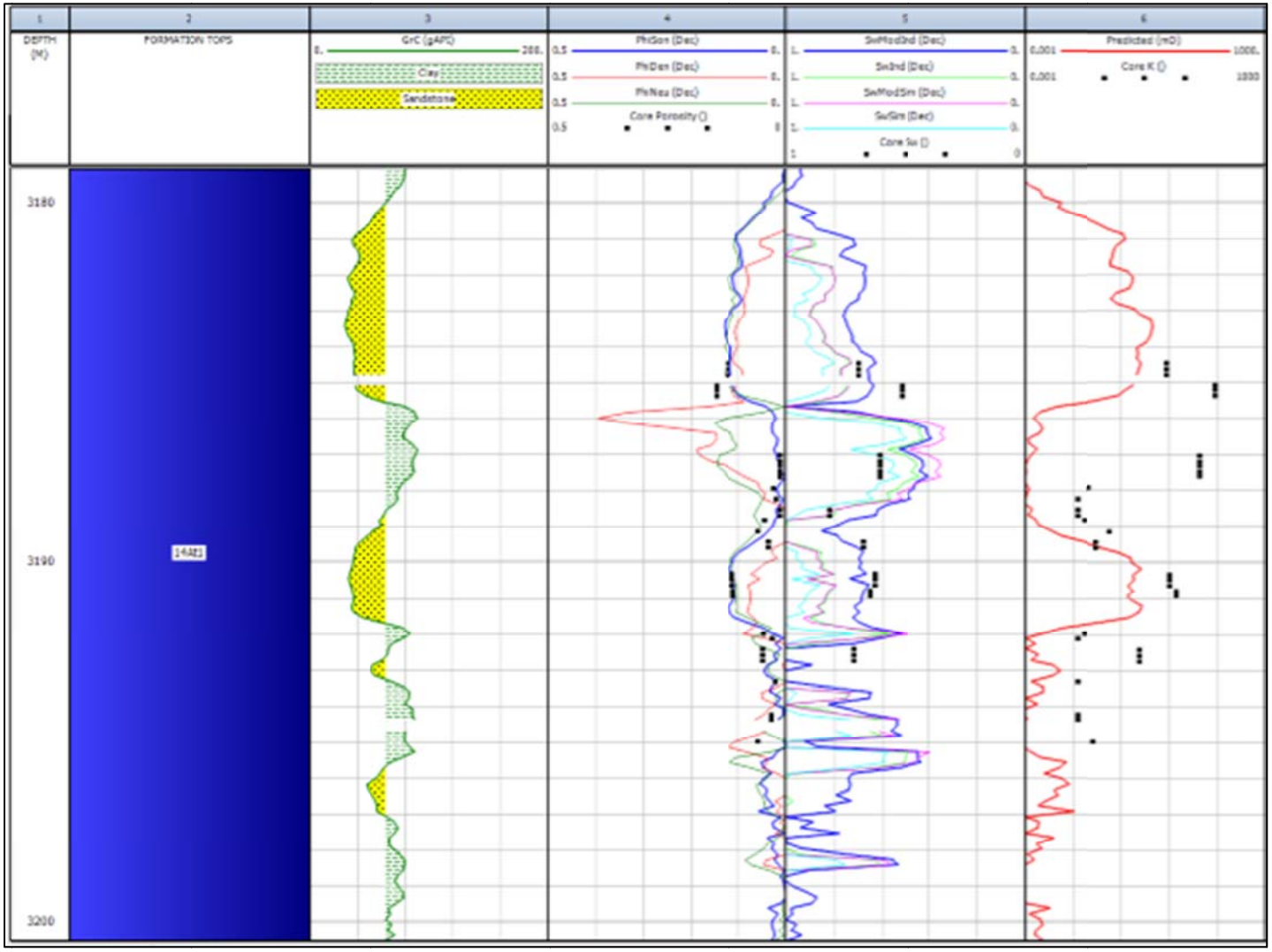

06 – Porosity vs Permeability Plot A-F1

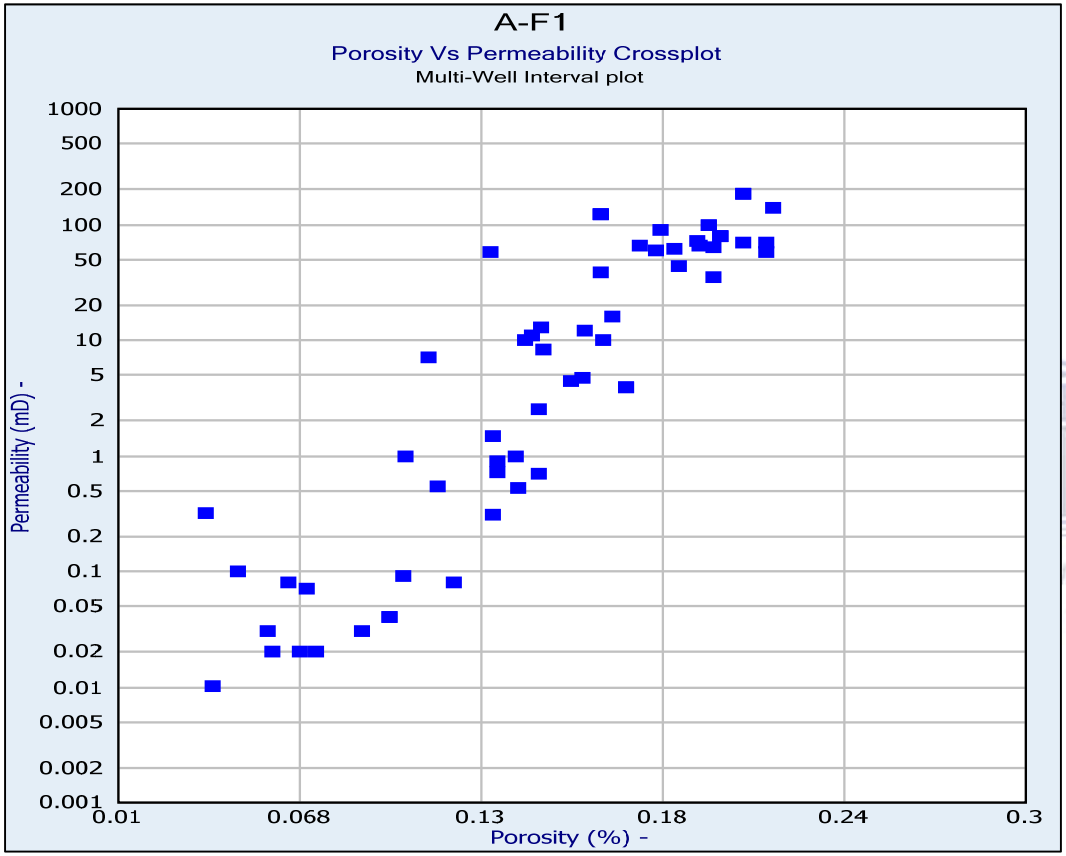

07– Volume of Shale vs Permeability Plot

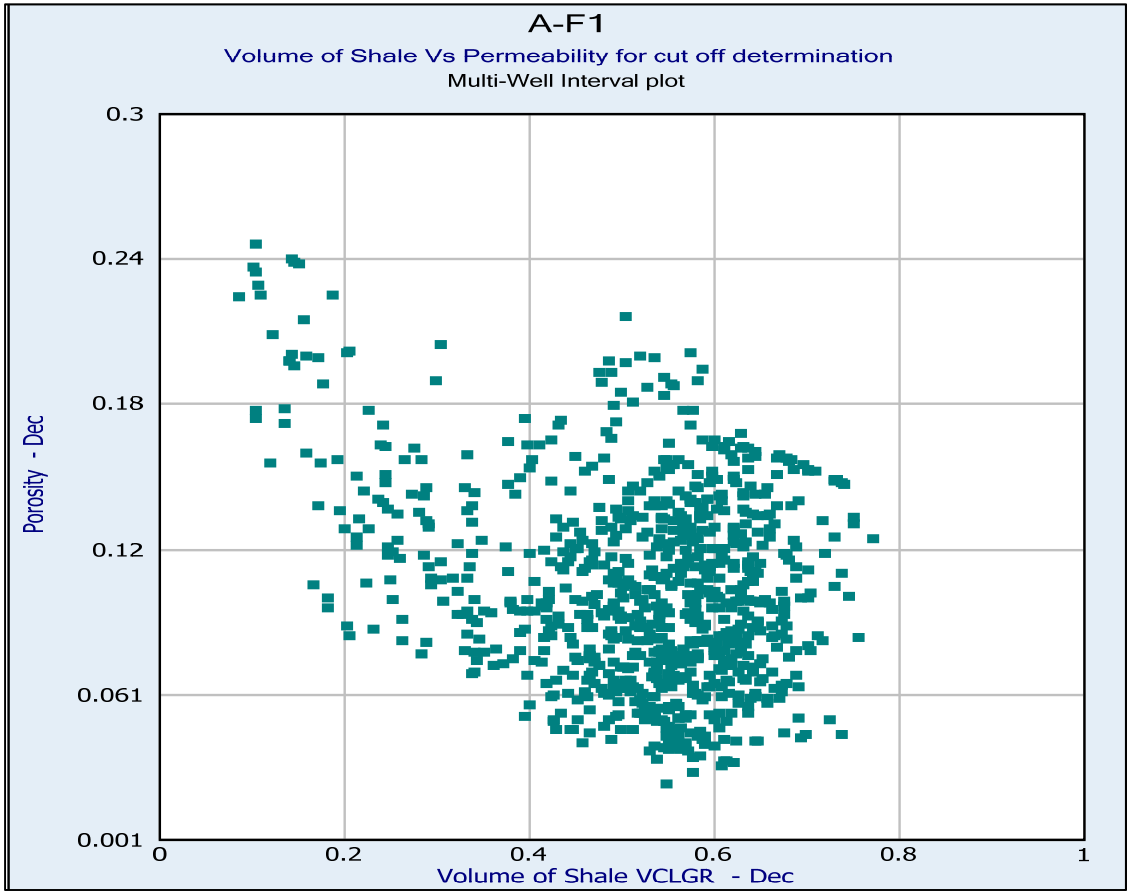

08 – Porosity vs Water Saturation plot

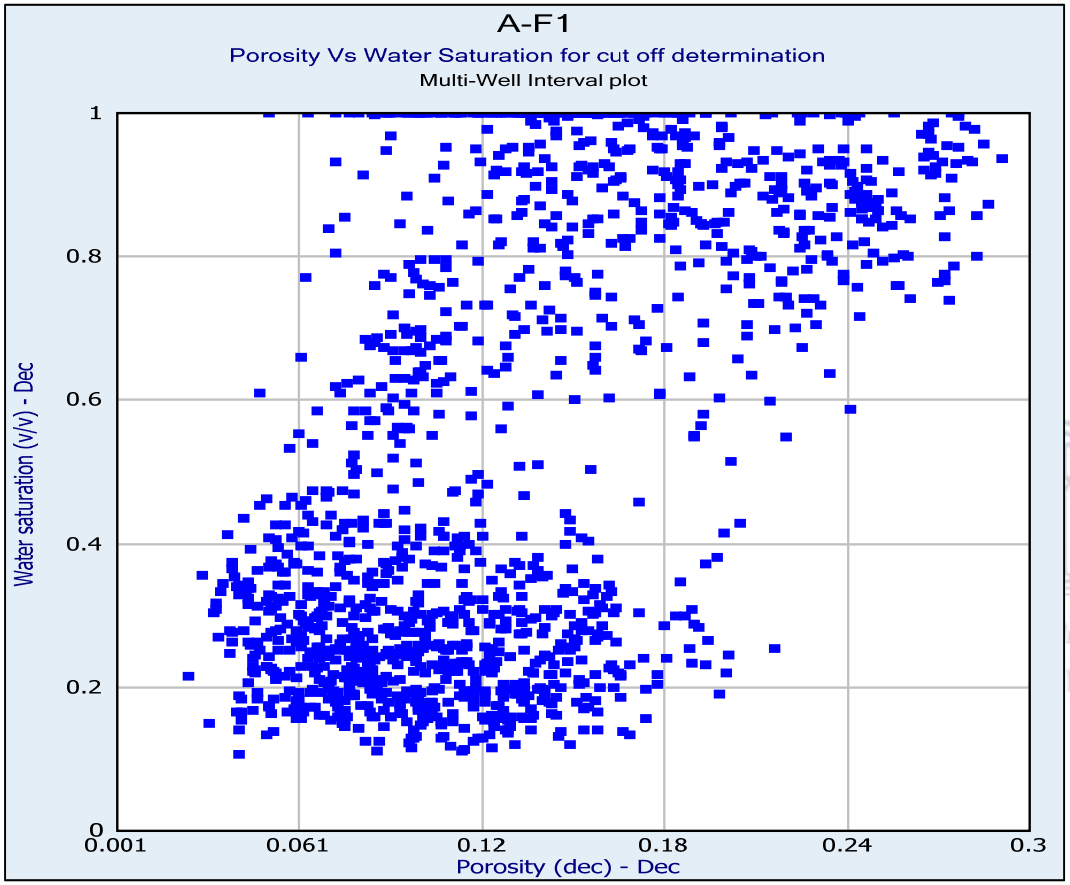

09 – TDR relationship – Depth vs Check shot (Interval Velocity)

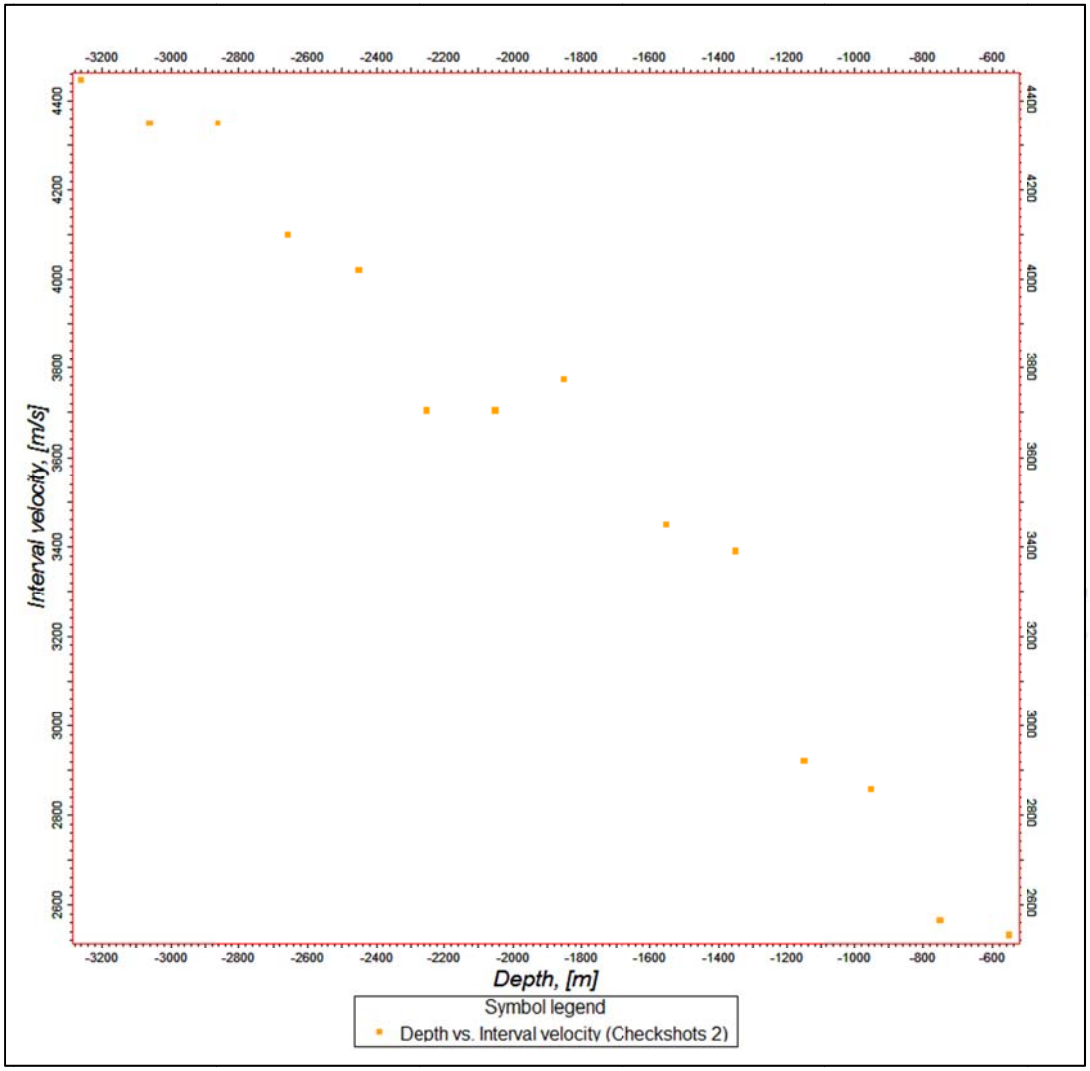

10 – Multi curve plot for 4 reservoir zones 14Ht1, well A-F1

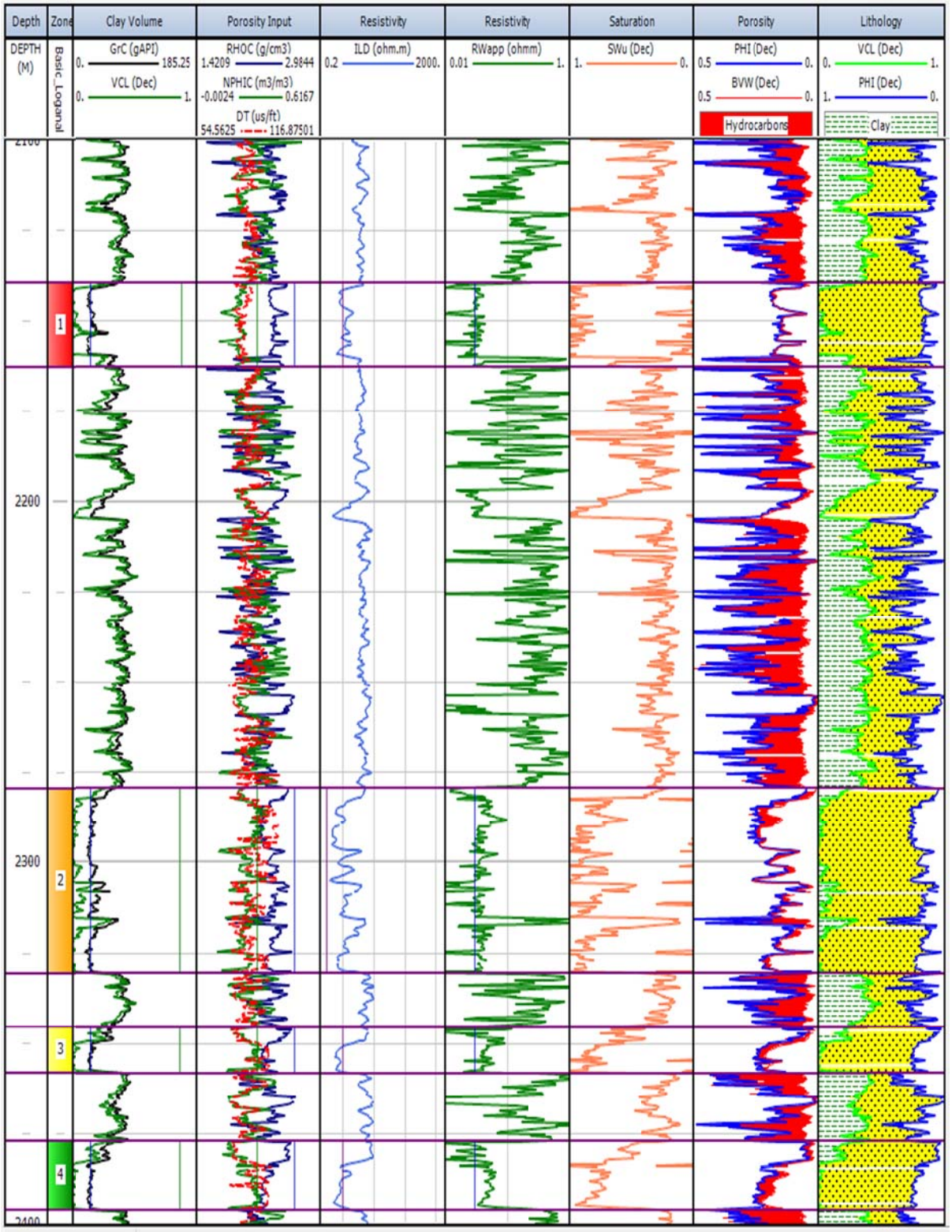

11 – Wireline logging tool descriptions (Schlumberger, 2017a).

Acoustic Amplitude (AMPL)

A measure of the maximum departure of an acoustic wave from the average value.

Bit Size (BS)

Nominal inside diameter of a borehole; often referred to a "bit size".

Bulk Density (RHOB)

Density of bulk material, including any void space or other materials contained in the subject volume. In well logging, it is the density of the rock, including fluid-filled pore space, as measured with a "Gamma-Gamma" type logging device

Bulk Density Correction (DRHO)

Correction to the Bulk Density log, as measured with a Gamma-gamma type logging device; used as an indication of hole condition to validate the Bulk Density measurement; conventionally abbreviated DRHO.

Cable Speed (CS)

Cable speed, generally measured at the surface as an approximation of tool speed.

Calibrated Induction Deep Conductivity (CILD)

The conductivity, measured by an induction log, which represents a measurement made several feet into the formation; generally considered a measurement of the undisturbed formation.

Caliper (CALI)

The inside diameter of a borehole.

Cement Bond Amplitude (CBL)

A measure of acoustic wave amplitude used for cement bond evaluation.

Density Porosity Limestone (DPL)

Porosity derived from a formation density measurement, assuming that the rock matrix material is calcite.

Gamma Ray (GR)

The intensity of natural gamma-ray radiation emitted from formations containing radioactive elements, such as Potassium, Thorium, and Uranium. Measured according to API specifications

Induction Deep Resistivity (ILD)

The resistivity, measured by an induction log, which represents a measurement made several feet into the formation; generally considered a measurement of the undisturbed formation.

Induction Medium Resistivity (ILM)

The resistivity, made by an induction log, which represents a measurement made approximately two to three feet into the formation.

Interval Transit time / Sonic Log (DT)

The time it takes for a compressional wave to traverse a fixed distance; reciprocal of Compressional Velocity.

Laterolog Deep Resistivity (LLD)

The resistivity, measured by a laterolog (or guard log) resistivity device, which represents a measurement made several feet into the formation; generally considered a measurement of the undisturbed formation.

Laterolog Shallow Resistivity (LLS)

The resistivity, measured by a laterolog (or guard log) resistivity device, which represents a measurement made approximately one to two feet into the formation; generally considered to measure the formation where it contains fluids which are comprised primarily of mud filtrate.

Magnetic Field Strength - along 3 axis with the second letter indicating axis (FX, FY, FZ)

Measurement of magnetic fields strength around the formation in all 3 axis using a magnetometer.

Matrix Density / Grain Density (RHGX)

The density of a unit volume of a mineral or other rock material at zero porosity. Sometimes called Matrix Density.

Micro Inverse Resistivity (MINV)

Micro Resistivity measurement using an "inverse" lateral electrode arrangement; traditionally combined with Micro Normal Resistivity in a Microlog survey for identifying permeable beds.

Micro Normal Resistivity (MNOR)

Micro Resistivity measurement using a "normal" electrode arrangement; traditionally combined with Micro Inverse Resistivity in a Microlog survey for identifying permeable beds.

Micro-spherically-focused Resistivity (MSFL)

A measurement of the resistivity of the formation, by a spherically focused tool, within the first few inches of the borehole wall.

Photoelectric Factor (PEF)

A measure of the probability that scattering due the Photoelectric Effect will occur; often expressed in an approximation unit barns/electron.]

Radius of Invasion (RI)

The radius of the "invaded zone", the region in which drilling mud filtrate has invaded porous and permeable rock around the borehole.

Raw Caliper (RCAL)

The inside diameter of a borehole.

Spherically Focussed Resistivity Un-averaged (SFLU)

The resistivity, measured by a spherically focused log, which represents the resistivity approximately one to two feet into the formation

Spontaneous Potential (SP)

The potential difference (DC voltage) between a movable electrode in the borehole and a distant reference electrode usually at surface. The voltage is due to currents generated by the electrochemical and electro-kinetic potentials.

Thermal Neutron Porosity (original Ratio Method) in Selected Lithology (NPHI)

Porosity as measured with a thermal neutron logging device.